EFFECT OF DISCONTINUITY ROUGHNESS AND ANISOTROPY ON SHEAR STRENGTH

A THESIS SUBMITTED TO
THE GRADUATE SCHOOL OF NATURAL AND APPLIED SCIENCES
OF
THE MIDDLE EAST TECHNICAL UNIVERSITY

BY

ALPER KAAN DENLİ

IN PARTIAL FULFILLMENT OF THE REQUIREMENTS FOR THE DEGREE

OF

MASTER OF SCIENCE

IN

THE DEPARTMENT OF MINING ENGINEERING

MAY 2004

Approval of the Graduate School of Natural and Applied Sciences.

_____

Prof. Dr. Canan Özgen

Director

I certify that this thesis satisfies all the requirements as a thesis for the degree of Master of Science.

_____

Prof. Dr. Ümit Atalay

Head of Department

This is to certify that we have read this thesis and that in our opinion it is fully adequate, in scope and quality, as a thesis for the degree of Master of Science.

_____	_____
Assist. Prof. Dr. H. Şebnem Düzgün	Prof. Dr. Celal Karpuz
Co-Supervisor	Supervisor

Examining Committee Members

Prof. Dr. Celal Karpuz	_____
Prof. Dr. Erdal Ünal	_____
Assoc. Prof. Dr. Levent Tutluoğlu	_____
Assist. Prof. Dr. Mehmet Ali Hindistan	_____
Assist. Prof. Dr. H. Şebnem Düzgün	_____

ABSTRACT

EFFECT OF DISCONTINUITY ROUGHNESS AND ANISOTROPY ON SHEAR STRENGTH

Denli, Alper Kaan

M.S., Department of Mining Engineering

Supervisor: Prof. Dr. Celal Karpuz

Co-supervisor: Assist. Prof. Dr. H. Şebnem Düzgün

May 2004, 109 pages

Discontinuity surfaces generally consist of undulations termed as roughness. It is well known that surface roughness plays an important role on the shear strength and shear behavior of discontinuities. However, the effect of roughness will not be the same when the direction of shearing changes. This effect causes variation of shear strength with shearing direction or in other words anisotropy on shear strength.

In this thesis, an experimental study was performed to investigate the effect of roughness and anisotropy on shear strength. For this purpose, joint samples were prepared using a model material and direct shear tests were conducted at different normal stress levels and shearing directions.

Key Words: Discontinuity, Roughness, Shear strength, Anisotropy

ÖZ

SÜREKSİZLERDEKİ YÜZEY PÜRÜZLÜLÜĞÜNÜN VE ANİZOTROPİNİN MAKASLAMA DAYANIMINA ETKİSİ

Denli, Alper Kaan
Yüksek Lisans, Maden Mühendisliği Bölümü
Tez Yöneticisi: Prof. Dr. Celal Karpuz
Ortak tez yöneticisi: Yrd. Doç. Dr. H. Şebnem Düzgün

Mayıs 2004, 109 sayfa

Süreksizlik yüzeyleri genellikle yüzey pürüzlülüğü olarak tanımladığımız ondülasyonlardan oluşur. Yüzey pürüzlülüğünün, süreksizliklerin makaslama dayanımına ve davranışına etkisi bilinmektedir. Ancak yüzey pürüzlülüğünün etkisi makaslama yönü değiştiği zaman aynı olmayacaktır. Bu etki makaslama dayanımının makaslama yönüne bağlı olarak değişmesine neden olur.

Bu tezde yüzey pürüzlülüğünün ve anizotropinin makaslama dayanımına etkisini incelemek amacıyla deneysel çalışma yapılmıştır. Bu amaçla, model malzemesi kullanılarak süreksizlik örnekleri hazırlandı ve makaslama deneyleri farklı normal gerilim seviyelerinde ve farklı makaslama yönlerinde yapıldı.

Anahtar Kelimeler: Süreksizlik, Yüzey pürüzlülüğü, Makaslama dayanımı, Anizotropi

To My Family

ACKNOWLEDGEMENTS

I would like to express my sincere appreciation to my supervisor Prof. Dr. Celal Karpuz and to my co-supervisor Assist. Prof. Dr. H. Şebnem Düzgün for their kind supervision, valuable suggestion and comments during this study.

I would like to express my sincere thanks to Nizamettin Aydemir and Mehmet Çakır for their help during laboratory experiments.

The author would like to thank to examining committee members for serving on the M. Sc. Thesis committe.

I would also like to express my gratitude to my family for their valuable support and patience.

TABLE OF CONTENTS

LIST OF TABLES

TABLE

LIST OF FIGURES

FIGURE

CHAPTER 1

INTRODUCTION

Rock discontinuities has a considerable influence on mechanical behavior of rock masses. Therefore, when stability of rock mass is considered, knowledge of shear strength of discontinuities gains importance. Surface of natural rock discontinuities generally consists of undulations or irregularities termed as roughness. Literature survey on this subject reveals that roughness plays an important role on the shear strength and shear behavior of discontinuities. Several models have been proposed which incorporate the effect of roughness on the shear strength of discontinuities (Patton, 1966; Ladanyi and Archambault, 1970; Barton and Choubey, 1977; Saeb, 1990). Nevertheless, shear strength was assumed to be independent of direction in most of these models.

Kulatilake (1995) stated that "Movements along discontinuities in foundations, dams, tunnels and slopes can occur in various directions, depending on the external forces such as external loads, water pressures, earthquake forces acting on the structure and on the kinematic constraints". Also, surface roughness of discontinuities usually exhibit variation in different direction on the same discontinuity surface and causes anisotropy on frictional characteristics.

In this thesis, an experimental study was performed to investigate the effect of roughness and anisotropy on shear strength. The investigation of anisotropy requires a number of joint samples with identical surface topography to be tested in

different directions and normal loads. Since it is impractical to use identical joints for each direction and normal load, the joint samples must have prepared artificially by casting method using a suitable model material. This method allows to repeat a particular surface geometry which represents roughness in each of the samples. Several researchers have used the casting method to replicate joints (Huang and Doong, 1990; Kulatilake et al., 1995; Jing et al., 1992; Lopez et al., 2003; Grasselli and Egger, 2003), however, a detailed procedure of sample preparation was not explained which is also important in terms of quality of replicating surface roughness and that of the tests.

It is usually difficult to construct a relationship between the surface properties and the observed mechanical behavior of natural discontinuities during shearing due to the complexity of surface morphology. However, Gentier et al. (2000) and Lopez et al. (2003) used geostatistical analyses for characterizion of surface morphology and investigated the effect of the morphological parameters on shear behavior.

In this study, simple joint geometry was used which allowed to identify the observed shear behavior more easily. For this purpose, joint roughness is simulated by saw-tooth geometry which is assumed to be an idealized shape of natural joint undulations. This type of roughness exhibit a characteristic anisotropy. Aydan et al. (1996) characterized the anisotropy of natural discontinuity surfaces by considering parameters associated with linear profiles (i.e height of asperities, inclination of asperity walls, length of asperity and periodicity of asperities) in two perpendicular directions , which are perpendicular to asperity ridge axis and parallel to it. They also estimated the parameters in other directions as a function of these two directions. Grasselli and Egger (2003) studied shear anisotropy, by creating joints both parallel and perpendicular to schistosity planes of two metamorphic rocks (serpentinite, gneiss which contains planes of schistosity). The joints tend to have a saw-tooth shape when they are perpendicular to schistosity planes and exhibit a characteristic anisotropic pattern.

The following outline in the thesis is used:

In Chapter 2, shear behavior of rock joints is reviewed. A literature survey on shear strength criteria for rough joints and previous investigations of anisotropy is given in Chapter 3. Experimental study, including detailed procedure for preparation and testing of samples, and test results are presented in Chapter 4. In Chapter 5, result of tests are analyzed in terms of variation of peak shear strengths, friction angles, peak dilation angles, shear stiffness with normal stress and shearing direction. The effect of roughness and anisotropy on these parameters is also discussed in this chapter. Finally conclusions and recommendations are presented in Chapter 6.

CHAPTER 2

REVIEW OF DISCONTINUITY BEHAVIOR

2.1 Introduction

Due to the fact that mechanical behavior of discontinuities has a significant effect on the rock mass deformation, various authors have investigated the deformational behavior of discontinuities (e.g. Bandis et al.,1983; Goodman, 1976,1989; Bandis, 1990; Saeb and Amadei, 1992).

The deformability of discontinuities are described by normal stiffness (K_n) and shear stiffness (K_s). Normal stiffness, K_n is defined as the rate of change of normal stress (σ_n) with respect to normal displacement (v) and shear stiffness, K_s is defined as the rate of change of shear stress (τ) with shear displacement (u) (Bandis et al., 1983).

2.2 Normal deformation behavior

Goodman (1976) showed that the interrelation between the normal stress and joint closure is non-linear and a typical curve is given in Figure 2.1. The curve indicates the rate of closure decreases with increasing normal stress and the curve becomes asymptotic to a vertical line which corresponds to limit of joint closure, V_m.

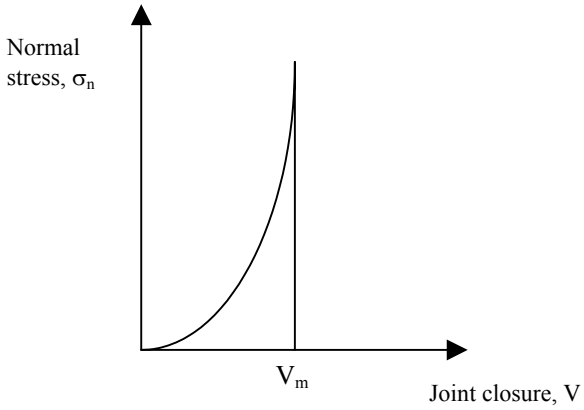

Figure 2.1 Typical normal stress vs. joint closure curve (After Goodman, 1976)

Based on the experiments on the interlocked and mismatched joints, Bandis et al. (1983) concluded that normal deformation for the interlocked and mismatched conditions are different and found much lower stiffness for the later. Unloading curves indicate the joint behavior is inelastic and result with hysteresis (Figure 2.2).

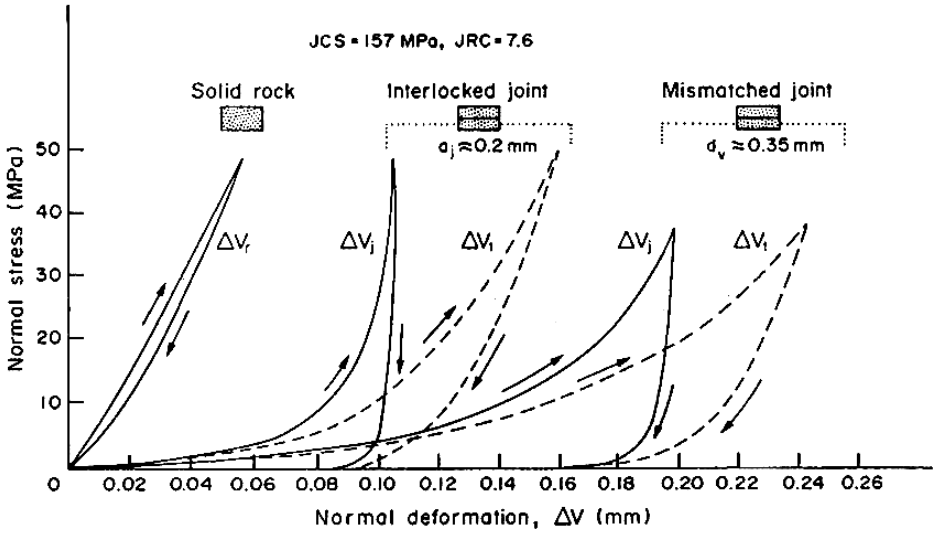

Figure 2.2 Normal deformation behavior (closure) of interlocked and mismatched joint (After Bandis et al.,1983)

Under normal load, the observed total normal deformation (ΔV_t) consists of compression of the intact rock (ΔV_r) and closure of the joint (ΔV_j). (Figure 2.2)
The joint deformation (closure) is given by ;

$\Delta V_j = \Delta V_t - \Delta V_r$

2.3 Shear behavior

Typical shear stress vs. displacement and normal displacement vs. shear displacement curve of a rough joint during direct shear test is shown in Figure 2.3 reported by Goodman (1989).

Shear stress-displacement curve in Figure 2.3 illustrates that, in the pre-peak region the shear stress (τ) rises quickly and attains maximum,τ_p after small shear displacement at $\Delta u = u_p$.

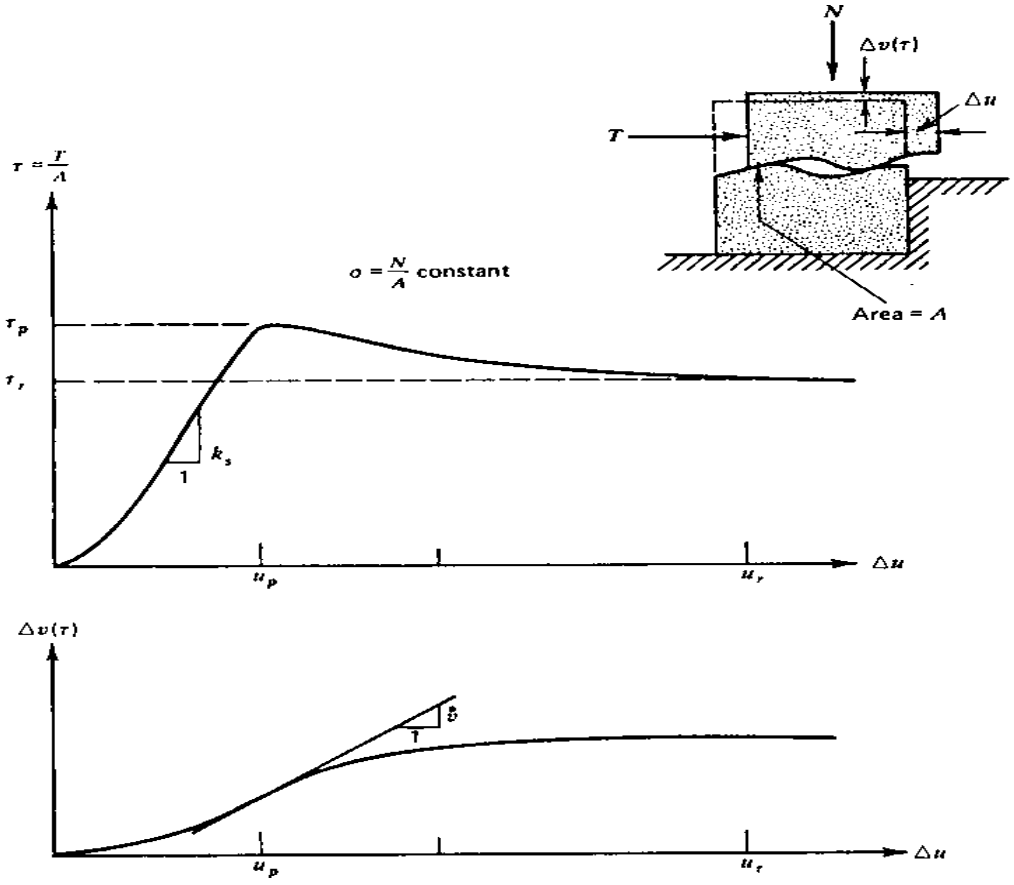

Figure 2.3 Tangential and normal displacements during direct shear of a rough joint (After Goodman, 1989)

In the post-peak region the shear stress decreases gradually until a constant residual shear strength is attained after large shear displacement at $\Delta u = u_r$.

2.3.1 Normal displacement of joint during shear

Due to undulations (roughness) on the surface of a non-planar joint, an upward displacement, Δv (dilation) occurs as the shear displacement takes place. In the Δv-Δu curve (Figure 2.3), as the shear stress builds, a period of adjustment with slight dilation followed by an increase in the rate of dilation; the rate of dilation is greatest at peak shear stress ($\Delta u = u_p$) and vanishes as the residual shear displacement is attained (Goodman,1989).

The amount of dilation depends on the surface roughness, the strength of the rock and the level of normal stress. With increasing normal stress dilation decreases due to degradation of surface roughness and the mode of failure changes from shear overriding to shear through (Bandis, 1993). Plesha (1987) stated that, even at lower normal stress levels, degradation of surface roughness can also arise from surface wear if the amount of slip is large.

2.3.2 Shear stiffness of rock joints

Goodman, Taylor, and Brekke, 1968 (Goodman, 1976) have introduced the term unit shear stiffness, K_s which is the slope of the τ-u curve as shown in Figure 2.3 characterizing the elastic region.

To describe the variation of shear behavior with normal stress, Goodman (1976) proposed two models which are constant stiffness and variable stiffness (constant peak displacement model) models. Constant stiffness model assumes that shear stiffness K_s is constant and does not depend on normal stress whereas constant peak displacement model assumes shear stiffness K_s varies with normal stress where both peak and residual displacements remain constant.

Bandis et al. (1983) used secant shear stiffness at peak shear stress, $K_{s,peak}$(secant) and based on the experiments on different joint types, concluded that peak shear stiffness increases with increasing normal stress in a non-linear fashion.

2.4 Effect of roughness on shear behavior

It is well known that, surface roughness has a great influence on shear strength and shear behavior of rock joints. Goodman (1989) stated that roughness controls not only the peak shear strength at low normal stresses but the shape of the shear stress versus shear displacement curve and rate of dilation. An experimental study performed by Yang and Chiang (2000) on the shear behavior of rock joints with tooth-shaped asperities demonstrated the two modes observed during shearing. They observed that, the shear stress-displacement curve shows a more ductile behavior at lower normal stress in slide-up mode and shows a brittle behavior at higher normal stress in shear-off mode (Figure 2.4).

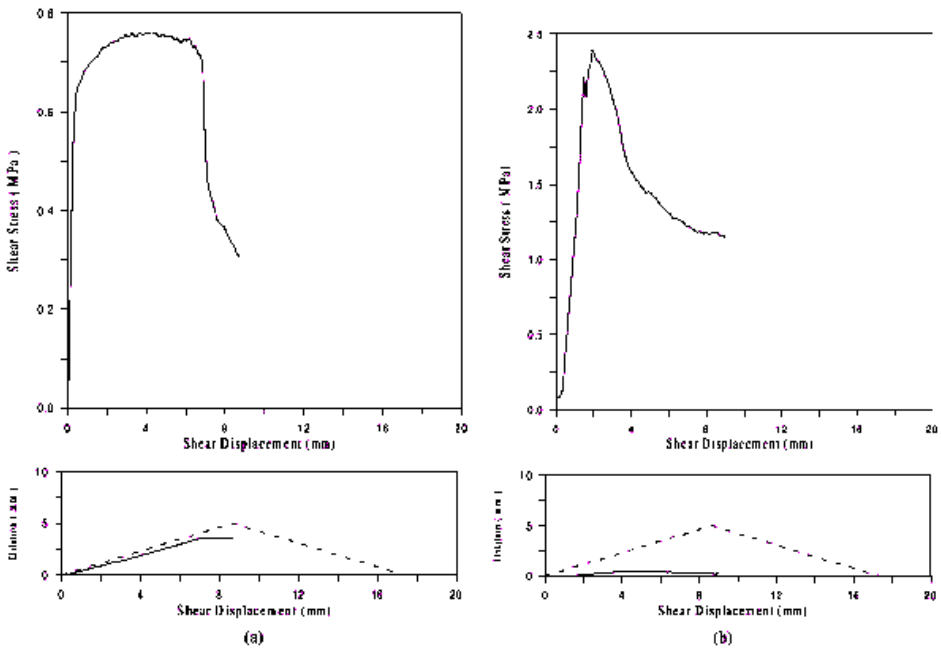

Figure 2.4 Two basic shear stress-displacement and dilation curves (a) Slide-up mode ; (b) Shear-off mode. (After Yang and Chiang, 2000)

Similarly, Huang et al. (2002) have observed different failure modes ranging from purely sliding to shearing-off asperities depending on normal stress. They found that when asperity failure occurs, subsequent sliding takes place on the newly formed fracture plane which means a decreased dilation angle.

Seidel and Haberfield (2002) have simulated roughness using regular and irregular tooth-shaped asperities. They concluded that joints with regular asperities display a higher peak shear strength and more brittle shear behavior compared to regular ones.

Yang et al. (2001) demonstrated that, at low normal stress levels a rougher joint shows a brittle behavior whereas a smoother joint shows a ductile behavior.

The above findings by previous researchers points out that, the surface roughness governs the shear behavior of rock joints to a great extent.

CHAPTER 3

LITERATURE SURVEY ON SHEAR STRENGTH OF DISCONTINUITIES

3.1 Introduction

In the first part of this chapter, different shear strength criteria proposed in the literature for non-planar (rough) joints are reviewed (Patton, 1966; Ladanyi and Archambault, 1970; Barton, 1977; Saeb, 1990). The effect of roughness on shear strength is also considered within the review of these models. In the second part, investigations on directional variation (anisotropy) of shear strength published in the literature are reviewed and shear strength criteria (Kulatilake, 1995; Grasselli and Egger, 2003) taking anisotropy into consideration are given.

3.2 Shear strength of discontinuities

Shear strength of two flat rock surfaces can be approximated by a linear envelope passing through the origin (Bandis, 1993) and described by ;

$$\tau = \sigma_n (\tan\phi_b) \qquad (3.1)$$

where;

ϕ_b is the basic friction angle (°)

The value of ϕ_b for smooth, unweathered rock surfaces lies between 25° and 35° (Barton, 1977).

For non-planar joints, the roughness features plays an important role on the shear strength. The effect of roughness on shear strength can be seen when Equation 3.2 developed by Newland and Alley (Barton,1976) is considered. In Equation 3.2 'i' value represents the contribution of roughness to shear strength which increases the basic friction angle (ϕ_b) by an angle equal to effective roughness angle (i).

$$\tau = \sigma_n \tan(\phi_b + i) \qquad (3.2)$$

where;

i = effective roughness angle (°)

Patton (1966), based on the experiments on saw-tooth joint geometry also used the same relation to define the shear strength at low normal stress levels. On the other hand, Patton found that Equation 3.2 is only valid at low values where the shear behavior is characterized by sliding or overriding in which the asperities remain intact. At higher stress levels, since the asperities are sheared-off he proposed the Coulomb relation given in Equation 3.3. Bilinear shear strength criterion is expressed as ;

$$\tau = \sigma_n \tan(\phi_b + i) \qquad \text{at lower } \sigma_n \text{ values}$$

$$\tau = C_a + \sigma_n \tan(\phi_r) \qquad \text{at higher } \sigma_n \text{ values} \qquad (3.3)$$

where;

C_a = apparent cohesion derived from the asperities

ϕ_r = residual friction angle

Ladanyi and Archambault (1970) proposed a curved shear strength envelope by considering variable dilation angle and shear area ratio in their shear strength criterion given by;

$$\tau = \frac{\sigma_n (1 - a_s)\left(\dot{v} + \tan \phi_b \right) + a_s S_r}{1 - (1 - a_s)\dot{v} \tan \phi_b} \qquad (3.4)$$

where ;

a_s = proportion of the joint area sheared through the asperities

$(1-a_s)$ = proportion on which sliding occurs

v = dilation rate at the peak shear stress, $\Delta v/\Delta u$

S_r = shear strength of the intact rock composing the asperities

Ladanyi and Archambault (1970) suggested the following relations (Equation 3.5, 3.6, 3.7) to express S_r, a_s and v;

$$S_r = \sigma_c \frac{(1+n)^{0.5} - 1}{\left(1 + n\frac{\sigma_n}{\sigma_c}\right)^{0.5}} \qquad (3.5)$$

where ;

σ_c is the uniaxial compressive strength and n is the ratio of uniaxial compressive to tensile strength of the rock.

$$a_s = 1 - \left(1 - \frac{\sigma_n}{\sigma_T}\right)^{k1} \qquad (3.6)$$

$$v = \left(1 - \frac{\sigma_n}{\sigma_T}\right)^{k2} \tan i_0 \qquad (3.7)$$

where ;

Suggested values for the exponents, k_1=1.5 and k_2=4

i_0 is the dilation angle at σ_n=0.

σ_T is the transition pressure and can be approximated by $\sigma_T = \sigma_c$ (Goodman, 1976).

Saeb (1990) revised the Ladanyi and Archambault's shear strength criterion and suggested the modified criterion given as ;

$$\tau = \sigma_n \tan(\phi_u + i)(1 - a_s) + a_s S_r \qquad (3.8)$$

$$i = \tan^{-1} \dot{v}$$

where; the parameters have same meaning of Ladanyi and Archambault's criterion which is given in Equation 3.4.

Barton and Choubey (1977) proposed an empirical shear strength criterion developed through quantification and testing of a wide range of natural rock joints given by ;

$$\tau = \sigma_n \tan\left[JRC \log\left(\frac{JCS}{\sigma_n} \right) + \phi_r \right] \qquad (3.9)$$

where;
JRC = Joint roughness coefficient (ranging 0-20 representing a scale of roughness from smooth, planar to rough, irregular joints)
JCS = Joint compressive strength

JRClog(JCS/σ_n), was termed as roughness component, describing both the geometrical and asperity strength contributions of roughness to shear strength (Bandis,1993). Equation 3.9 is applicable for predicting the peak shear strength of both weathered and unweathered surfaces. If the joint surfaces are unweathered, JCS can be taken equal to σ_c (unconfined compressive strength) also ϕ_b can be used instead of ϕ_r such that , $\phi_r = \phi_b$ (Barton and Choubey,1977).

Barton and Choubey (1977) introduced the term ‘damage coefficient’ and defined the peak dilation angle, $d_n°$ as;

$$d_n^{\circ} = \frac{JRC}{M}\log\left(\frac{JCS}{\sigma_n}\right) \qquad (3.10)$$

where;
M is damage coefficient and approximately takes values, 1 at low σ_n values with little asperity damage occurs, may be high as 2 at higher σ_n values with increasing asperity damage (Barton et al., 1990).

If asperity damage is slight ‘M’ will be equal to 1 and peak dilation angle will be equal to ;

$$d_n^{\circ} = JRC\log\left(JCS/\sigma_n\right)$$

and Equation 3.11 may be used as a first approximation to peak shear strength (Barton and Choubey, 1977).

$$\tau = \sigma_n \tan\left(d_n^{\circ} + \phi_r\right) \qquad (3.11)$$

Both JRC (joint roughness coefficient) and JCS (joint compressive strength) are scale dependent and scale correction Equations 3.12, 3.13 are proposed when assigning field values from laboratory-determined values (Barton et al., 1990).

$$JRC_n \approx JRC_0\left(L_n/L_0\right)^{-0{\cdot}02JRC_0} \qquad (3.12)$$

$$JCS_n \approx JCS_0\left(L_n/L_0\right)^{-0{\cdot}03JRC_0} \qquad (3.13)$$

Where L is length of the joint and subscript ($_0$) and (n) refers to laboratory and field scale respectively.

3.3 Effect of anisotropy on shear strength

Shear strength criteria mentioned in the previous section consider variation of shear strength with normal stress, effect of roughness and frictional properties of rock such as basic friction angle. However, these shear strength criteria doesn't take into account the directional dependence of shear strength which can be anisotropic. In the literature, the emphasis given on the effect of anisotropy in shear strength and behavior of discontinuities is limited. Some of the investigations which considers this concept (Huang and Doong, 1990; Jing et al.,1992; Kulatilake et al., 1995,1999; Riss et al., 1997; Gentier et al., 2000; Grasselli and Egger, 2003; Lopez et al., 2003) are briefly reviewed.

Huang and Doong (1990) investigated the anisotropic shear strength by conducting shear tests and roughness measurements on model joints prepared from natural joint surfaces and found that shear strength of rock joints depends both on the normal stress as well as on the direction of shearing. Another result concluded by them is the anisotropy of shear strength might be significant and its effect decreases with increasing normal stress.

Kulatilake et al. (1995) performed similar experiments and roughness profile measurements on model joints of three different natural rock joints at different directions. their results also show both joint roughness and peak shear strength are anisotropic. They proposed a strength criteria that captures roughness arising from both stationary (or small scale roughness) and non-stationary parts (or large-scale undulations) of a joint profile. They introduced a parameter 'I' to model non-stationary part. In order to model stationary (small-scale rougness) part they introduced a roughness parameter 'SRP' and they used different methods of quantification of joint surface roughness which includes conventional statistical parameters, fractal parameters, spectral/fractal parameters and variogram/fractal parameters as roughness measures. By means of these different parameters as roughness measures, they suggested four options to represent 'SRP'. Shear strength criterion reported by Kulatilake et al.(1995) takes the general form given by ;

$$\tau = \sigma_n \tan\left(\phi_b + a(SRP)^c \left[\log\left(\frac{\sigma_J}{\sigma} \right) \right]^d + I \right) \qquad (3.14)$$

Where ;

Coefficients a, c, d are determined by performing regression analysis on the experimental data.

σ_j = joint compressive strength

SRP denotes stationary roughness parameter

I represents non-stationary part and is the average inclination angle along the direction of the joint surface considered.

For smooth joint surfaces, the value of $a(SRP)^c$ becomes 0 and the equation reduces to which is applicable for smooth inclined joint surfaces.

$$\tau = \sigma_n \tan(\phi_b + I) \qquad (3.15)$$

And for smooth horizontal joint surfaces ;

$$\tau = \sigma_n \tan \phi_b \qquad (3.16)$$

The shear strength criterion given in Equation 3.14 is applicable only at low normal stresses where only the effect of dilation considered. As the normal stress increases both dilation and shearing-through contributes peak shear strength and the equation was further improved to include the effect of dilation and shearing through the asperities by Kulatilake et al. (1999).

Jing et al. (1992) have found existence of anisotropy in both the frictional strength and deformability of joints with rough surfaces. They observed that, the directional (anisotropic) distribution of friction angle is not completely random but has some principal directions and explained the relation by defining an asperity ellipse such that in the case of isotropy the ellipse will take the form of circle. Similarly, associated with anisotropy of shear strength, Wang et.al. (2003) have

used an anisotropy parameter defined by an ellipse function and incorporated the parameter into their constitutive model for joints.

The characterization of damaged zones occurring during shear tests with various normal stresses, shear directions and shear displacement is reported by Riss et al., 1997 and Gentier et al., 2000. By means of geostatistical methods and image analysis, they concluded that there is an increase in damaged areas with increasing normal stress and shear displacement, on the other hand size, shape and spatial distribution of damaged areas are related to shear directions and anisotropic. Lopez et al. (2003) have used geostatistical methods to estimate morphological parameters which are characterizing the anisotropic surface roughness and investigated the relationship between these morphological parameters and the observed shear behavior.

Grasselli and Egger (2003), proposed the peak shear strength criterion given in Equation 3.17 which shows the directional dependency of shear strength.

$$\tau = \sigma_n \tan\phi_r \left[1 + e^{-\left(\theta^*_{\max} / 9A_0 C\right)(\sigma_n / \sigma_t)} \right] \qquad (3.17)$$

where;

ϕ_r = residual friction angle; σ_t = tensile strength of rock; A_0 = maximum potential contact area for the specified shear direction; θ^*_{max} = maximum apparent dip angle with respect to the shear direction and C = roughness parameter which characterizes the distribution of the apparent dip angles over the surface.

Estimation of the parameters $A_{0,}$ θ^*_{max} and C was described by Grasselli et al. (2002) which includes measurement and discretisation of the natural discontinuity surface.

CHAPTER 4

EXPERIMENTAL STUDY

4.1 Introduction

In order to investigate the effect of roughness and anisotropy on shear strength, artificial joint samples were casted using a model material. The advantage of the casting method is the ability to make several joint samples (replicas) with identical surface geometry. This allows to investigate the parameters effecting shear strength and directional dependency of shear strength which requires many joint samples (but with identical geometry) to be tested along different shear loading directions. Direct shear testing of joint samples was performed on a large shear-box machine under constant normal load conditions. The procedure followed in sample preparation and shear tests, is in accordance with the ISRM suggested methods for determination of direct shear strength (Brown,1981).

In this chapter, first a description of model material, preparation of artificial joint samples and procedure followed in the direct shear testing of samples are given. Subsequently, the test results obtained from standard direct shear tests are given in the form of graphs.

4.2 Model material

Cement-based grout was chosen as a model material due to its relatively high compressive strength values, homogeneity of dry mix, good flow

characteristics. Water/dry-mix ratio was kept at 0.14 by weight for all samples.

Samples for compression tests are prepared by pouring the model material (water added) into cylindrical tubes having a diameter of 54 mm and 130 mm length (Figure 4.1) and the mix was left to set for a day. After that, samples were removed and left to cure for a period of 15, 21 and 28 days.

Figure 4.1 Samples prepared for compressive strength tests

As mentioned, the water ratio was kept constant and uniaxial compressive strength (σ_c) values were measured for different curing periods at room temperature (Table 4.1). Obviously, model material gains strength as the curing time extends and has attained the highest compressive strength value at 28 days. Curing period of 28 days was chosen for the model material, therefore all samples have an average compressive strength (σ_c) of 43.5 MPa.

Table 4.1 Uniaxial compressive strength values of model material for different curing periods

Curing period (days)	No. of samples	Uniaxial compressive strength (MPa)	
		Average	Standard Deviation
15	3	36.5	1.57
21	6	38.6	1.29
28	6	43.5	2.78

4.3 Sample preparation

Previously determined joint surface geometry (i.e. height or number of asperities) was initially machined at the workshop by milling cutter on an aluminum sheet to a final circular cross-section the diameter of which is equal to 10 cm. The surface geometry was reproduced using a two component casting epoxy, so a perfectly matching lower and upper half-mold was obtained. These epoxy molds were then placed at the bottom of the steel tube with inner diameter equal to 10 cm and the model material (grout) was poured into each half. Afterwards, the model material was left to set for a day at room temperature and then separated from the mold. By means of that procedure, several pairs of matching joint samples with identical surface geometry was casted. It should be noted that, using a relatively flexible epoxy as an intermediate mold and application of a very thin film of releasing agent which doesn't alter the surface properties (i.e removed easily when dryed) prevented bonding of grout to the mold. Figure 4.2 shows the casting procedure and prepared joint samples.

Two types of artificially prepared joint samples with the method mentioned above were used in this study. These include;

Type1 : Joints with regularly indented saw-tooth geometry. Each asperity (teeth) has an inclination angle, $\theta = 7.6°$ with a height of 2 mm and a base length of 30 mm.

Type2 : Joints with regularly indented saw-tooth geometry. Each asperity (teeth) has an inclination angle, $\theta = 7.6°$ with a height of 1 mm and a base length of 15 mm.

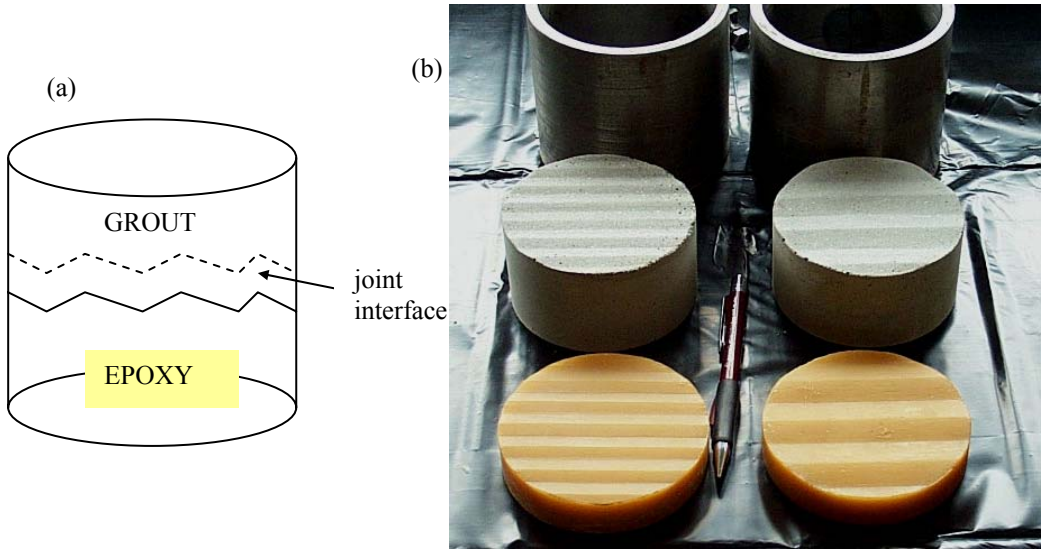

Figure 4.2 (a) Schematic representation of casting of joint samples (b) Photograph of steel-tubes, prepared samples and epoxy molds (from top to bottom)

For the second type of joints, both the height and base length of asperities are half of the first type so that the number of asperities over the total joint surface or periodicity of asperities is twice the first type. Illustration of Type1 and Type2 joints are shown in Figure 4.3.

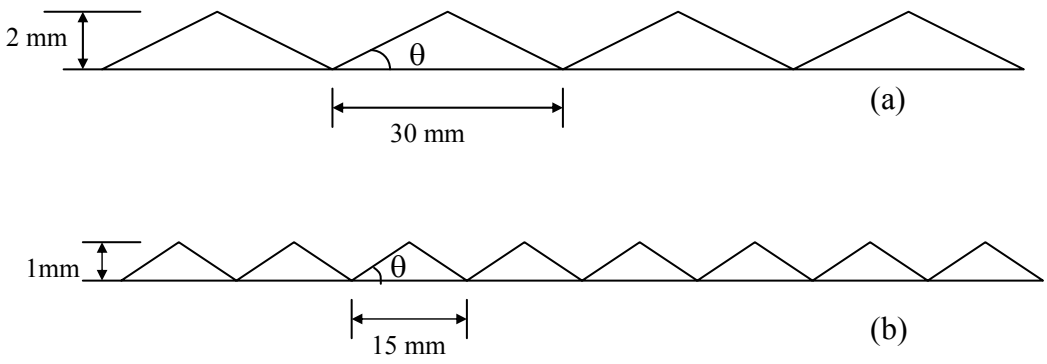

Figure 4.3 Schematic view of (a) Type1 and (b) Type2 joint profiles, θ is the geometric inclination angle (in asperity dip direction)

Flat, smooth joints were also prepared to measure the angle of basic friction, ϕ_b. Model material was poured into steel tube (inner diameter is 10 cm) on a flat glass plate and left to set for a day. After that, surface of the joint sample halves were further smoothed using a lapping machine.

4.4 Preparation of joint samples for shear testing

Joint sample was encapsulated using cement mortar in order to fix inside the shear-box for direct shear test. Figure 4.4 shows a test sample built-in the shear box. Cement mortar that used for encapsulation of joint sample is a mix of cement, sand and water. The stages followed for preparation of joint samples for shear testing is as follows;

(1) The two matching lower and upper half joint samples are tied up with a binding wire to prevent movement during the following stages.
(2) Joint sample is secured in correct position (previously determined direction of shearing) and the shear plane is leveled horizontally by means of a locating clamp with adjustable screws.

Figure 4.4 Photograph of a test sample built-in shear box

(3) Locating clamp with joint sample, is centered on the lower shear-box mold.

(4) Cement mortar is poured into the lower shear-box mold up to the marked line on the joint sample which leaves a zone of about 5mm free from encapsulation.

(5) After the cement mortar has set, upper-shear box mold is filled with cement mortar similarly. The lower shear-box mold with the joint sample in place is turned over and lowered onto the upper shear-box mold ensuring both molds coincide with each other.

(6) Subsequent to setting of mortar, the wire holding the samples together is cut and joint samples are left to cure for 28 days.

4.5 Testing apparatus

All of the direct shear tests of joint samples were carried out using a large shear-box machine (WF25505) manufactured by Wykeham Farrance. A general view of the machine is shown in Figure 4.5. The testing machine have square cross-section shear-box of size 30 cm.

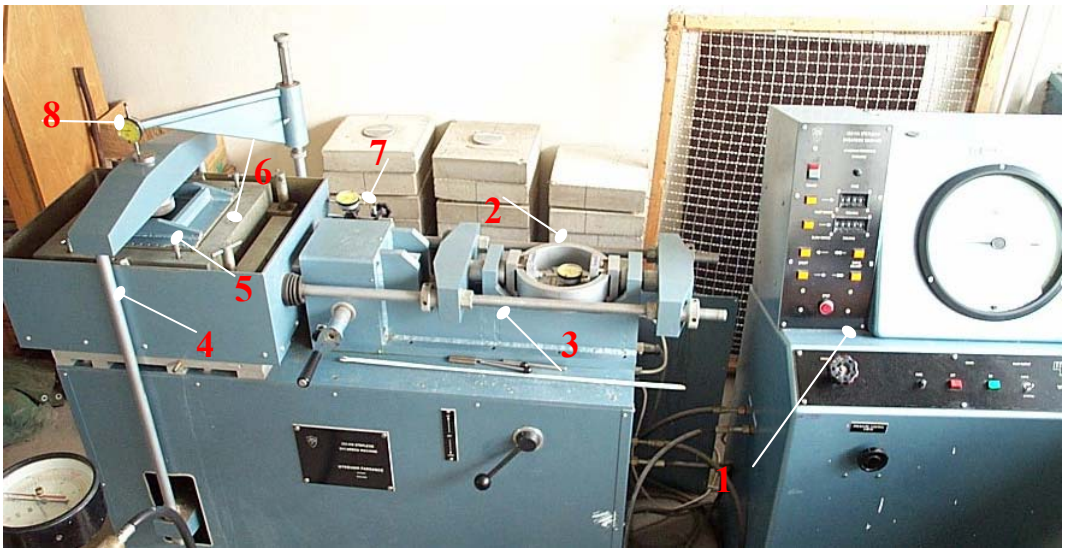

Figure 4.5 General view of the large shearbox machine, 1.Control unit ; 2.Proving ring ; 3.Horizontal tension bars ; 4.Vertical loading yoke ; 5.Loading plate ; 6.Shearbox ; 7.Horizontal displacement gauge ; 8.Normal displacement gauge

The consolidation (normal) force applied through a loading yoke is produced by a hydraulic system having a sensitive sprung loaded valve which, once adjusted manually to the desired load, automatically maintains that load. Horizontal shearing force is produced by two direct current stepless motors through a rubber belt drive.

With the sample in place and the horizontal loading system applying a force to the bottom half of the shearbox, a shear force is transmitted through the sample to the top half of the shearbox. Attached to this half are horizontal tension bars. A proving ring is used to measure this load (Figure 4.6).

The proving ring measures shear load as a function of displacement. Vertical (normal) and horizontal (shear) displacements are recorded by dial gauges during shear tests. The accuracy of the measuring system for proving ring is 0.002mm and is 0.01mm for both normal and shear displacements.

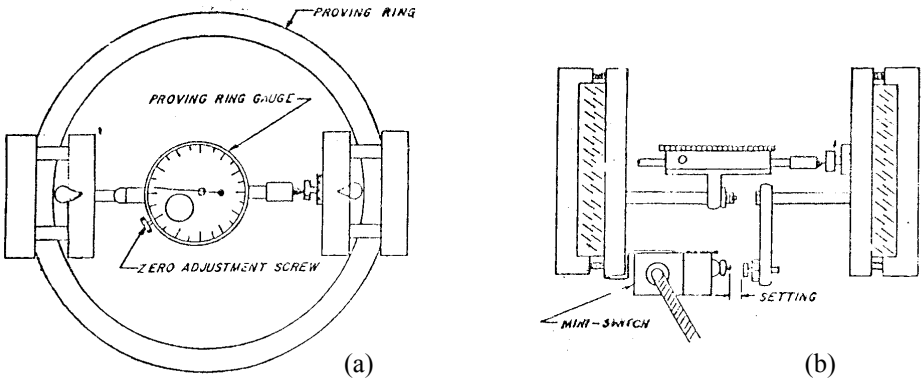

Figure 4.6 Schematics of proving ring (a) Top view (b) Side view

4.6 Direct shear test procedure

After 28 days of curing, joint samples were ready to test in shear machine. Direct shear tests were performed under constant normal load ranging from 5 to 34 kN. The rate of shear displacement was 0.1 mm/min with the maximum being 0.3 mm/min (usually increased after the peak shear resistance is attained) and total shear displacement was in the range between 7.5 to 10 mm.

4.6.1 Calculation of shear and normal stresses

Both shear stress and normal stress values were calculated by dividing the shear load and normal load by the corrected nominal area respectively. Nominal joint area (gross contact area) is corrected according to change in joint area during shear.

Normal stress is equal to;

$$\sigma_n = \frac{F_n}{A} \qquad (4.1)$$

where;

F_n = normal load (kN)

A = corrected nominal area of the joint surface (mm^2)

Shear stress is equal to ;

$$\tau = \frac{F_s}{A} \qquad (4.2)$$

where;

F_s = shear load (kN)

A = corrected nominal area of the joint surface (mm^2)

Normal loads used in the shear tests are 5 kN, 10 kN, 16 kN, 23 kN, 34 kN. Equivalent initial normal stresses are calculated as ;

Initial joint area for all samples is ;

$$A = \frac{\pi(100)^2}{4} = 7854 mm^2$$

and according to Equation 4.1 initial normal stresses are equal to 0.64, 1.27, 2.04, 2.93, 4.33 MPa respectively. Initial normal stresses were used only to distinguish plots of shear stress vs. shear displacement.

As mentioned previously, normal stresses are changing continuously due to changing joint area and so these corrected values were used in the interpretation of results.

Shear stresses were calculated according to Equation 4.2 using the measured shear loads in the tests. In Figure 4.7, two shear stress vs. shear displacement curves of the same test are drawn. One curve is plotted considering constant original area while the other is plotted considering corrected area. The amount of increase in shear stress at 7.5 mm shear displacement is about 10.5 % of the value of shear stress for original area. Due to this significant change in shear stress all test results were plotted using the corrected values.

4.6.2 Test program

Totally 35 samples including flat and rough joints were prepared and tested. Properties and total number of samples for each joint type are shown in Table 4.2.

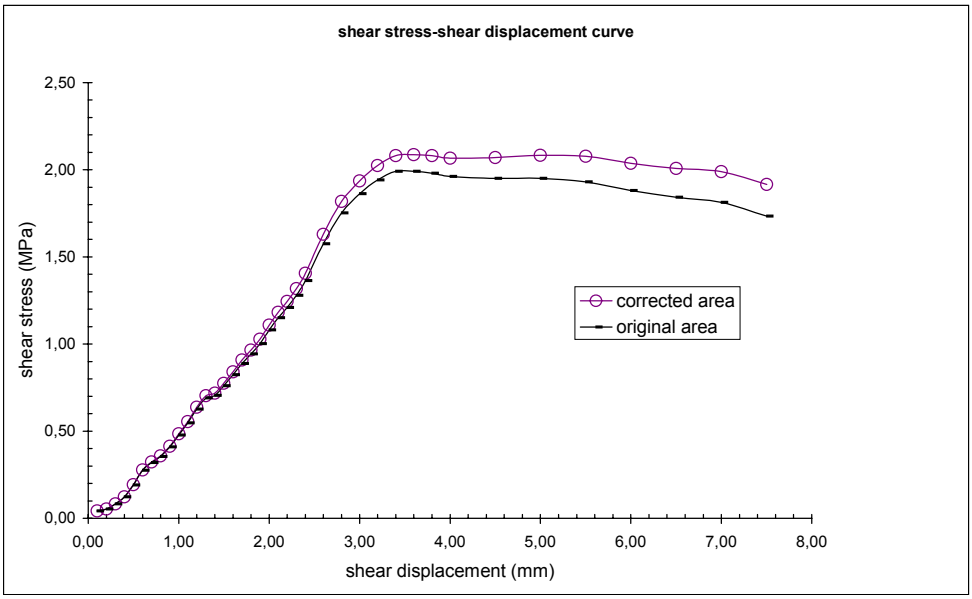

Figure 4.7 Comparison of shear stress vs. shear displacement curves plotted using original area and corrected area

Table 4.2 Properties and number of samples

Joint sample name	Joint profile	Sample diameter, D (cm)	Model material	Curing period (days)	Number of samples
Flat	Flat	10	Cement-based grout	28	4
Type1	Saw-tooth	10	Cement-based grout	28	16
Type2	Saw-tooth	10	Cement-based grout	28	15

The test samples of Type1 and Type2 were further subdivided into groups according to predetermined direction of shearing to investigate the effect of anisotropy. Shearing direction was denoted by α and the definition was represented on the lower half of joint surface in Figure 4.8. Direction of shearing normal to the asperities is taken as 90° (y-axis) shearing direction, other directions are measured clockwise at 30° intervals where 0° (x-axis) corresponds to direction of shearing parallel to the asperities.

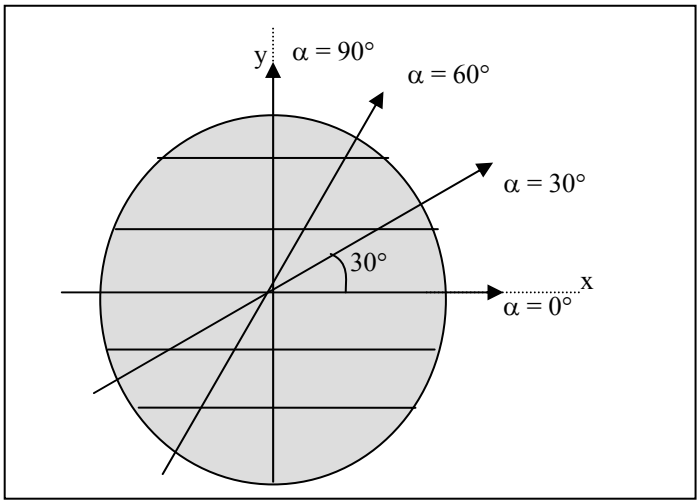

Figure 4.8 Definition of shearing direction, α, represented on the lower joint surface

Three groups were formed for both type of joint (5 sample in each group) according to shearing directions 90°, 60°, 30°. Since it can be assumed that there is no effect of roughness for direction 0°, only one sample of Type1 joint was tested for comparison. Distribution of samples with different shear direction is shown in Table 4.3.

Table 4.3 Distribution of samples

Joint type	Direction of shearing, α	No. of samples
Type1	90 °	5
	60 °	5
	30 °	5
	0 °	1
Type2	90 °	5
	60 °	5
	30 °	5

Within a particular joint type and shearing direction, each of the five sample was sheared at a different constant normal load. This means the shear response of a joint for each normal load level, but having same surface geometry and sheared in the same direction, could have obtained in separate tests.

However, each sample was also further subjected to shearing cycles at different loads where the same sample was returned to its initial position at the end of each run. On the other hand, normal stress applied during the first run (cycle) of shear test σ_n* was kept different among the five samples as mentioned. Other normal stresses in subsequent cycles were applied in an incremental order.

Ratio of the initial normal stress to compressive strength of joint sample, σ_n / σ_c ranges between 0.015 and 0.1. Despite low ranges of σ_n / σ_c values, the results where only the first run of shear tests taken into consideration were interpreted separately. Since a fresh joint sample was used in the first run, the possible effect of wearing or degradation of joint surface was excluded.

4.7 Shear test results

Results of shear tests of smooth, flat joints and Type1, Type2 are presented in graphical form. Typical curves obtained from the direct shear test results are;

- Shear stress vs. shear displacement (τ-u) curves
- Normal displacement vs. shear displacement (v-u) curves

In normal displacement response, dilation of joint is reckoned positive.

4.7.1 Shear test results of smooth, flat joints

The shear tests of this type of joint was conducted to determine the basic friction angle of the model material from which the joint samples were prepared. Totally, four samples are prepared and tested. Figure 4.9 presents a typical result of direct shear test on smooth-flat joint in terms of shear stress vs. shear displacement (τ-u) and normal displacement vs. shear displacement (v-u) response at five different constant normal loads. Test results of three other samples are given from Figure A.1 to Figure A.6 in terms of τ-u and v-u curves in Appendix A.1.

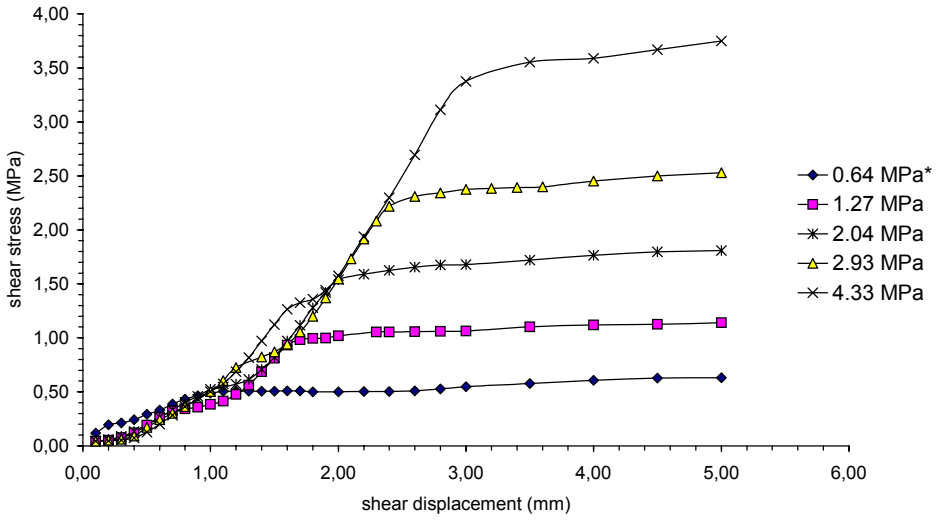

(a)

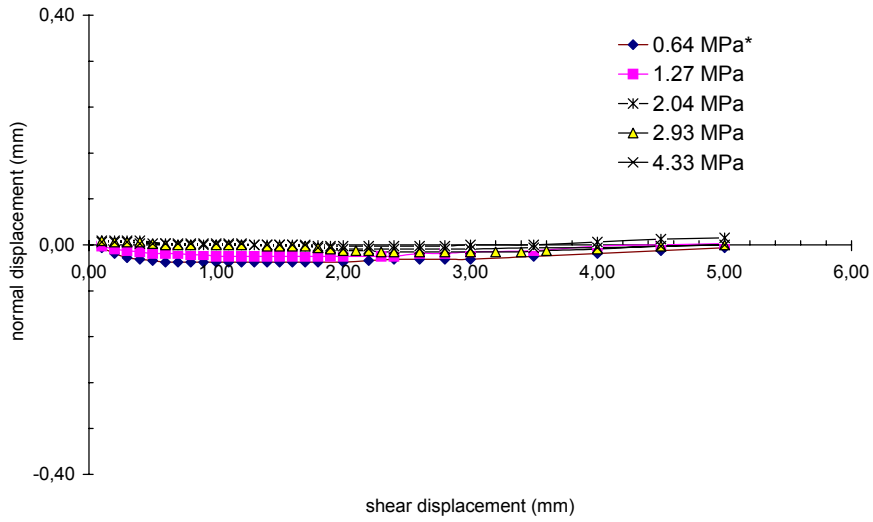

(b)

Figure 4.9 (a) Shear stress vs. shear displacement curves (b) Normal displacement vs. shear displacement curves, of a flat joint (Flat-4) at different normal stress levels applied sequentially in a series of shear tests where the sample was returned to its initial position at the end of each run

*original normal stress in the first run

4.7.2 Shear test results of rough joints

Shear test result of a Type1 joint sheared in the direction 0° is shown in Figure 4.10. The curves in Figure 4.10 (b) do not show any variation in normal displacement except the test at σ_n= 4.33 MPa that demonstrates an increase about 0.1mm in normal displacement which could also assumed to be insignificant.

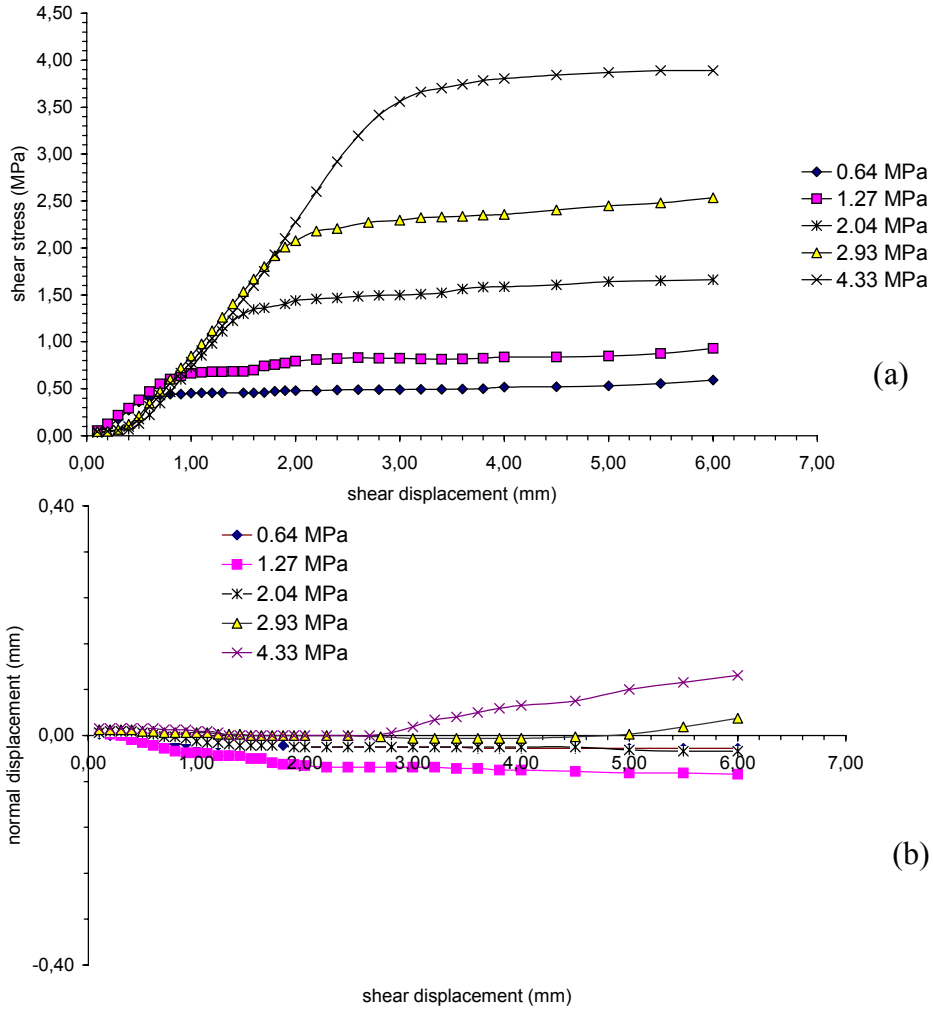

Figure 4.10 (a) Shear stress vs. shear displacement curves and (b) normal displacement vs. shear displacement curves, of Type1 joint sheared in $\alpha = 0°$ and at different normal stress levels applied sequentially in a series of shear tests where the sample was returned to its initial position at the end of each run (Sample N-1)

Shear test results of Type1 joints sheared in the direction 90° are shown in Figure 4.11.

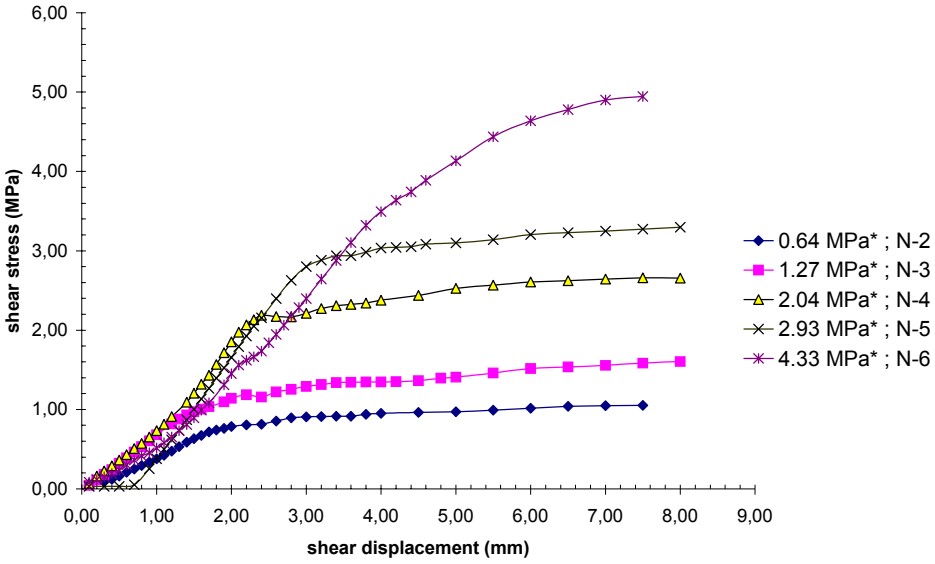

(a)

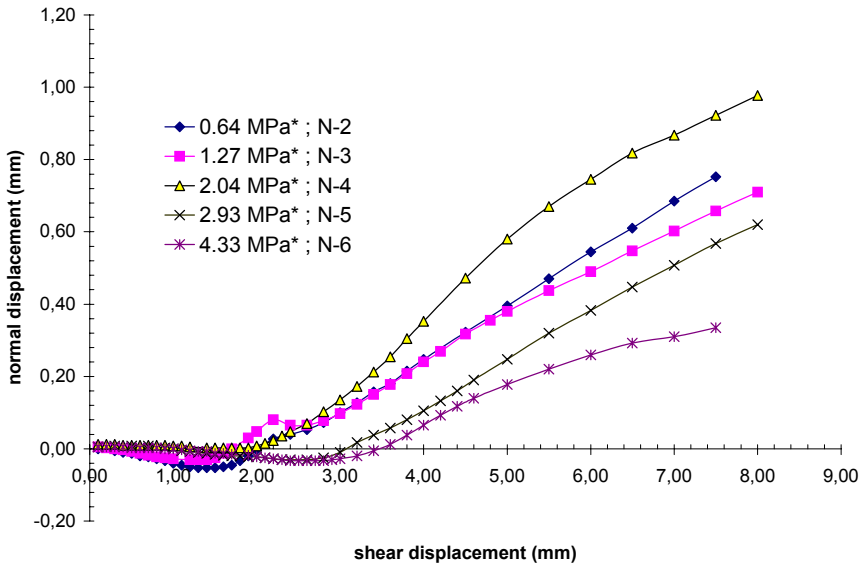

(b)

Figure 4.11 (a) Shear stress vs. shear displacement curves (b) Normal displacement vs. shear displacement curves, of Type1 joints sheared in $\alpha = 90°$

*original normal stress in the first run ; N is the sample number

Shear test results of Type1 joints sheared in the direction 60° are shown in Figure 4.12.

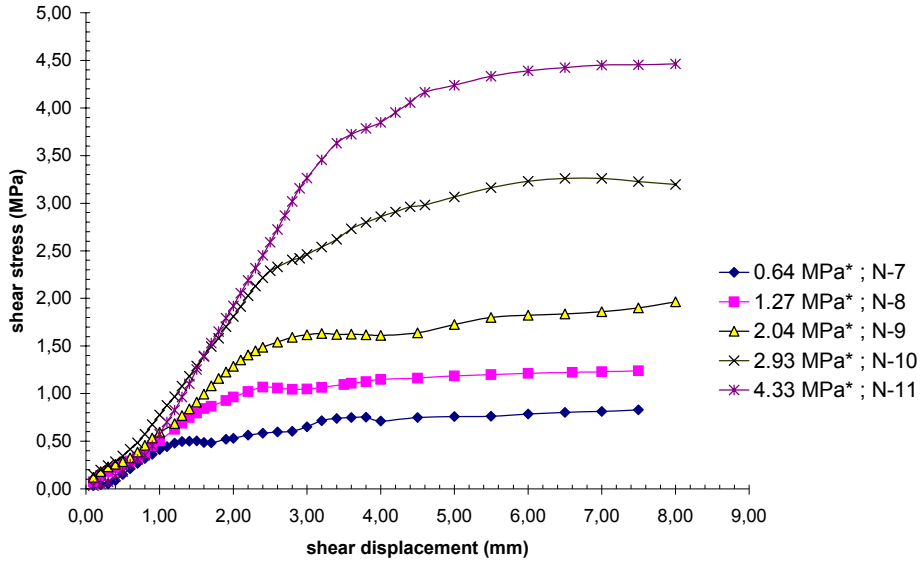

(a)

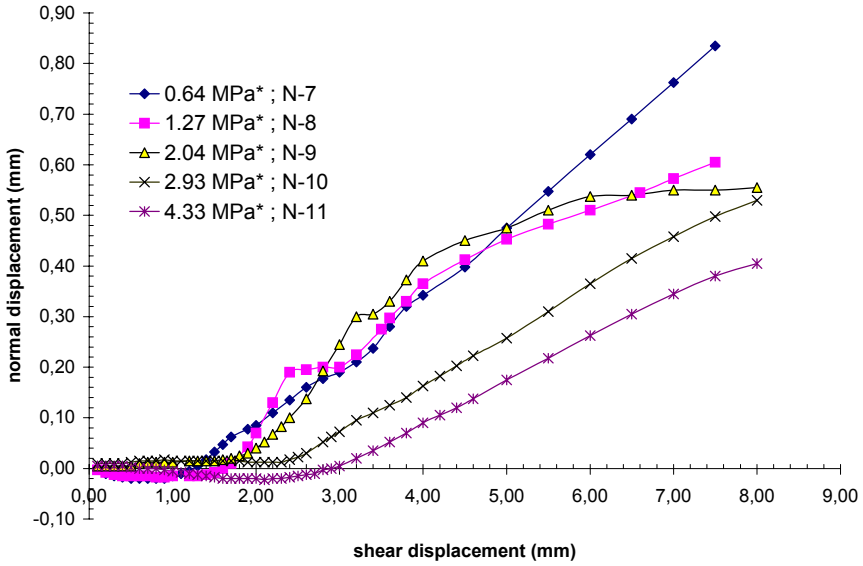

(b)

Figure 4.12 (a) Shear stress vs. shear displacement curves (b) Normal displacement vs. shear displacement curves, of Type1 joints sheared in $\alpha = 60°$

*original normal stress in the first run ; N = sample number

Shear test results of Type1 joints sheared in the direction 30° are shown in Figure 4.13.

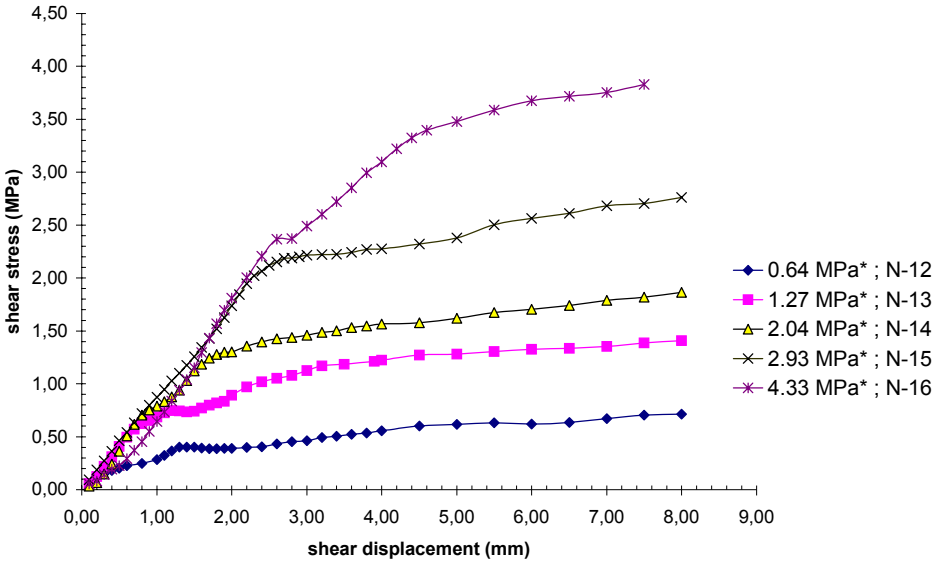

(a)

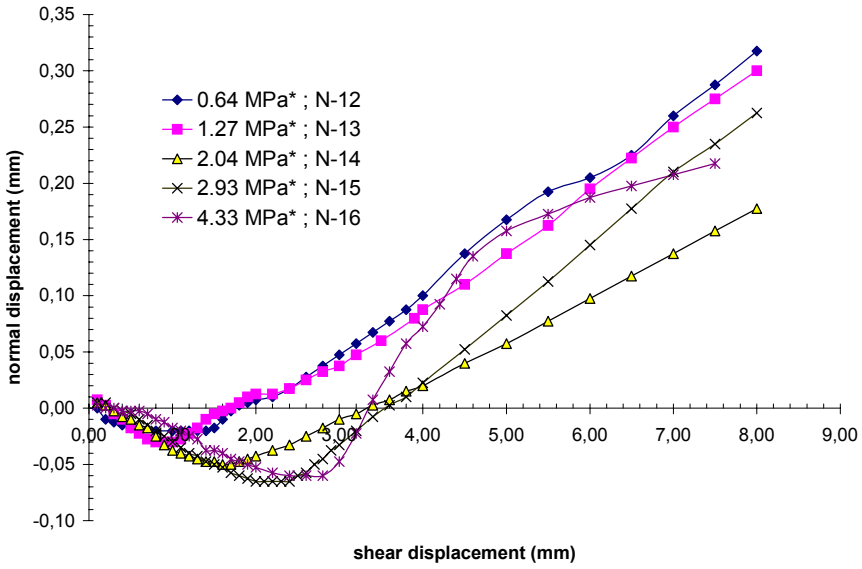

(b)

Figure 4.13 (a) Shear stress vs. shear displacement curves (b) Normal displacement vs. shear displacement curves, of Type1 joints sheared in $\alpha = 30°$

*original normal stress in the first run ; N = sample number

Shear test results of Type2 joints sheared in the direction 90° are shown in Figure 4.14.

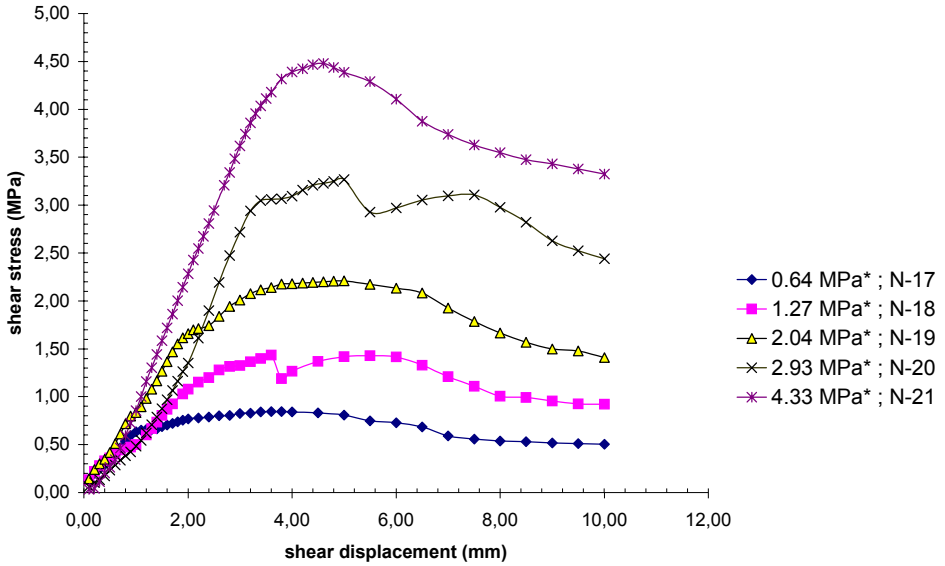

(a)

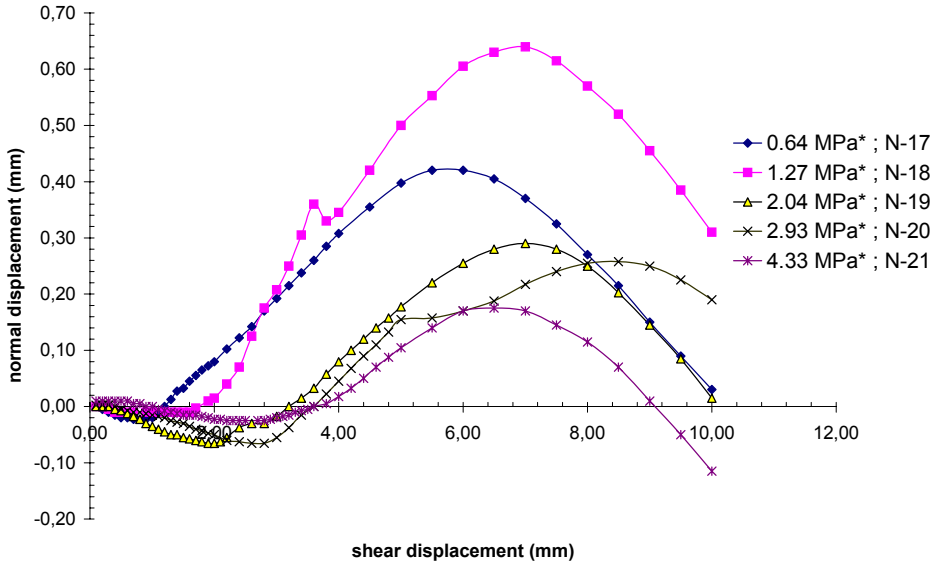

(b)

Figure 4.14 (a) Shear stress vs. shear displacement curves (b) Normal displacement vs. shear displacement curves, of Type2 joints sheared in $\alpha = 90°$

*original normal stress in the first run ; N = sample number

Shear test results of Type2 joints sheared in the direction 60° are shown in Figure 4.15.

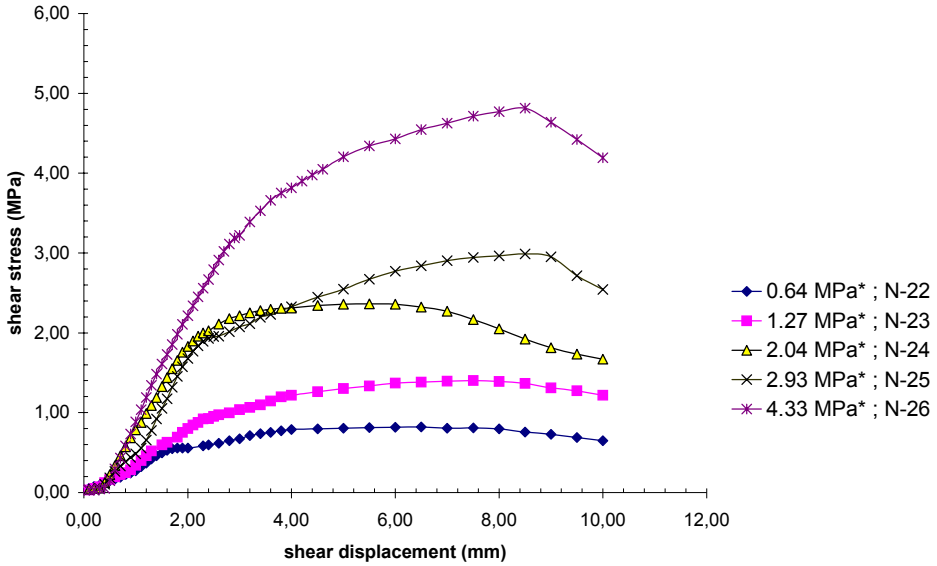

(a)

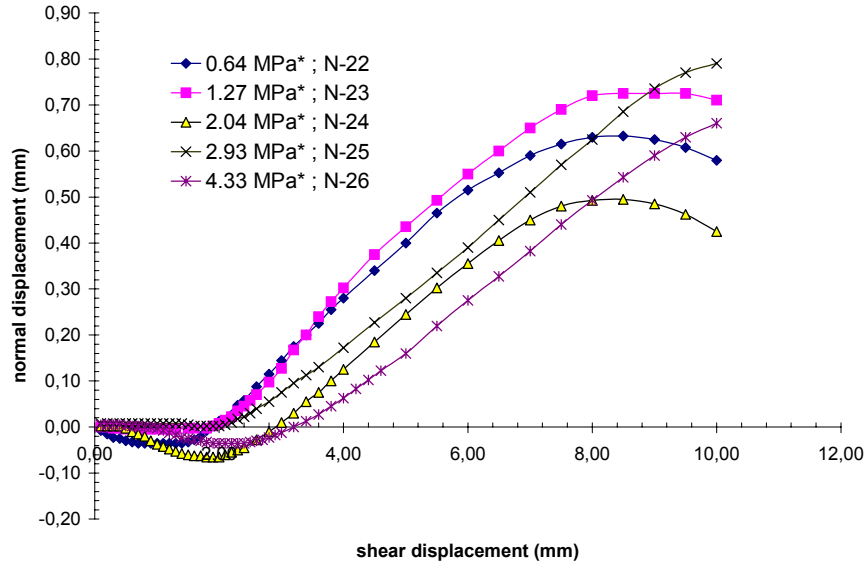

(b)

Figure 4.15 (a) Shear stress vs. shear displacement curves (b) Normal displacement vs. shear displacement curves, of Type2 joints sheared in α=60°

*original normal stress in the first run ; N = sample number

Shear test results of Type2 joints sheared in the direction 30° are shown in Figure 4.16.

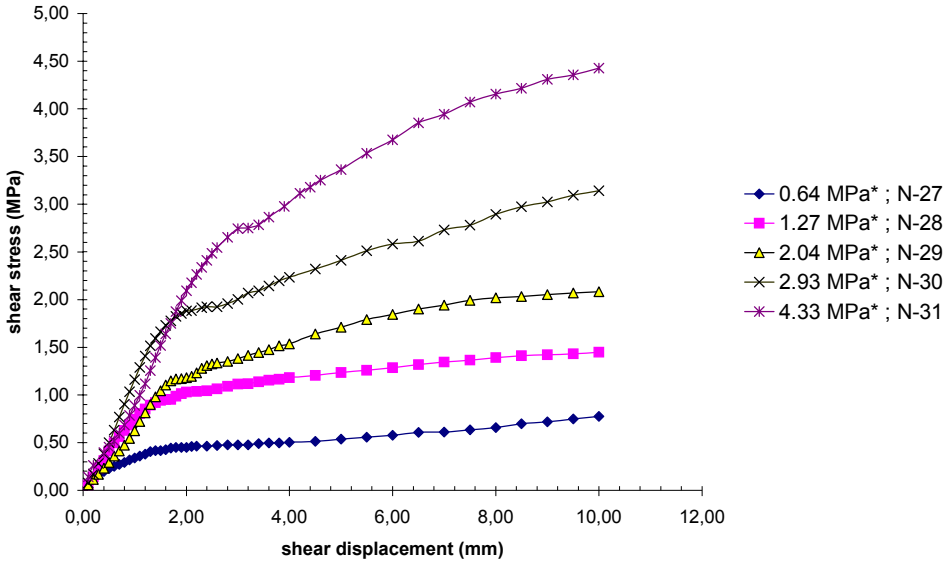

(a)

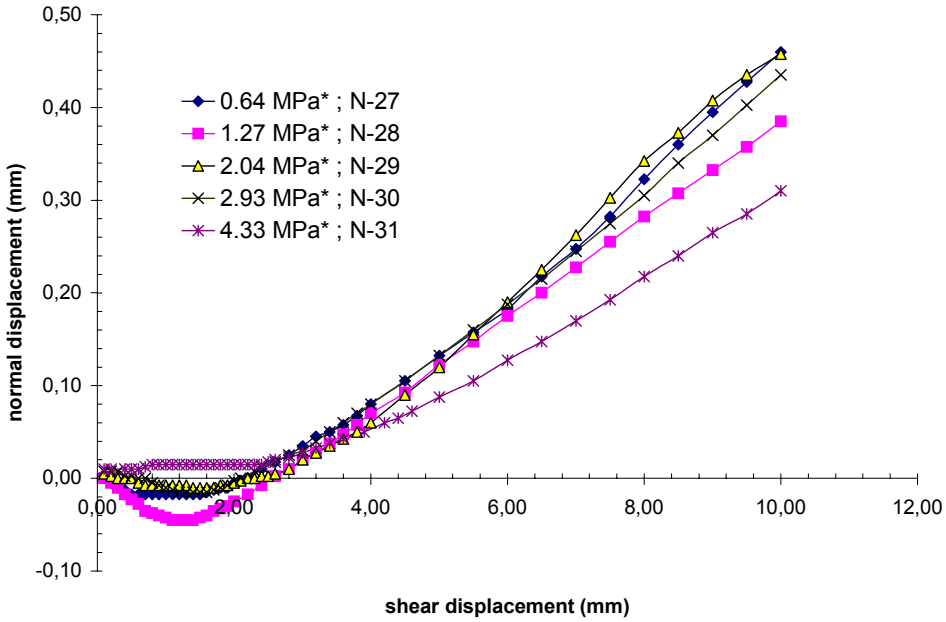

(b)

Figure 4.16 (a) Shear stress vs. shear displacement curves (b) Normal displacement vs. shear displacement curves, of Type2 joints sheared in $\alpha = 30°$

*original normal stress in the first run ; N = sample number

Shear stress vs. shear displacement and normal displacement vs. shear displacement curves for rough joints demonstrate that, peak shear stress increases as normal stress level increases, while the amount of dilation decreases with the increase of normal stress. However, it was noticed that some samples does not follow the usual trend in dilation behavior. For example, in Figure 4.11(b) sample N-4, which was sheared at σ_n^*=2.04 MPa, shows a higher amount of dilation than sample N-2, which was sheared at σ_n^*=0.64 MPa. Similarly, in Figure 4.14(b) sample N-18 shows a higher amount of dilation than N-17. This is probably due to slight differences in seating position within samples which was encountered during building sample halves into the large shear box. The difficulty in satisfying the perfect seating of samples was also reported by Hutson and Dowding (1990) and defined it as index (or zero position) error. This explains to some extent the observed behavior mentioned above in Figure 4.14 (b) such that, the shift in index position causes one sample to dilate lower amount (reach the asperity peak more quickly) compared to the other sample in which there is initially no or less index error.

Except the inconsistent results in some curves, normal displacement curves generally show an expected trend demonstrating the effect of normal stress and shear direction. Also, normal displacement curves indicate that, the range of normal stress levels could be larger than the range used in these tests. Accordingly, the difference in normal displacement curves will probably be more clear.

CHAPTER 5

ANALYSIS OF TEST RESULTS

5.1 Introduction

From the results of shear tests on smooth, flat joints basic friction angle for joint samples is calculated which is later used in the interpretation of results for rough joints. Results obtained for Type1 and Type2 joints which are representative of rough joints are used to calculate peak shear strengths, friction angles, peak dilation angles and shear stiffness values for both joint type. The variation of these parameters with normal stress and shearing direction is also discussed. Results, where only the first run of shear tests taken into consideration and where shear tests continued on the same sample were analyzed separately.

5.2 Basic friction angle

Basic friction angle, ϕ_b of the model material of joints were calculated based on the shear tests on smooth, flat joint surfaces. Since ϕ_b represents the shear resistance of smooth, flat surfaces, it can be considered as material constant and can be used to compare the results obtained for rough joints. Basic friction angle is also a constant which does not depend on the shear direction.

Four flat joint samples were prepared and tested over a range of normal load. Using shear test results, shear strength versus normal stress relations (area corrected) were obtained for the four samples.

The relation between shear strength and normal stress is linear and expressed by linear envelopes passing through origin as shown in Figure 5.1.

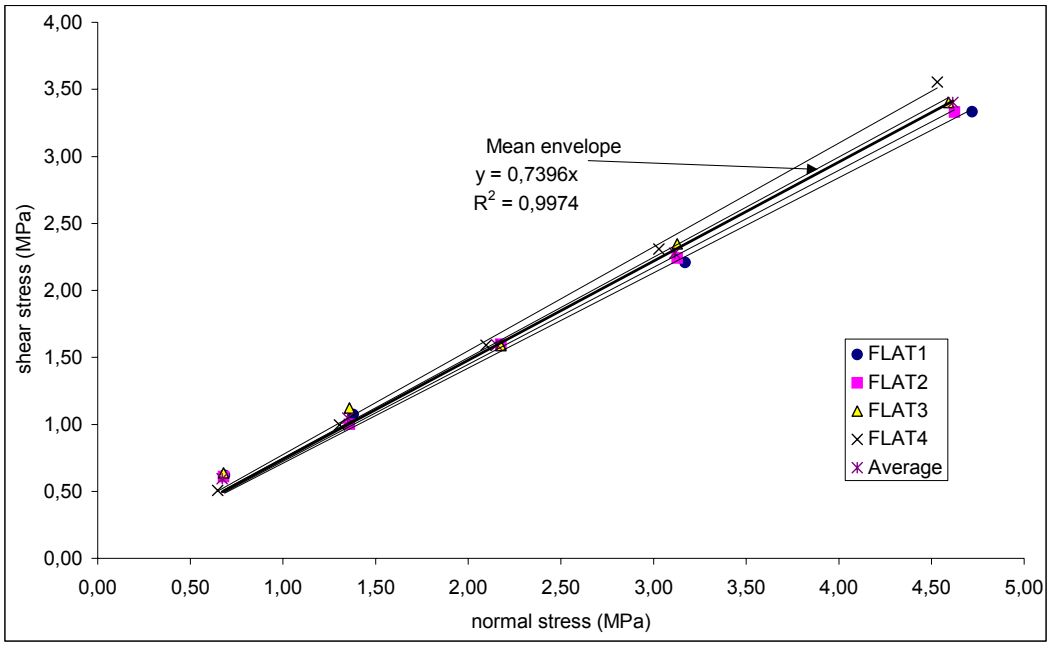

Figure 5.1 Shear strength vs. normal stress graph for flat joints

Friction angles are calculated as ;

$$\phi = \tan^{-1} \mu \qquad (5.1)$$

where;

μ is the slope of linear shear strength envelope.

Friction angles obtained for the four samples are presented in Table 5.1. Mean of the four friction angles is calculated and accepted as the basic friction angle (ϕ_b). Basic friction angle for the model material, ϕ_b is equal to 36.5°.

Table 5.1 Friction angles obtained for smooth, flat joints

Sample name	Friction angle (degree)	Mean friction angle, ϕ_b (degree)	Standard deviation
Flat-1	35.4	36.5	±1.05
Flat-2	35.9		
Flat-3	36.8		
Flat-4	37.8		

5.3 Peak shear strength of rough joints

Shear stress-shear displacement curves obtained from the direct shear tests of Type1 and Type2 joints, generally demonstrate a rise of shear stress with almost constant stiffness followed by a decrease in the rate and finally remains relatively constant with increasing shear displacement. A fall in shear stress or softening behavior, so a well-defined peak is not usually observed. Instead, some curves demonstrate a slight increase in shear stress (hardening behavior) especially the ones sheared in direction α=30°. Only those sheared in direction α=90° of Type2 joints displayed a fall in shear stress so the peak is relatively distinguishable. So that, the instant that the maximum shear stress observed is taken as the peak shear strength value and for curves which demonstrates a slight increase in shear stress, the maximum at the final displacement, is accepted as peak shear strength.

Three typical shear stress vs. shear displacement and normal displacement responses, obtained from the shear tests, are shown in Figure 5.2. The curves are divided into three segments similar to Sun et al. (1985) since the observed behavior sharing the characteristics observed by them (from shear tests on large scale natural joints).

In Segment I shear stress increase with almost constant shear stiffness in which normal displacement usually displays contraction at first followed sometimes by steady behavior (dilation doesn't occur at this stage). In some tests, the extent of initial contraction was relatively larger indicating a slight mismatch of the joint. Contrary to fully interlocked position the joint will contract first and then dilate.

The rate of increase in shear stress, reduces in segment II accompanied by the initiation of dilation of the joint i.e relative sliding along the asperity faces exists. Peak shear strength is usually attained at the end of this stage for curves displaying similar behavior to curves in Category-A and Category-C as shown in Figure 5.2.

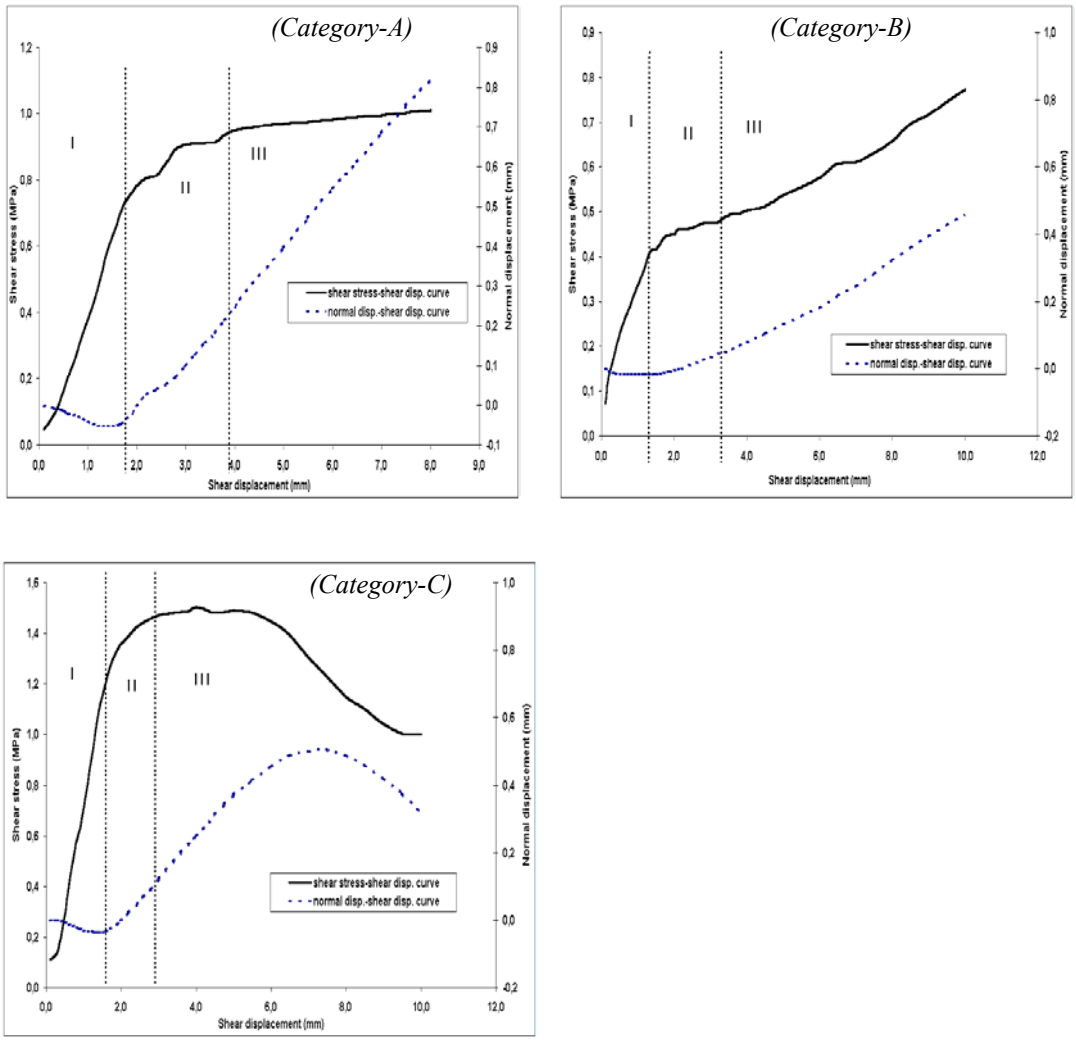

Figure 5.2 Typical shear stress vs. shear displacement and normal displacement vs. shear displacement curves (*categorized*) obtained from the shear tests divided into segments according to observed behavior

Segment III is characterized by sliding along the joint following the inclined path on asperity face. This segment forms the basic for the categorization of typical responses. The shear stress at this stage generally shows a steady state or a slight increase with minor fluctuations (Category-A) for Type1 joints sheared in α=90° as mentioned. Shear stress drop occurs for Type2 joints (Category-C), particularly in α=90°, because the shear displacement exceeds the half of the asperity base length and upper part of the joint starts to slide down-slope as shown in Figure 5.3. Category-B shear behavior was mostly displayed by joint samples, of both type, sheared in α=30° and particularly at higher normal stresses.

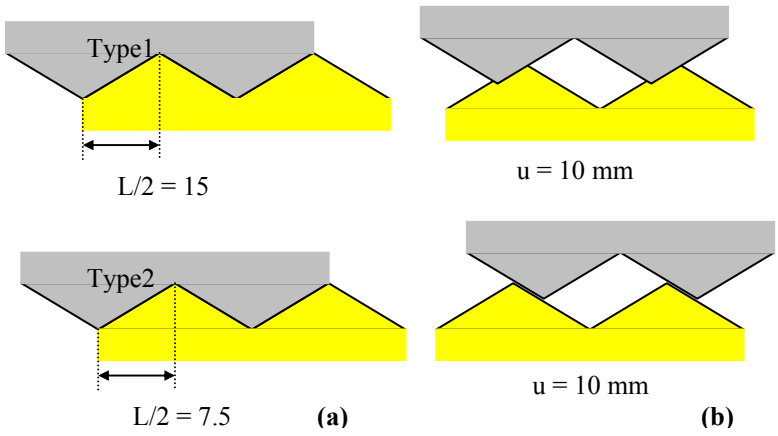

Figure 5.3 Schematic of asperity position for Type1 and Type2 joints for α=90° at (a) initial ; u = 0 and (b) final ; u = 10 mm (L = base length of asperity ; u = shear displacement)

5.3.1 Analysis of peak shear strengths obtained from the first run of shear tests only

Measured peak shear strengths from the test results at following original normal stresses and shearing directions are given in Table 5.2. Each measured data point, represents an individual sample and was obtained from the first run (1st cycle) of shear test for that sample.

Table 5.2 Peak shear strengths obtained from the first run of shear tests only

		Peak shear strengths (τ_p), MPa				
Joint type	Shearing direction, α (degree)	σ_n = 0.64 (MPa)	σ_n = 1.27 (MPa)	σ_n = 2.04 (MPa)	σ_n = 2.93 (MPa)	σ_n = 4.33 (MPa)
Type1	90	0.95	1.61	2.61	3.20	4.94
	60	0.83	1.21	1.96	3.26	4.39
	30	0.71	1.41	1.86	2.76	3.83
	0	0.49	0.83	1.50	2.33	3.66
Type2	90	0.84	1.43	2.21	3.27	4.48
	60	0.79	1.38	2.34	2.94	4.82
	30	0.77	1.41	2.02	3.14	4.43

Only one sample (N-1) of Type1 joint is tested in the 0° shearing direction for comparison since it can be assumed that there is no effect of roughness in that direction.

Using the values in Table 5.2, linear peak shear strength envelopes passing through the origin are drawn in Figure 5.4 for Type1 and in Figure 5.5 for Type2 joints. Statistically, linear envelopes fits the data with high coefficient of correlation values indicating that the relation between the shear strength and normal stress is linear within the range of normal stresses used in the tests. Shear strength envelope for flat joints, angle of which is equal to basic friction, is also plotted for comparison.

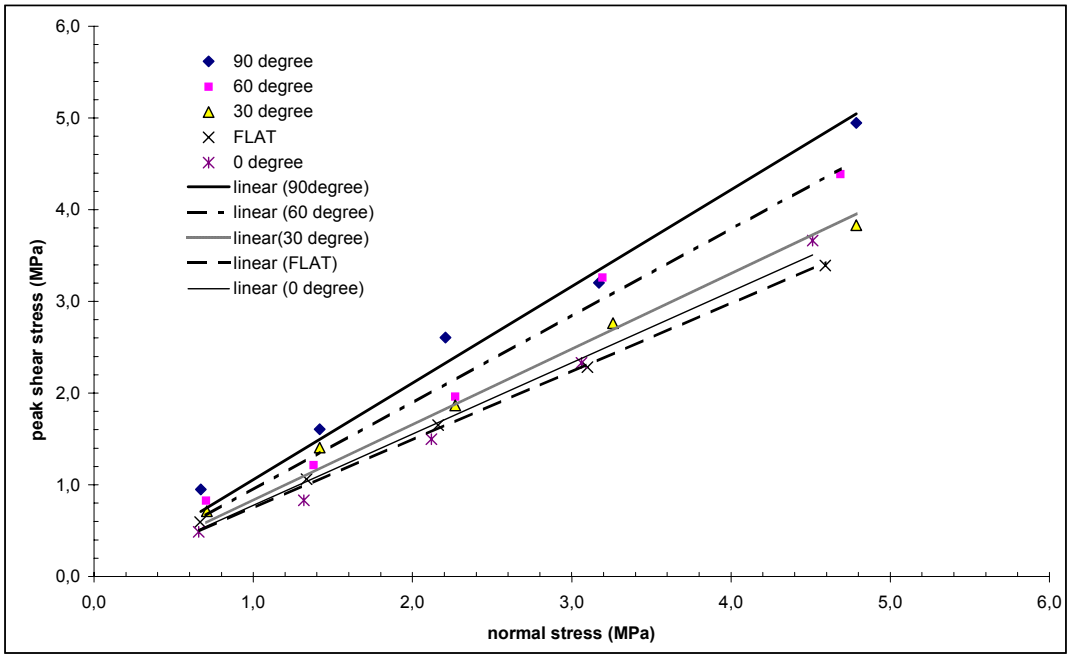

Figure 5.4 Peak shear strength lines fitted to the experimental data for Type1 joints in different shearing directions

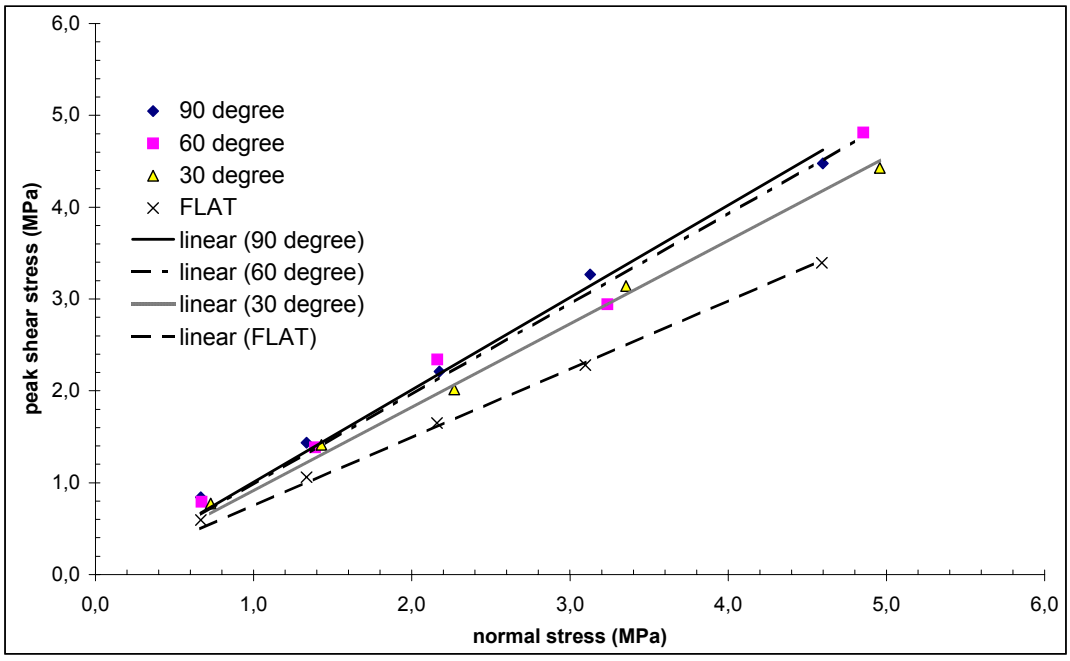

Figure 5.5 Peak shear strength lines fitted to the experimental data for Type2 joints in different shearing directions

Equations of linear shear strength envelopes and calculated friction angles (ϕ) from the first run of shear tests are given in Table 5.3. The Equation 3.2 given by Patton (1966) for prediction of peak shear strength, is also in linear form where the shear behavior is characterized by sliding.

In this equation, friction angle is composed two components which are basic friction angle and effective roughness angle. Since ϕ_b is known and equal to 36.5°, effective roughness angles are back calculated from the test results according to Equation 5.2 .

$$\phi = \phi_b + i \qquad (5.2)$$

where;
ϕ is friction angle, ϕ_b is basic friction angle and i is effective roughness angle

Table 5.3 Equations of peak shear strength envelopes and friction angles

Joint Type	Shearing direction α (degree)	Mathematical equation of shear strength envelope	Coefficient of correlation, R^2	Friction angle ϕ (degree)	Effective roughness angle, $i=\phi-\phi_b$ (degree)
Type1	90	$\tau_p = 1.0548(\sigma_n)$	0.9812	46.5	10.0
	60	$\tau_p = 0.9491(\sigma_n)$	0.9855	43.5	7.0
	30	$\tau_p = 0.827(\sigma_n)$	0.9843	39.6	3.1
	0	$\tau_p = 0.7764(\sigma_n)$	0.9868	37.8	1.3
Type2	90	$\tau_p = 1.0055(\sigma_n)$	0.9912	45.2	8.7
	60	$\tau_p = 0.9838(\sigma_n)$	0.9873	44.5	8.0
	30	$\tau_p = 0.9103(\sigma_n)$	0.995	42.3	5.8

Although there is little cohesion exists, peak shear strength lines were also expressed in terms of Coulomb parameters c and ϕ_a satisfying the linear relation with a cohesion intercept given in Equation 5.3 ;

$$\tau = c + \sigma_n \tan\phi_a \qquad (5.3)$$

where;

τ is peak shear strength, c is cohesion intercept and ϕ_a is the apparent friction angle.

Table 5.4 Equations of peak shear strength envelopes in terms of c and ϕ_a

Joint Type	Shearing direction α (degree)	Mathematical equation of shear strength envelope	Coefficient of correlation, R^2	Apparent friction angle ϕ_a (degree)	Cohesion, c (MPa)
Type1	90 60 30	$\tau_p = 0.9615(\sigma_n) + 0.31$ $\tau_p = 0.9378(\sigma_n) + 0.04$ $\tau_p = 0.7567(\sigma_n) + 0.23$	0.9937 0.9857 0.9957	43.9 43.2 37.1	0.31 0.04 0.23
Type2	90 60 30	$\tau_p = 0.9399(\sigma_n)+0.21$ $\tau_p = 0.946(\sigma_n)+0.13$ $\tau_p = 0.8696(\sigma_n)+0.14$	0.9977 0.9894 0.9979	43.2 43.4 41.0	0.21 0.13 0.14

5.3.2 Interpretation of peak shear strengths

Peak shear strength increases as normal stress increases for both type. Variation of peak shear strengths with normal stress is linear for the range of σ_n used in the tests.

Highest shear strength values were measured for those sheared in direction 90° while lowest shear strength values were measured for those sheared in direction 30° of all the Type1 joint samples. For samples sheared in direction 60°, measured shear strength values are between those sheared in direction 30° and 90°.

According to these results, we can conclude that Type1 joint samples show anisotropy on peak shear strength.

An important and well known point is that the contribution of an interlocked roughness to shear resistance of rock joints. For Type1 joints, the increment in friction angle measured perpendicular to asperity plane (α=90°) is high as 27% of the value for flat joints. On the other hand, the difference in friction angle for α=90° and α=60° is about %17 and %10 of the value for α=30° respectively. This variation in shear strength with the direction of shearing is also remarkable at higher normal stress levels, which means the asperities are still intact at this level and creates directional variation in shear strength.

The degree of anisotropy for Type2 joints is not strong as it is for Type1 joints. The friction angle difference for α=90° and α=60° is about %7 and %5 of the value for α=30° respectively. The reason for this can be related with the total shear displacement. As shown previously in Figure 5.3, the upper part asperity pass the tip of the lower asperity and caused the lower asperity tip to fail. This behavior was probably narrowed the extent of anisotropy.

It can be noticed that, effective roughness angles (i values) back calculated from the measured friction angles in α=90° during the tests are higher than the original asperity inclination angle (θ) in that direction which is about 7.6° for both joint types. This means that, the measured peak shear strength is higher than the peak shear strength predicted by Equation 3.2. On the other hand, the i value measured for α=0° is 1.3° which should be zero since the effect of roughness at this direction is absent (that is parallel to roughness features) and indicates some difference.

In order to analyze the physical appearance of the joint surfaces, photographs of the samples were taken after shear tests.

Unfortunately breaking of the lower halves at the edges was common for all samples. This was due to stress concentration at the edges as the shearing progress. An example for two lower halves after shear test is shown in Figure 5.6.

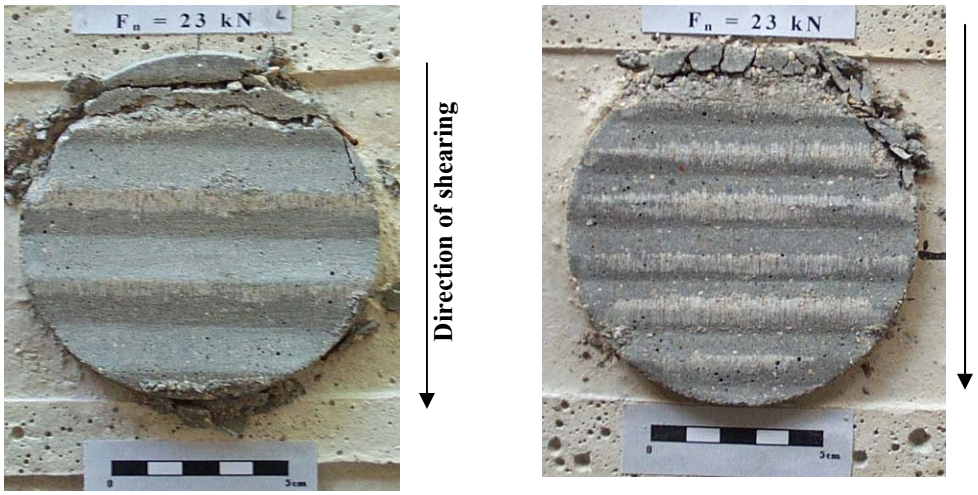

Figure 5.6 Photograph of lower halves for two different type of sample after shear test at F_n=23 kN where the failure at the edges of samples was common

Another example is given in Figure 5.7 which shows the side view of a lower half joint sample after shear test conducted at normal load equal to 5 kN. Failure of sample edge occurred also at that normal load.

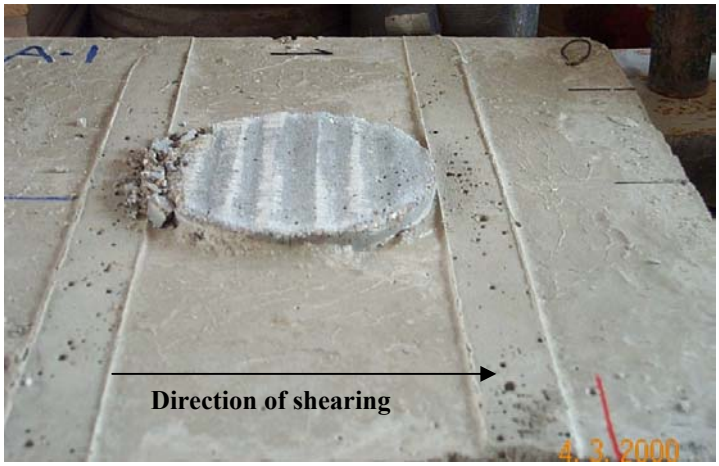

Figure 5.7 Side view of a lower half sample after shear test at 5 kN, fail of the edge also occurred at that normal load level

Failure of the sample edges was absent for upper halves. Photographs showing the appearance of Type1 joint samples after shear tests at different normal loads and shearing directions are given in Figure 5.8, 5.9, 5.10 for α=90°, α=60°, α=30° respectively and appearance of Type2 joint samples are shown in Figure 5.11, 5.12, 5.13 for α=90°, α=60°, α=30° respectively. The scratched areas demonstrates the traces of sliding surfaces at contact. From these figures, it can generally be deduced that the contact area is increasing as the normal load increases whatever is the shearing direction. Approximately, contact area changes within %30 to %40 of the whole sample surface. On the other hand, change in contact area doesn't seem to depend on shear direction. Figures from 5.8 to 5.10 demonstrate that, there isn't any asperity failure at the end of shearing for Type1 joints whereas Figure 5.11 and 5.12 demonstrate degradation of asperity due to failure at asperity tips for Type2 joints particularly at α=90° and α=60°.

σ_n = 0.64 MPa, sample N-2

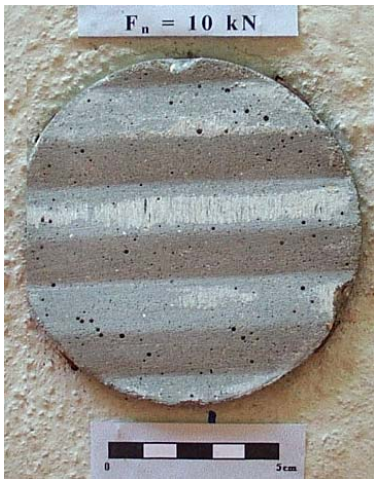

σ_n = 1.27 MPa, sample N-3

σ_n = 2.04 MPa, sample N-4

σ_n = 2.93 MPa, sample N-5

σ_n = 4.33 MPa, sample N-6

Figure 5.8 Appearance of Type1 joint samples after shearing at α=90°

σ_n = 0.64 MPa, sample N-7

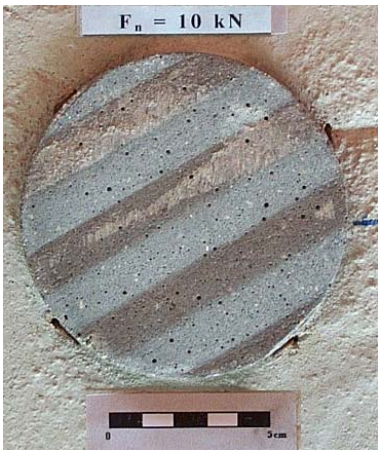

σ_n = 1.27 MPa, sample N-8

σ_n = 2.04 MPa, sample N-9

σ_n = 2.93 MPa, sample N-10

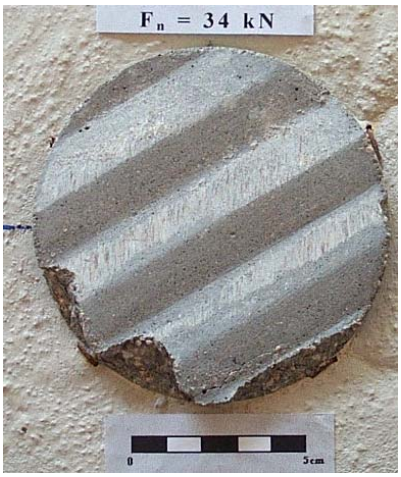

σ_n = 4.33 MPa, sample N-11

Figure 5.9 Appearance of Type1 joint samples after shearing at α=60°

σ_n = 0.64 MPa, sample N-12

σ_n = 1.27 MPa, sample N-13

σ_n = 2.04 MPa, sample N-14

σ_n = 2.93 MPa, sample N-15

σ_n = 4.33 MPa, sample N-16

Figure 5.10 Appearance of Type1 joint samples after shearing at α=30°

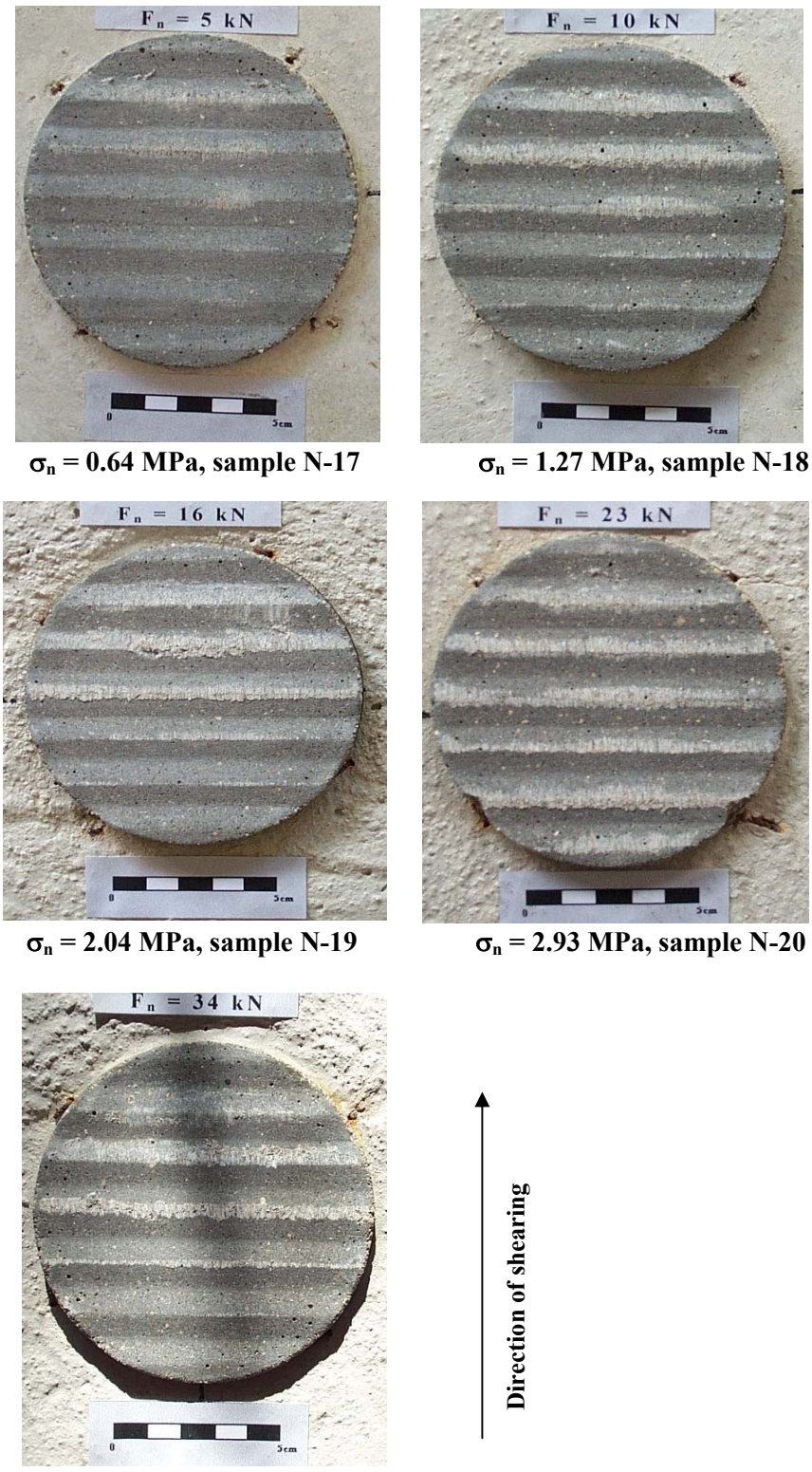

Figure 5.11 Appearance of Type2 joint samples after shearing at α=90°

σ_n = 0.64 MPa, sample N-22

σ_n = 1.27 MPa, sample N-23

σ_n = 2.04 MPa, sample N-24

σ_n = 2.93 MPa, sample N-25

σ_n = 4.33 MPa, sample N-26

Figure 5.12 Appearance of Type2 joint samples after shearing at α=60°

σ_n = 0.64 MPa, sample N-27

σ_n = 1.27 MPa, sample N-28

σ_n = 2.04 MPa, sample N-29

σ_n = 2.93 MPa, sample N-30

σ_n = 4.33 MPa, sample N-31

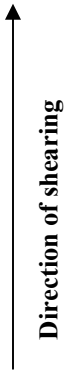

Figure 5.13 Appearance of Type2 joint samples after shearing at α=30°

5.3.3 Peak shear strengths including all shear cycles (at different normal loads) on the same sample

After a sample was sheared at a prescribed normal load, the shear tests were further progressed at other normal loads in an incremental way. Due to low ratio of σ_n/σ_c which ranges between 0.015 and 0.1, wearing effect was expected to be minimum. If this is the case, the results at same normal loads for different samples can be compared to check the repeatability otherwise can be used to observe the effect on the results.

All peak shear strength data was given in Table 5.5 and Table 5.6 including the ones obtained from the shear tests on the same sample. Shear stress vs. shear displacement and normal displacement vs. shear displacement curves at different normal stresses for each sample are given in Appendix A.2 and A.3.

Table 5.5 Peak shear strength, τ_p (MPa) values for Type1 joints

		Peak shear strength, τ_p (MPa)				
Joint sample Name	Shearing direction, α (degree)	σ_n = 0.64 (MPa)	σ_n = 1.27 (MPa)	σ_n = 2.04 (MPa)	σ_n = 2.93 (MPa)	σ_n = 4.33 (MPa)
N-1	0	0.49	0.83	1.50	2.33	3.66
N-2	90	0.95*	1.73	-	3.55	4.90
N-3	90	-	1.61*	-	3.32	-
N-4	90	1.06	1.79	2.61*	3.76	5.16
N-5	90	0.90	1.65	2.54	3.20*	5.09
N-6	90	0.94	1.58	2.36	3.30	4.94*
N-7	60	0.83*	1.56	2.30	3.20	4.63
N-8	60	0.77	1.21*	2.08	2.87	3.90
N-9	60	0.82	1.41	1.96*	2.93	4.05
N-10	60	0.84	1.48	2.35	3.26*	4.66
N-11	60	-	-	-	-	4.39*
N-12	30	0.71*	1.33	2.09	2.91	4.00
N-13	30	0.86	1.41*	2.13	3.04	4.55
N-14	30	0.73	1.34	1.86*	2.93	4.29
N-15	30	0.78	1.49	2.30	2.76*	4.28
N-16	30	0.74	1.37	2.12	2.96	3.83*

* indicates peak shear strength values measured in the first run of shear test for that sample where the related normal stress is initially applied

Table 5.6 Peak shear strength, τ_p (MPa) values for Type2 joints

		Peak shear strength, τ_p (MPa)				
Joint sample Name	Shearing direction, α (degree)	σ_n = 0.64 (MPa)	σ_n = 1.27 (MPa)	σ_n = 2.04 (MPa)	σ_n = 2.93 (MPa)	σ_n = 4.33 (MPa)
N-17	90	0.84*	1.50	2.36	3.28	4.45
N-18	90	0.85	1.43*	2.24	2.83	4.09
N-19	90	-	-	2.21*	-	-
N-20	90	-	-	-	3.27*	-
N-21	90	-	-	-	-	4.48*
N-22	60	0.79*	1.41	2.20	3.06	4.45
N-23	60	0.72	1.38*	1.99	2.96	4.26
N-24	60	0.89	1.54	2.34*	3.21	4.59
N-25	60	0.87	1.53	2.40	2.94*	-
N-26	60	0.90	1.51	2.25	3.15	4.82*
N-27	30	0.77*	1.39	2.32	3.33	4.84
N-28	30	0.83	1.41*	2.23	3.27	4.76
N-29	30	0.83	1.49	2.02*	3.04	4.50
N-30	30	0.82	1.49	2.31	3.14*	4.68
N-31	30	0.76	1.41	2.14	3.04	4.43*

* indicates peak shear strength values measured in the first run of shear test for that sample where the related normal stress is initially applied

5.3.4 Variation of shear strength with normal stress and shearing direction

All peak shear strength, τ_p values are plotted in graphs of Figure 5.14 and Figure 5.15 for Type1 and Type2 joints respectively. Peak shear strengths measured for samples tested in the same direction (for instance 90°) are grouped and denoted only by the shearing direction without referring the sample name. By means of that, the variation of peak shear strength with shear direction can more easily be distinguished.

Plots in Figure 5.14 demonstrate the effect of normal stress and shearing direction on peak shear strength. The anisotropy in peak shear strength can clearly be observed, since the data points for a particular direction are accumulated and are distinct from data points measured in other directions.

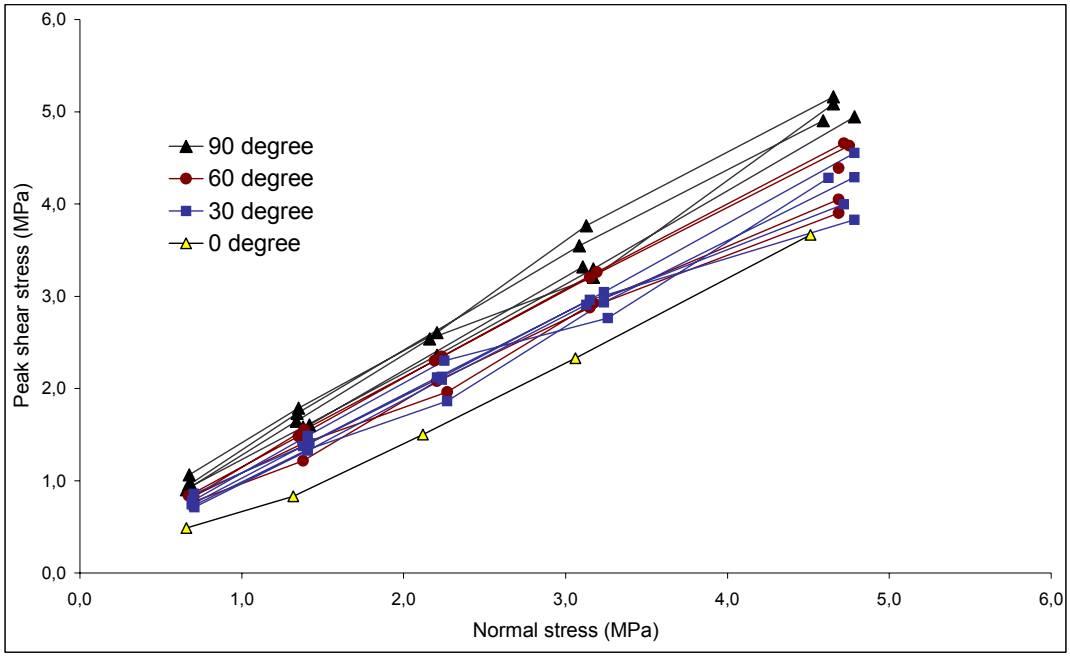

Figure 5.14 Variation of peak shear strength values for Type1 joints

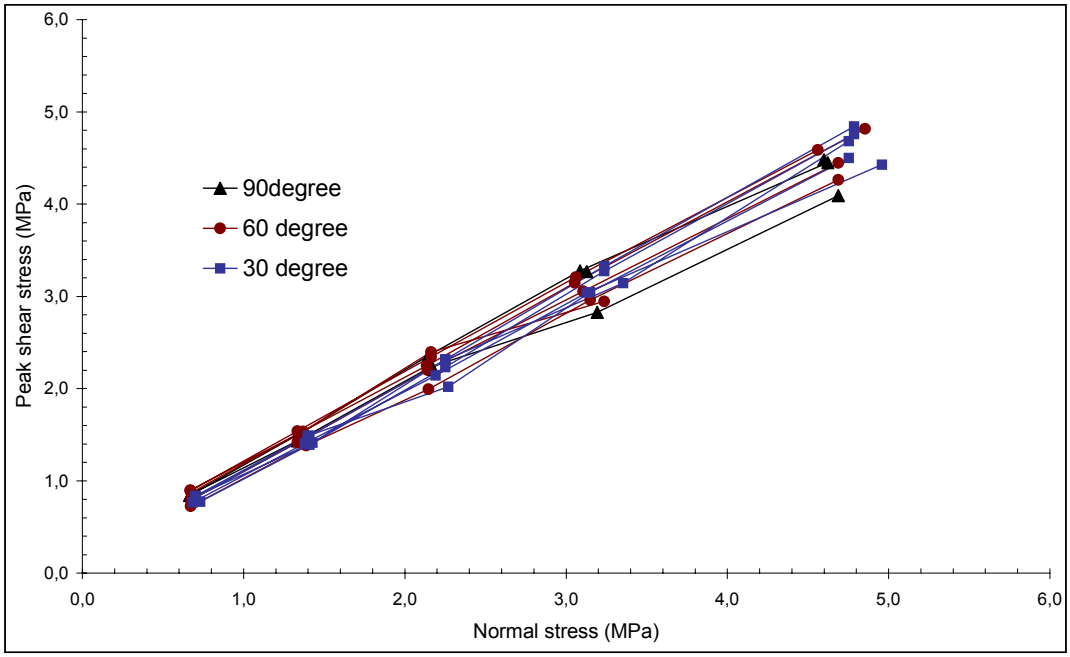

Figure 5.15 Variation of peak shear strength values for Type2 joints

On the other hand, plots in Figure 5.15 demonstrates a lower degree of anisotropy in peak shear strength which was probably due degradation of asperity especially for 90° and 60° shearing direction as it became more pronounced when the same sample further subjected to shearing at different normal load.

Mean peak shear strength envelopes are drawn using, the data obtained for a particular direction, in Figures 5.16 and 5.17 for Type1 and Type2 joints respectively. Shear strength envelope for smooth, flat joints is also drawn in order to compare with the peak shear strength envelopes for rough joints.

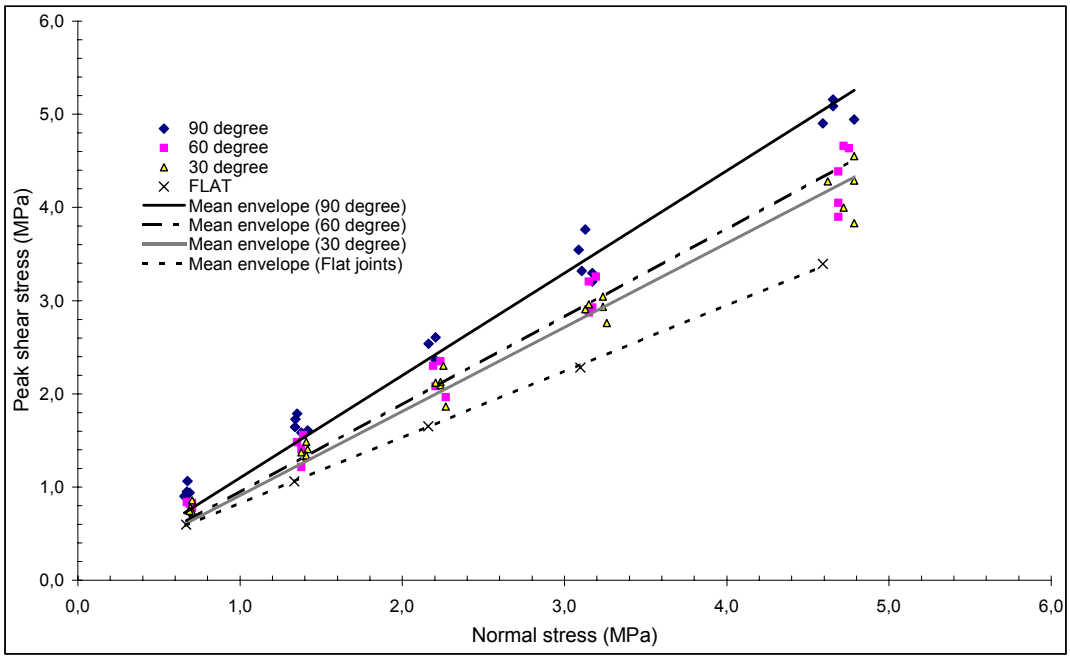

Figure 5.16 Mean peak shear strength envelopes for different shearing directions (Type1)

Equations of the mean peak shear strength envelopes with the coefficient of correlation values are given in Table 5.7. Using the equations of mean shear strength envelopes, friction angles, ϕ are calculated for each shearing direction and also effective roughness angles are back calculated according to Equation 3.2.

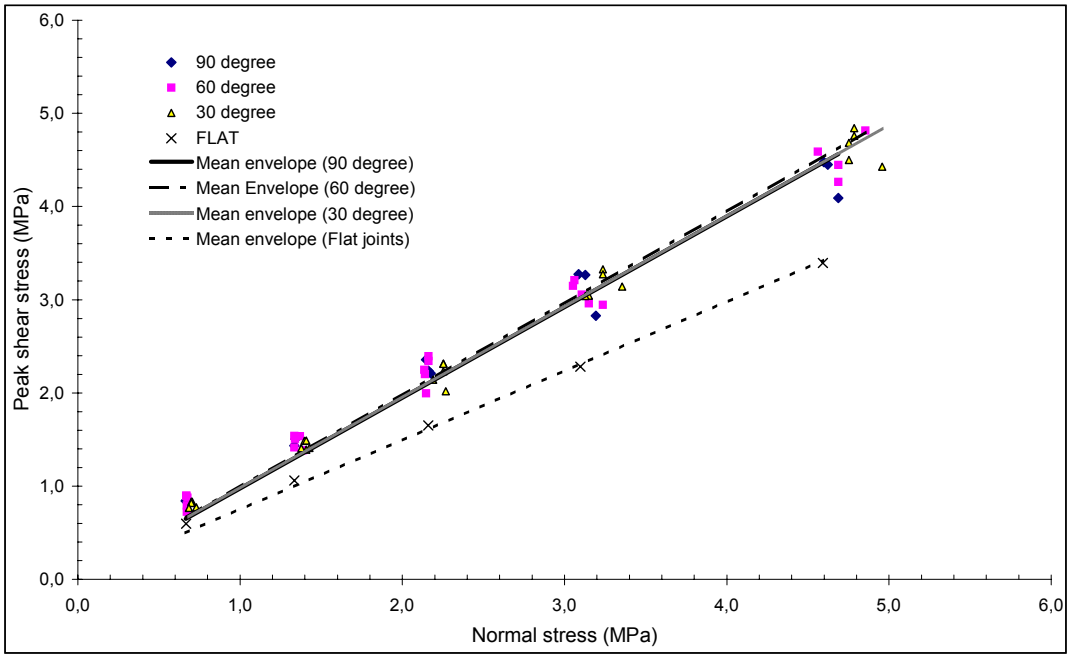

Figure 5.17 Mean peak shear strength envelopes for different shearing directions (Type2)

Table 5.7 Equations of mean peak shear strength envelopes for different shearing directions

Joint Type	Shearing direction α (degree)	Mathematical equation of shear strength envelope	Coefficient of correlation, R^2	Friction angle ϕ (degree)	Effective roughness angle, $i=\phi-\phi_b$ (degree)
Type1	90 60 30	$\tau_p = 1.0988\ (\sigma_n)$ $\tau_p = 0.944\ (\sigma_n)$ $\tau_p = 0.9052\ (\sigma_n)$	0.9798 0.9721 0.9789	47.7 43.4 42.2	11.2 6.9 5.7
Type2	90 60 30	$\tau_p = 0.9734(\sigma_n)$ $\tau_p = 0.9894(\sigma_n)$ $\tau_p = 0.9766(\sigma_n)$	0.9657 0.9795 0.9899	44.2 44.7 44.3	7.7 8.2 7.8

The difference in friction angle at α=90°and α=60° is about %13 and %3 of the value at α=30° respectively for Type1 joints. On the other hand, the difference in friction angle is totally absent for Type2 joints.

If we define mean peak shear strength envelopes in terms of Coulomb's parameters, c and ϕ_a the following results in Table 5.8 are obtained.

Table 5.8 Equations of mean peak shear strength envelopes in terms of c and ϕ_a for different shearing directions

Joint Type	Shearing direction α (degree)	Mathematical equation of shear strength envelope	Coefficient of correlation, R^2	Apparent friction angle ϕ_a (degree)	Cohesion, c (MPa)
Type1	90	$\tau_p = 1.010(\sigma_n) + 0.28$	0.99	45.3	0.28
	60	$\tau_p = 0.879(\sigma_n) + 0.22$	0.9792	41.3	0.22
	30	$\tau_p = 0.8463(\sigma_n) + 0.19$	0.9853	40.2	0.19
Type2	90	$\tau_p = 0.8758(\sigma_n) + 0.32$	0.9813	41.2	0.32
	60	$\tau_p = 0.9119(\sigma_n) + 0.24$	0.9891	42.4	0.24
	30	$\tau_p = 0.9371(\sigma_n) + 0.13$	0.9922	43.1	0.13

5.3.5 Comparison of mean shear strengths and shear strengths obtained from the first run of shear tests

Comparison can be made by considering the two observed cases. First, the original joint surfaces exhibit some slippery characteristics relative to its immediate underlying material, which occurred during curing of samples. This slippery surface was completely disappeared after first shearing run (cycle), thus caused some sort of increased friction at subsequent shearing runs. Second, when if degradation occurred after first shearing run, this became more pronounced at subsequent runs

which mainly caused the degree of anisotropy to decrease further or cause it to be diminished. The graphs given in Figure 5.18 and 5.19 demonstrates the effect of these two cases. For example in Figure 5.18, shear strength curves obtained from the first shear runs shows lower friction angles then mean shear strengths.

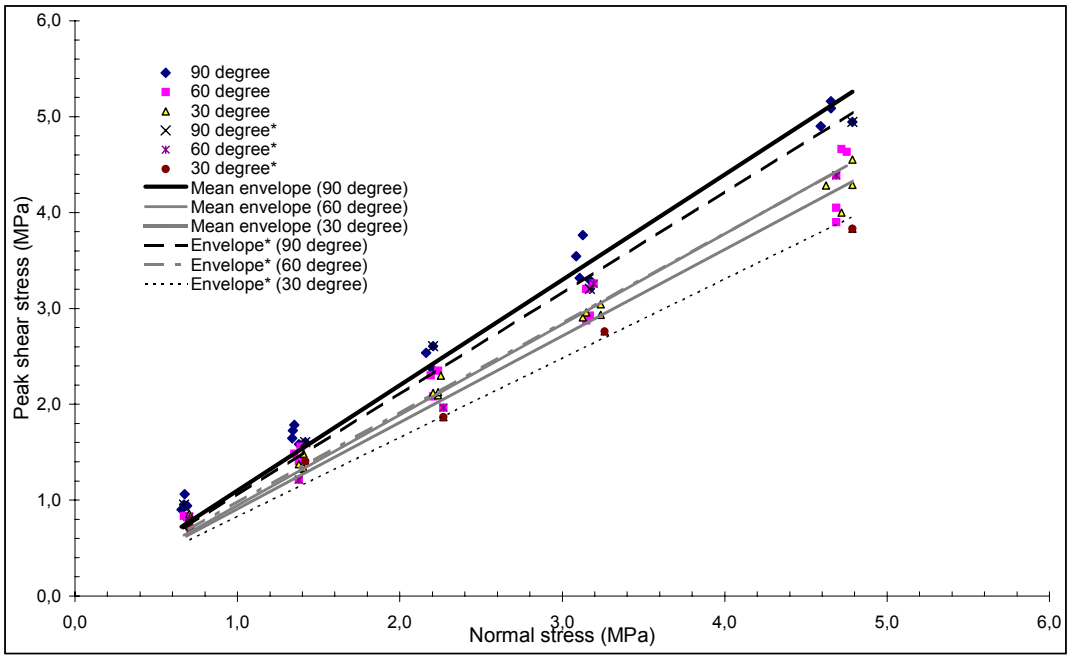

Figure 5.18 Comparison of mean shear strengths and shear strengths measured in the first run of shear tests for Type1 joints

On the other hand, any difference was not observed between the shear strength curves obtained in the first run and mean shear strength curves in Figure 5.19.

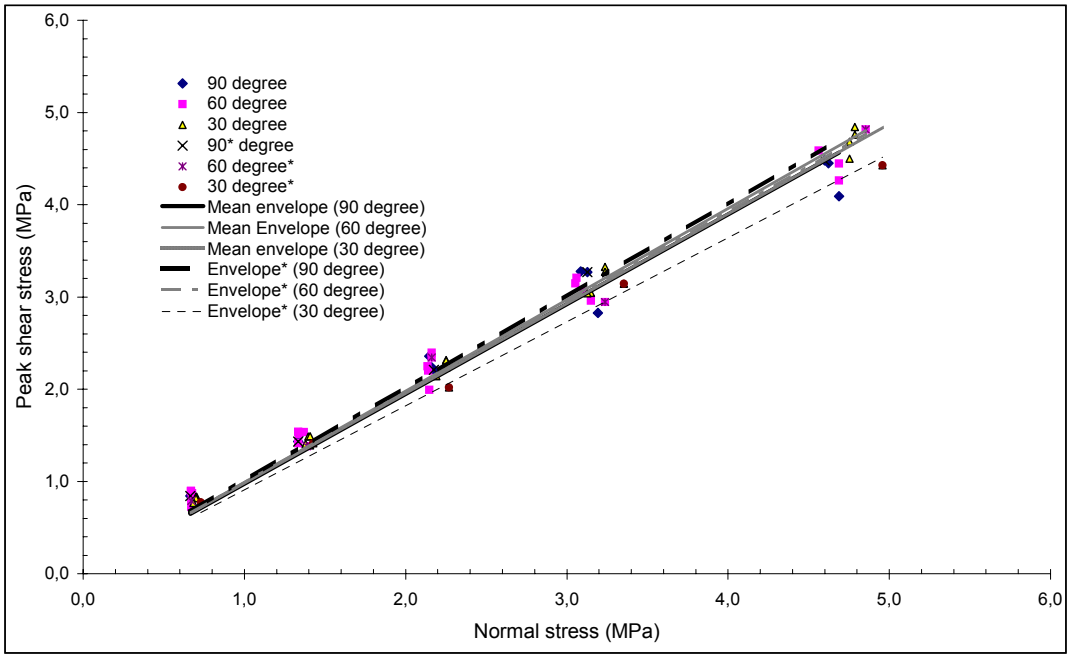

Figure 5.19 Comparison of mean shear strengths and shear strengths measured in the first run of shear tests for Type2 joints.

5.4 Shear stiffness (K_s)

Shear stiffness, K_s is taken as the slope of the tangent line at 50% of the peak shear stress (τ_p) in shear stress-displacement curve (τ-u). In most of the curves, shear stress increase with shear displacement is linear at that point. The definition of shear stiffness, K_s is shown in Figure 5.20.

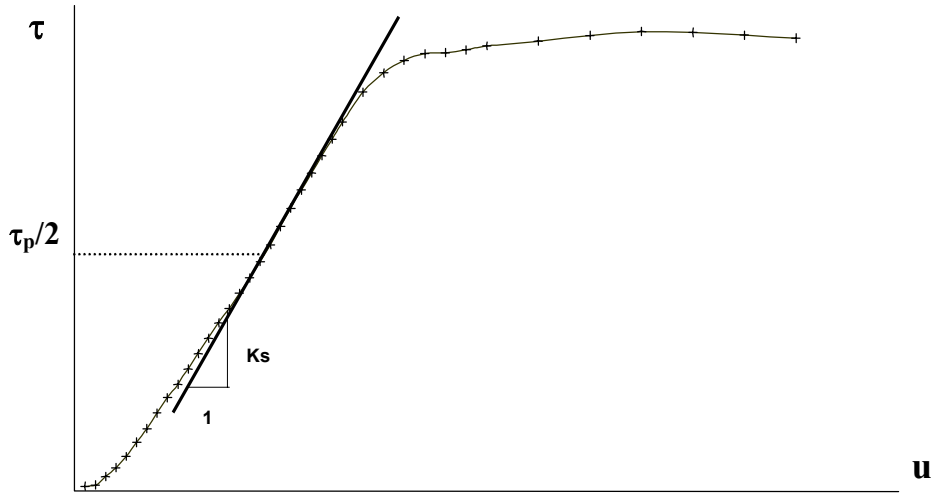

Figure 5.20 Definition of shear stiffness, K_s

5.4.1 Shear stiffness values obtained from the first run of shear tests only

Shear stiffness values, calculated as defined in Figure 5.20, at different normal stresses and shearing directions. Calculated K_s values from the first run of shear tests are given in Table 5.9 for both joint type.

Best fit envelopes drawn using the values given in Table 5.9 are shown in Figure 5.21 and Figure 5.22 for Type1 and Type2 respectively.

Table 5.9 Shear stiffness,K_s (MPa/mm) values (obtained from the first run of shear tests only)

		Shear stiffness,K_s (MPa/mm)				
Joint type	Shearing direction, α (degree)	σ_n = 0.64 (MPa)	σ_n = 1.27 (MPa)	σ_n = 2.04 (MPa)	σ_n = 2.93 (MPa)	σ_n = 4.33 (MPa)
Type1	90	0.52	0.67	1.09	1.26	1.12
	60	0.47	0.59	0.74	0.91	1.29
	30	0.40	0.37	0.52	0.82	1.16
Type2	90	0.54	0.84	1.09	1.43	1.38
	60	0.47	0.37	0.99	1.36	1.11
	30	0.20	0.59	0.82	1.11	1.04

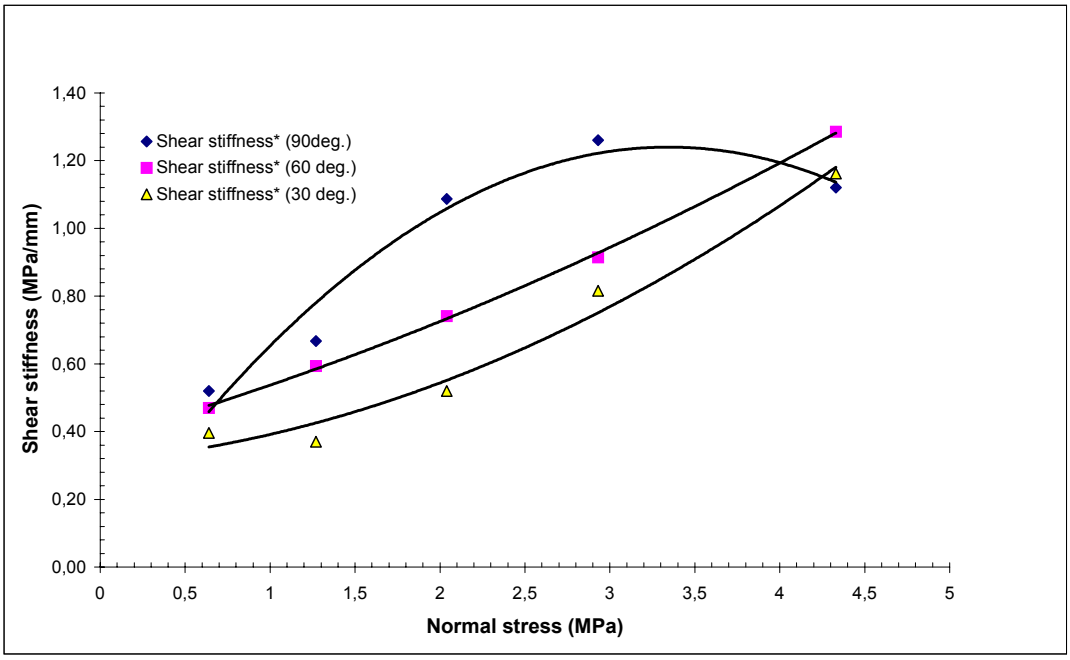

Figure 5.21 Best fit shear stiffness (K_s) envelopes for Type1 joints (obtained from the first run of shear tests)

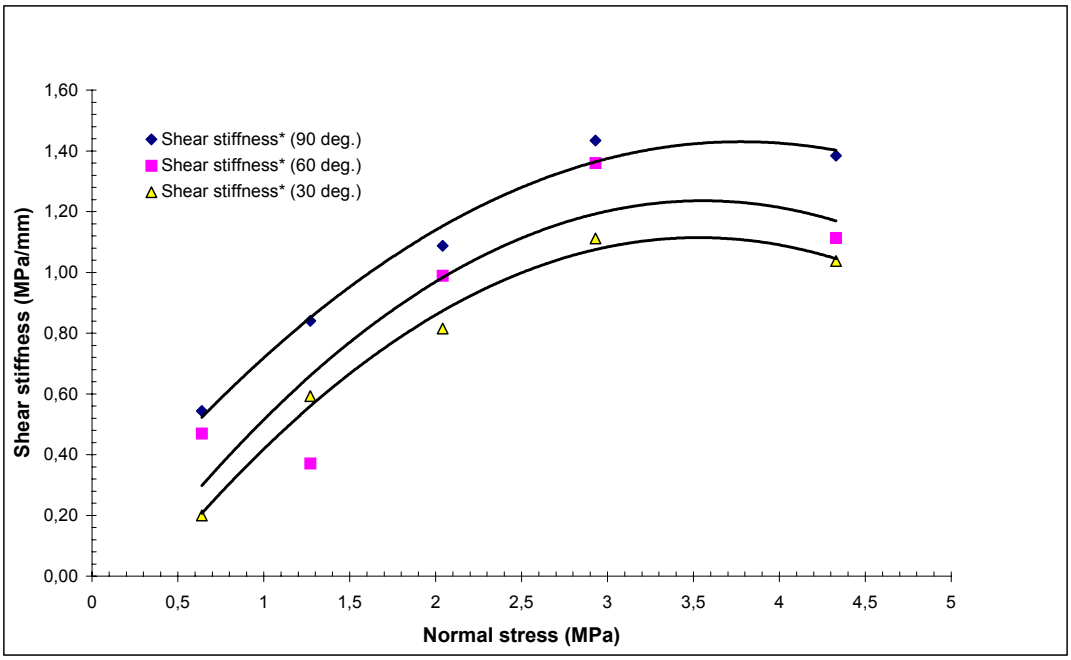

Figure 5.22 Best fit shear stiffness (K_s) envelopes for Type2 joints (obtained from the first run of shear tests)

5.4.2 Interpretation of shear stiffness results

Shear stiffness increases with the increase in normal stress in every shearing direction. Jing et. al. (1992) linked this behaviour to the increased contact area with the increasing normal stress since the degree of interlocking between two opposite joint surfaces will increase and the joint will become more stiff. Similar observation can be made in the same way that, Figures from 5.8 to 5.13 showing the appearance of joint surfaces also indicate an increased contact area with normal stress.

Generally highest shear stiffness values were calculated for α=90° and lowest for α=30°. Without being remarkable shear stiffness also varies with shear direction.

Best fit shear stiffness envelopes have curved shape and similar shaped envelopes were reported by Bandis et al. (1983) to decribe the variation of secant shear stiffness of different natural joints with normal stress.

5.5 Peak dilation angle ($d_n°$)

Peak dilation angle ($d_n°$) is taken as the angle of tangent line drawn to normal displacement (ν) vs. shear displacement curve (u) at peak shear displacement (u_p) as shown in Figure 5.23.

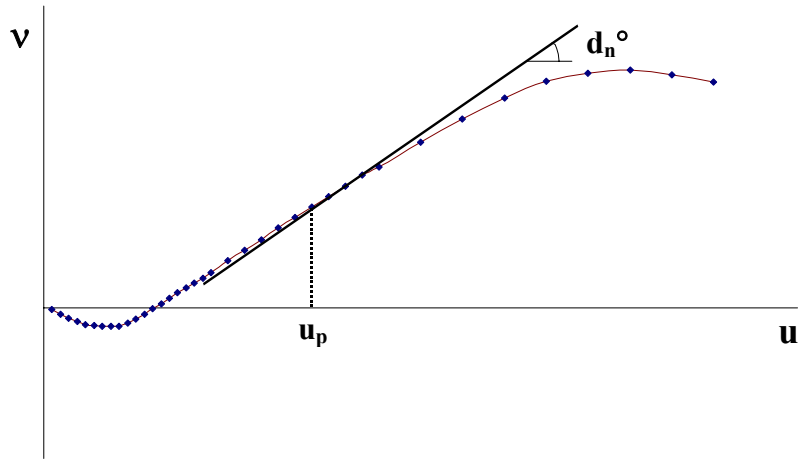

Figure 5.23 Definition of peak dilation angle, $d_n°$

5.5.1 Peak dilation angles obtained from the first run of shear tests only

Calculated $d_n°$ values from the first run of shear tests are given in Table 5.10 for both joint type. Best fit envelopes were drawn as shown in Figure 5.24 and Figure 5.25 for Type1 and Type2, respectively.

Table 5.10 Peak dilation angles, $d_n°$ (obtained from the first run of shear tests)

		Peak dilation angles, $d_n°$				
Joint type	Shearing direction, α (degree)	σ_n = 0.64 (MPa)	σ_n = 1.27 (MPa)	σ_n = 2.04 (MPa)	σ_n = 2.93 (MPa)	σ_n = 4.33 (MPa)
Type1	90	9.09	6.84	8.53	6.84	4.57
	60	7.97	3.43	3.43	5.14	5.14
	30	3.43	2.86	2.29	2.86	1.43
Type2	90	8.53	7.97	5.14	7.41	3.15
	60	6.84	5.71	6.84	6.84	5.71
	30	3.72	3.43	4.00	4.00	2.58

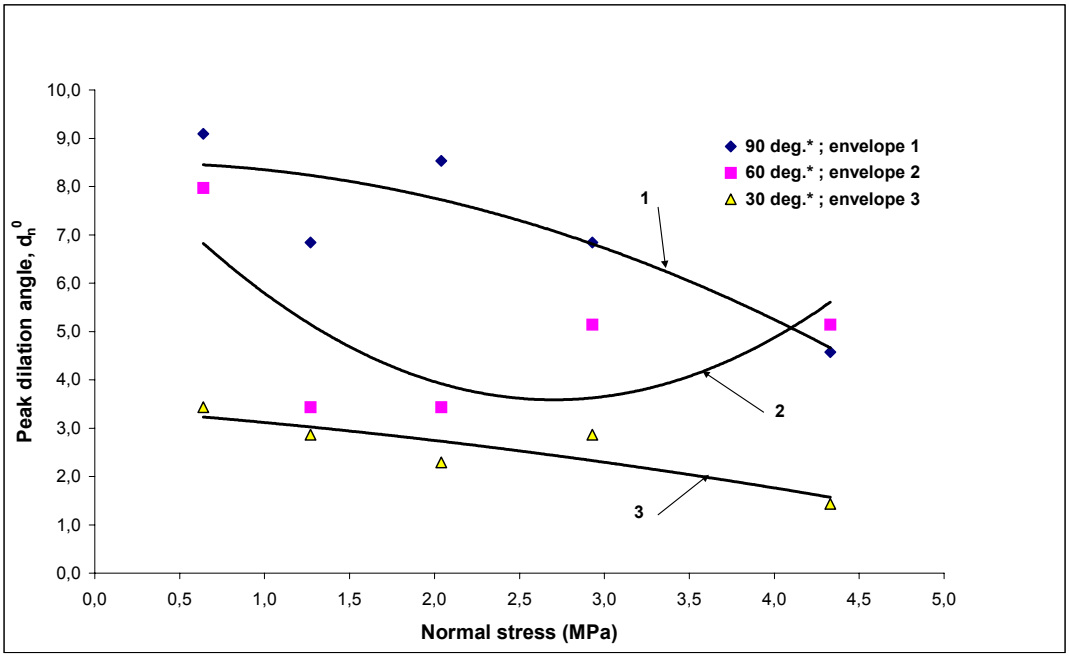

Figure 5.24 Peak dilation angle vs. normal stress (obtained from the first run of shear test) (Type1)

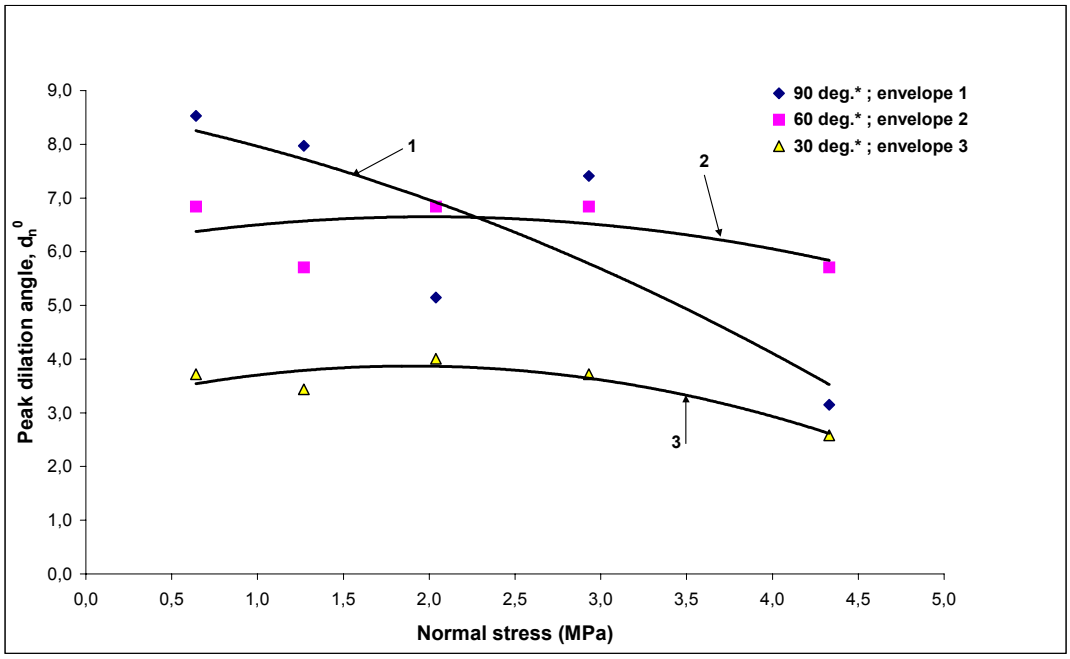

Figure 5.25 Peak dilation angle vs. normal stress (obtained from the first run of shear test) (Type2)

5.5.2 Peak dilation angles including all shear cycles

Values of $d_n°$, calculated for all shear tests including the shear cycles on the same sample, are given in Table 5.11 and Table 5.12 for Type1 and Tpye2 joints respectively.

Mean of peak dilation angles are calculated for the samples tested in the same shearing direction and normal stress level. Best fit envelopes using the mean peak dilation angles are drawn in Figure 5.26 and Figure 5.27 for Type1 and Type2 joints respectively. Best fit envelope 1 is drawn for $\alpha = 90°$, 2 for $\alpha = 60°$ and 3 for $\alpha = 30°$.

Table 5.11 Peak dilation angles for Type1 joints

		Peak dilation angles, d_n°				
Joint sample Name	Shearing direction, α (degree)	σ_n = 0.64 (MPa)	σ_n = 1.27 (MPa)	σ_n = 2.04 (MPa)	σ_n = 2.93 (MPa)	σ_n = 4.33 (MPa)
N-2	90	9.09*	7.97	-	9.65	9.65
N-3	90	-	6.84*	-	6.28	-
N-4	90	9.09	8.53	8.53*	9.09	7.97
N-5	90	7.97	7.97	7.97	6.84*	6.84
N-6	90	7.13	6.84	6.28	5.71	4.57*
N-7	60	7.97*	6.28	5.71	5.14	3.43
N-8	60	5.14	3.43*	3.43	4.57	3.43
N-9	60	4.00	4.00	3.43*	3.43	2.86
N-10	60	5.71	5.71	4.57	5.14*	4.00
N-11	60	-	-	-	-	5.14*
N-12	30	3.43*	2.86	2.86	2.29	0.57
N-13	30	3.43	2.86*	3.15	2.86	2.86
N-14	30	2.86	2.58	2.29*	2.29	2.29
N-15	30	3.72	3.43	3.43	2.86*	2.86
N-16	30	2.29	1.72	1.72	1.72	1.43*

Table 5.12 Peak dilation angles for Type2 joints

		Peak dilation angles, d_n°				
Joint sample Name	Shearing direction, α (degree)	σ_n = 0.64 (MPa)	σ_n = 1.27 (MPa)	σ_n = 2.04 (MPa)	σ_n = 2.93 (MPa)	σ_n = 4.33 (MPa)
N-17	90	8.53*	7.97	6.84	5.71	3.43
N-18	90	8.25	7.97*	6.28	5.14	2.86
N-19	90	-	-	5.14*	-	-
N-20	90	-	-	-	7.41*	-
N-21	90	-	-	-	-	3.15*
N-22	60	6.84*	6.84	5.71	4.57	3.43
N-23	60	5.14	5.71*	4.00	4.00	3.43
N-24	60	6.56	6.28	6.84*	6.28	5.14
N-25	60	6.84	7.41	6.84	6.84*	6.28
N-26	60	6.56	6.28	5.71	5.71	5.71*
N-27	30	3.72*	3.43	3.43	3.43	3.43
N-28	30	3.43	3.43*	3.43	3.43	2.86
N-29	30	3.72	3.15	4.00*	2.86	2.29
N-30	30	4.00	4.00	4.00	4.00*	4.00
N-31	30	2.86	2.86	2.86	2.86	2.58*

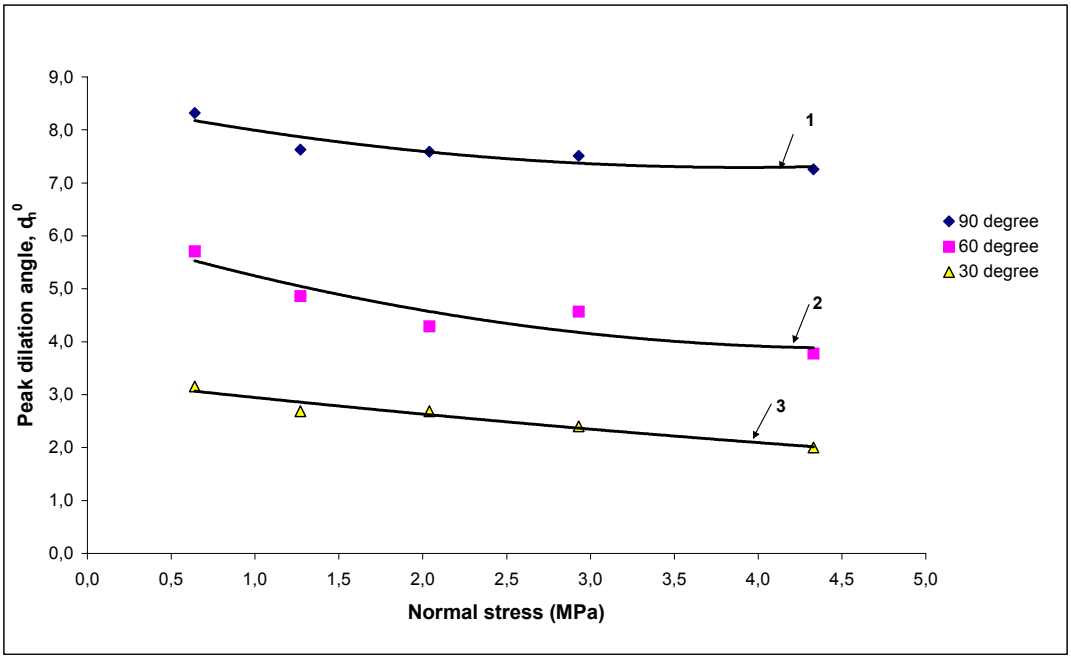

Figure 5.26 Peak dilation angle vs. normal stress (Type1)

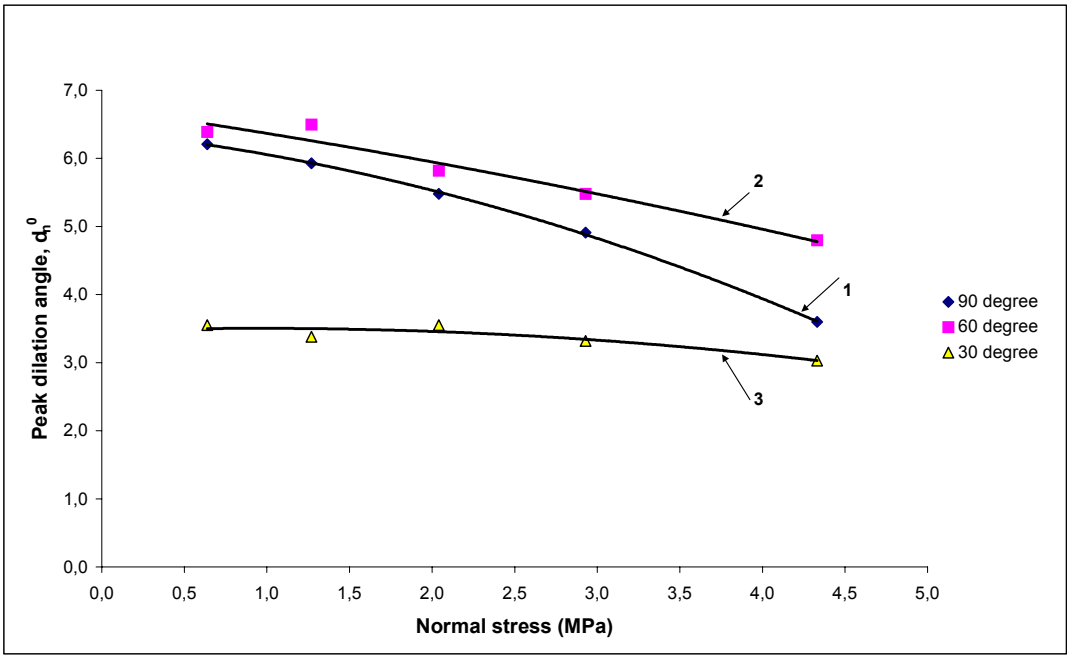

Figure 5.27 Peak dilation angle vs. normal stress (Type2)

5.5.3 Interpretation of peak dilation angles ($d_n°$)

Peak dilation angle decreses with increasing normal load for both joint type and the amount of decreament is generally lowest for α=30° and highest for α=90°.

For Type1 joints, peak dilation angles are highest for α=90° and lowest for α=30°. This is also valid at higher normal stress levels.

For Type2 joints, peak dilation angles are highest for α=90° at low normal stress levels but close to α=30° at high normal stress levels. This extensive decreament in peak dilation angle for α=90° might be responsible for relatively lower shear strengths when compared to Type1 samples in the same shearing direction.

Since dilation of joint is a result of sliding on or over-riding of asperities, decrease in dilation angle means a decrease in over-riding of asperities wheras an increment in behavior of shear-through asperities. This behavior was explained by the relation given by Barton (1973) in which friction angle (ϕ) is composed of angular components i.e $\phi = \phi_b + d_n + s_n$ where d_n is peak dilation angle and s_n is angluar component due to shearing-through asperities or failure of asperities.

Therefore, for Type2 joints, extensive decreament in d_n value particularly in 90° shearing direction is a result of failure on the asperity tips. Consequently, effect of roughness decreases and might be responsible for non-existence of anisotropy on shear strength for Type2 joints.

CHAPTER 6

CONCLUSION

Effect of roughness and anisotropy on shear strength and shear behavior was investigated using artificially prepared joint samples by conducting shear tests in different directions and normal stress levels. Most of the shear stress-displacement curves show ductile behavior in which peak shear stress is less distinguishable. Normal vs. shear displacement curves show a contraction at the beginning followed by dilation of the joint. In some tests, however, dilation starts after a relatively large shear displacement most probably due to slight mismatch in the joint.

From the experimental results following conclusions can be obtained ;

i) Shear stress vs. shear displacement and normal displacement vs. shear displacement curves display different responses with changing shearing directions which indicates anisotropic shear behavior.

ii) Peak shear strength of joints change with the shearing direction and the degree of anisotropy is significant if the asperity degradation is absent and contrarily if there is asperity degradation the anisotropy on shear strength decreases or can be completely disappeared.

iii) Effect of increasing normal stress on the degree of anisotropy of shear strength is not much at least for the range of normal stress to compressive strength ratios used in the tests.

iv) Anisotropy on shear strength, appears to be dependent also on the amount of shear displacement. For instance as the shear displacement is larger than the mean asperity length (such as in the case of Type2 joints) anisotropy may be weaker and may disappear (isotropy) at subsequent shear runs (cycles).

v) Contact area is increasing as the normal load increases and seems to depend much more on normal load rather than shearing direction.

vi) Shear stiffness increases with increasing normal stress and without being remarkable also varies with shearing direction.

vii) Peak dilation angles generally decrease with increasing normal stress. In the perpendicular direction to asperity plane the dilation angle is the highest, on the other hand the amount of decrement is also larger in the direction perpendicular to asperity compared to the other directions.

viii) Results of shear tests confirms the anisotropy on shear strength and should be taken into account particularly at low normal stress to compressive strength ratios (σ_n / σ_c).

Recommendations for future study;

i) Sample size could be larger and the upper half could be prepared smaller than the lower half in order to ensure the continued contact between the two opposite joint surfaces. Failure at the sample edges will be avoided by means of that.

ii) Dilation curves indicates that, the range of normal stress level could be larger than the range in this study in order to see the differences more clearly.

iii) Directional variation of shear strength and scale effects on anisotropy could be investigated using a model material with a proper similitude properties. The emphasis given on the variation of shear behavior of rock joints with shearing directions is less in literature and could be investigated thoroughly with the support of numerical methods.

REFERENCES

Aydan, Ö., Shimizu, Y. and Kawamoto, T., 1996. The Anisotropy of surface morphology characteristics of rock discontinuities, Rock Mech. Rock Engng, 29, pp. 47-59.

Bandis, S.C., Lumsden, A.C. and Barton, N.R., 1983. Fundamentals of rock joint deformation, Int. J. Rock Mech. Min. Sci. & Geomech. Abstr., 20, pp. 249-268.

Bandis, S.C., 1990. Mechanical properties of rock joints, Rock Joints, Balkema, Rotterdam, pp.125- 140.

Bandis, S.C.,1993. Engineering properties and characterization of rock discontinuities, Comprehensive Rock Engineering Principle Practice & Projects, 1 , pp.155-182.

Barton, N., 1973. Review of a new shear-strength criterion for rock joints, Engineering Geology, 7, pp. 287-332.

Barton, N. , 1976. The shear strength of rock and rock joints, Int. J. Rock Mech. Min. Sci. & Geomech. Abstr., 13, pp. 255-279.

Barton, N. and Choubey, V., 1977. The shear strength of rock joints in theory and practice, Rock Mechanics, 10, pp.1-54.

Barton, N. and Bandis, S.C., 1990. Review of predictive capabilities of JRC-JCS model in engineering practice, Rock Joints, , Balkema, Rotterdam, pp. 603-610.

Brown, E.T.,1981. Rock characterization testing and monitoring, ISRM suggested methods, Pergamon press, pp. 129-140.

Gentier, S., Riss, J., Archambault, R., Flamand, R. and Hopkins, D., 2000. Influence of fracture geometry on shear behavior, International Journal of Rock Mechanics and Mining Sciences, 37, pp. 161-174.

Goodman, R.E., 1976. Methods of Geological Engineering in Discontinuous Rocks, West, New York

Goodman, R.E., 1989. Introduction to Rock Mechanics, John Wiley & Sons, pp.156-170.

Grasselli, G., Wirth, J., Egger, P., 2002. Quantitative three-dimensional description of a rough surface and paraneter evolution with shearing, International Journal of Rock Mechanics and Mining Sciences, 39, pp. 789-800

Grasselli, G. and Egger, P., 2003. Constitutive law for the shear strength of rock joints based on three-dimensional surface parameters, International Journal of Rock Mechanics and Mining Sciences, 40, pp. 25-40.

Huang, T. H. and Doong, Y.S., 1990. Anisotropic shear strength of rock joints, Rock Joints, Balkema, Rotterdam, pp. 211-218.

Huang, T. H., Chang, C.S., Chao, C.Y., 2002. Experimental and mathematical modeling for fracture of rock joint with regular asperities, Engineering Fracture Mechanics, 69, pp. 1977-1996

Hutson, R.W. and Dowding, C.H., 1990. Joint asperity degradation during cyclic shear, Int. J. Rock Mech. Min. Sci. & Geomech. Abstr., 27, pp.109-119

Jing, L., Nordlund, E. and Stephansson, O., 1992. An experimental study on the anisotropy and stress-dependency of the strength and deformability of rock joints, Int. J. Rock Mech. Min. Sci. & Geomech . Abstr., 29, pp. 535-542.

Kulatilake, P.H.S.W., Shou, G., Huang, T.H. and Morgan, R.M., 1995. New peak shear-strength criterion for anisotropic rock joints, Int. J. Rock Mech. Min. Sci. & Geomech., 32, pp. 673-697.

Kulatilake, P.H.S.W., Asce, J.Um, Panda, B.B. and Nghiem, N., 1999. Development of new peak shear-strength criterion for anisotropic rock joints, Journal of Engineering Mechanics, pp. 1010-1017.

Ladanyi, B. and Archambault, G., 1970. Simulation of shear behavior of a jointed rock mass, Proc. 11th Symp. on Rock Mechanics, pp. 105-125.

Lopez, P., Riss, J., Archambault, G., 2003. An experimental method to link morphological properties of rock fracture surfaces to their mechanical proporties, International Journal of Rock Mechanics and Mining Sciences, 40, pp. 947-954.

Patton, F.D., 1966. Multiple modes of shear failure in rock, Proc. 1st Congress Int. Society of Rock Mechanics, 1966, pp. 509-513.

Plesha, M.E., 1987. Constitutive models for rock discontinuities with dilatancy and surface degradation, International Journal for Numerical and Analytical Methods in Geomechanics, 11, pp. 345-362

Riss, J., Gentier, S., Archambault, G. and Flamand, R., 1997. Sheared rock joints: Dependence of damage zones on morphological anisotropy, Int. J. Rock Mech. Min. Sci. &Geomech., 34, pp. 3-4.

Saeb, S., 1990. A variance on the Ladanyi and Archambault's shear strength criterion, Rock Joints, Balkema, Rotterdam, pp. 701-705

Saeb, S. and Amadei, B., 1992. Modelling rock joints under shear and normal loading, Int. J. Rock Mech. Min. Sci. &Geomech., 29, pp. 267-278.

Seidel, J. P. and Haberfield, C. M., 2002. Laboratory testing of concrete-rock joints in constant normal stiffness direct shear, Geotechnical Testing Journal, 25, pp. 1-14

Sun, Z., Gerrard, C. and Stephansson, O., 1985. Rock joint compliance tests for compression and shear loads, Int. J. Rock Mech. Min. Sci. &Geomech., 22, pp. 197-213

Wang, J.G., Ichikawa, Y., Leung, C.F., 2003. A constitutive model for rock interfaces and joints, International Journal of Rock Mechanics and Mining Sciences, 40, pp. 41-53

Yang, Z.Y., Di, C.C. and Yen, K.C., 2001. The effect of asperity order on the roughness of rock joints, International Journal of Rock Mechanics and Mining Sciences, 38, pp. 745-752.

Yang, Z.Y. and Chiang, D.Y., 2000. An experimental study on the progressive shear behavior of rock joints with tooth-shaped asperities, International Journal of Rock Mechanics and Mining Sciences, 37, pp. 1247-1259.

APPENDIX A

SHEAR TEST CURVES

A.1 Shear test curves of flat joints

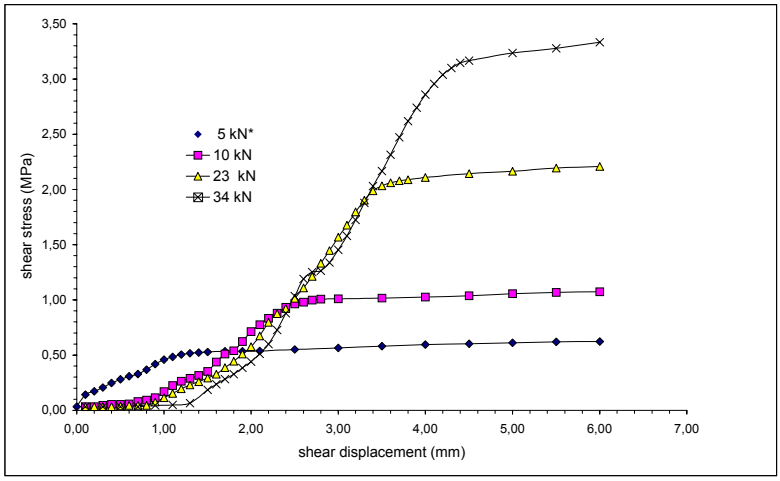

Figure A.1 Shear stress vs. shear displacement for flat joints (Flat –1)

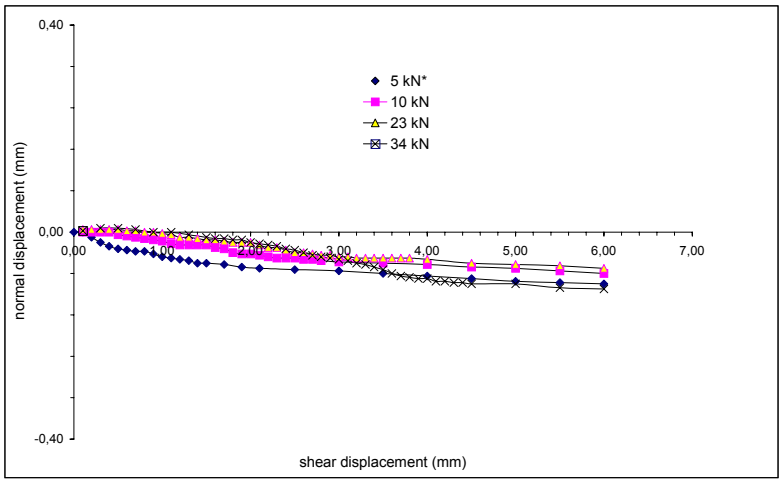

Figure A.2 Normal vs. shear displacement curves for flat joints (Flat-1)

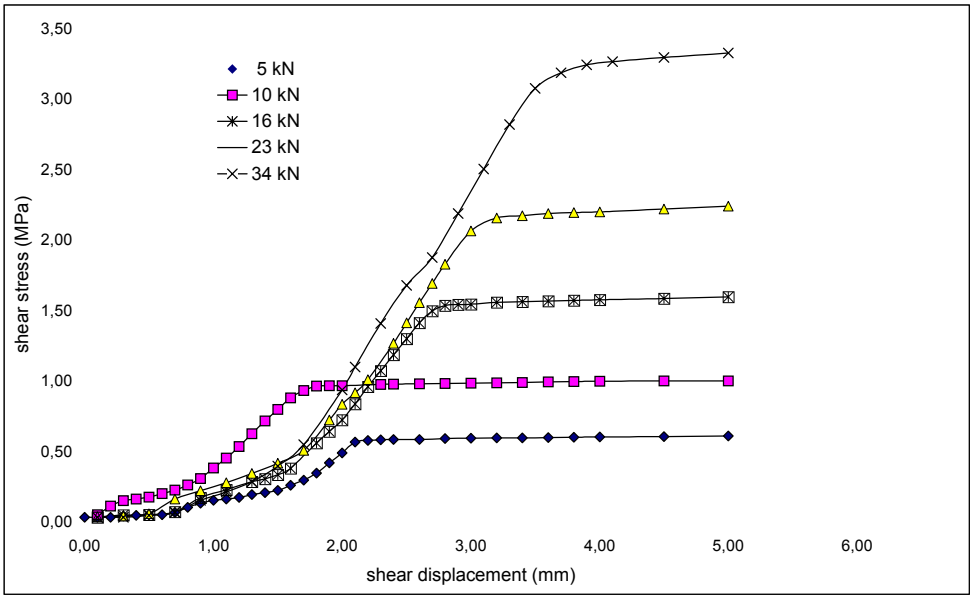

Figure A.3 Shear stress vs. shear displacement curves for flat joints (Flat –2)

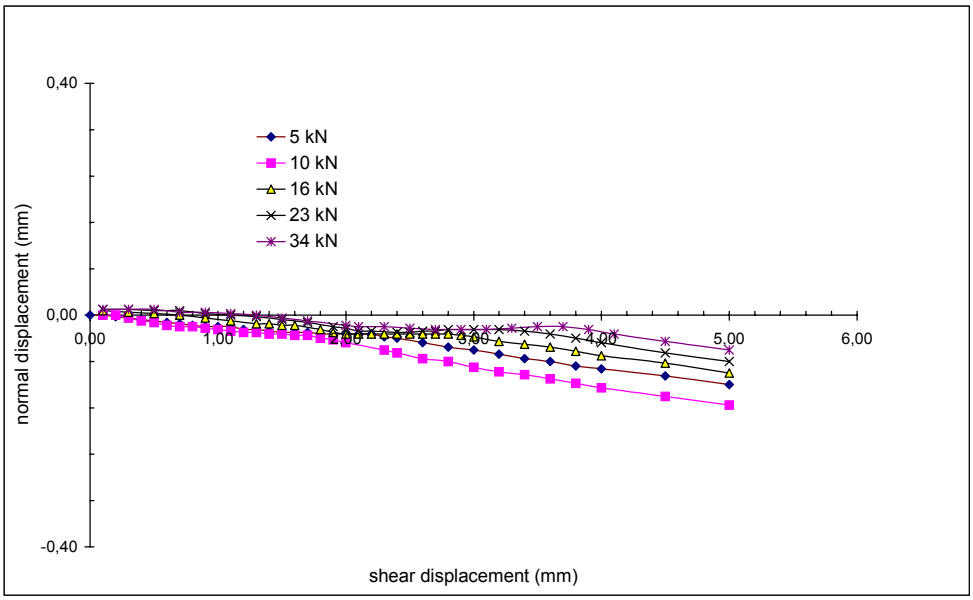

Figure A.4 Normal vs. shear displacement curves for flat joints (Flat-2)

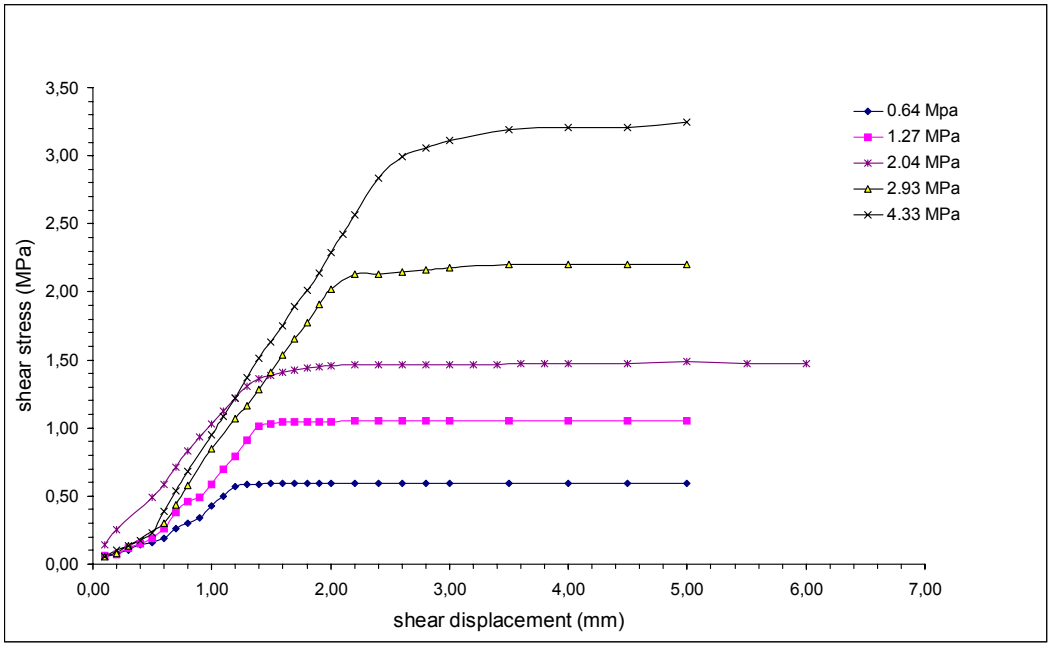

Figure A.5 Shear stress vs. shear displacement curves for flat joints (Flat-3)

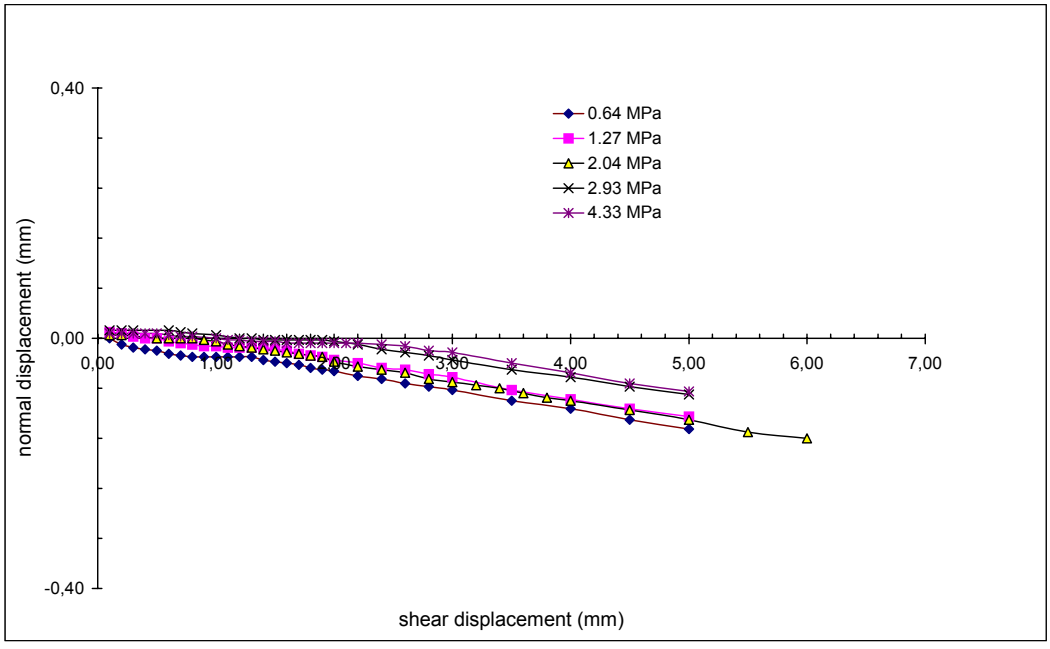

Figure A.6 Normal vs. shear displacement curves for flat joints (Flat-3)

A.2 Shear test curves of Type1 joints

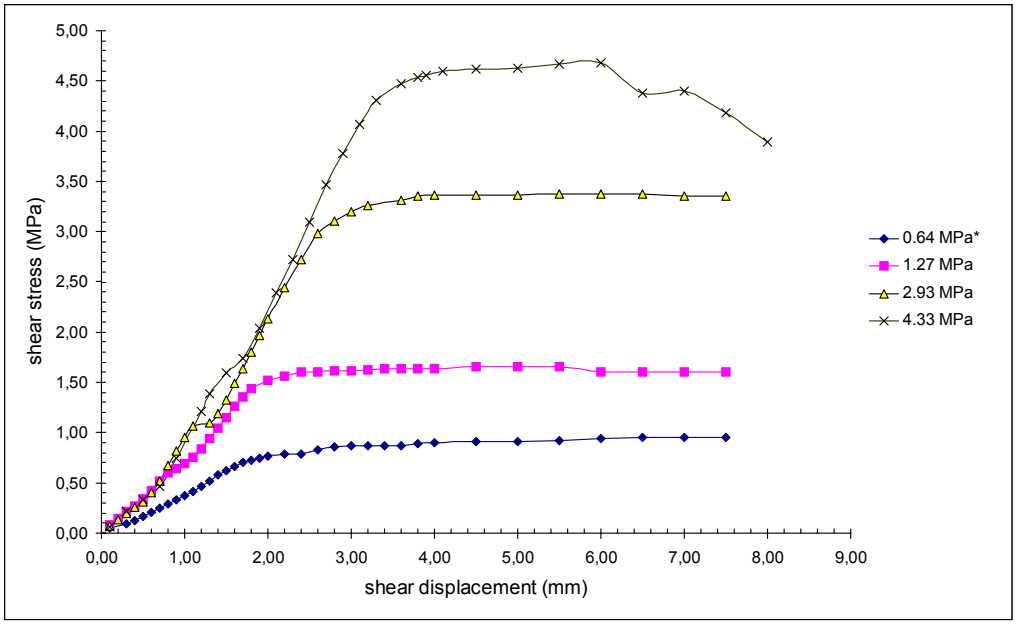

Figure A.7 Shear stress vs. shear displacement curves for Type1, α=90° (σ_n* = 0.64 MPa)

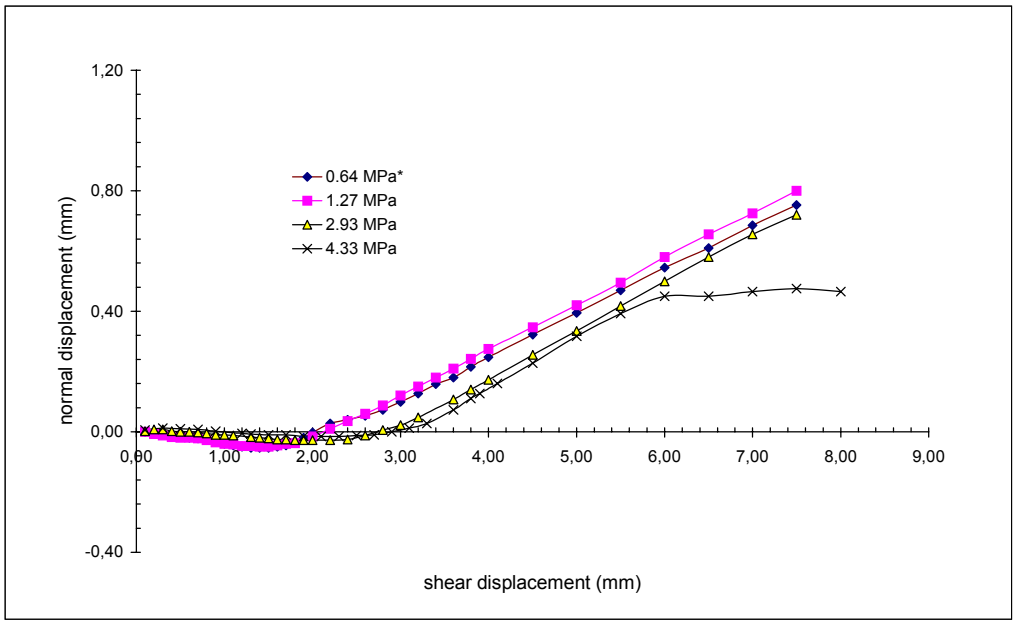

Figure A.8 Normal displacement vs. shear displacement curves for Type1, α=90° (σ_n* = 0.64 MPa)

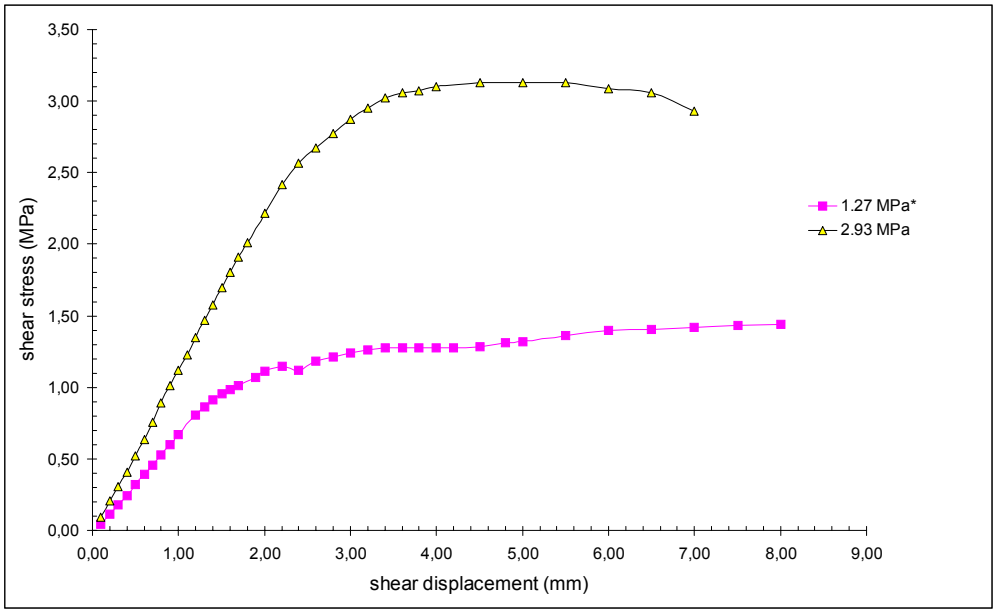

Figure A.9 Shear stress vs. shear displacement curves for Type1, α=90° (σ_n* = 1.27 MPa)

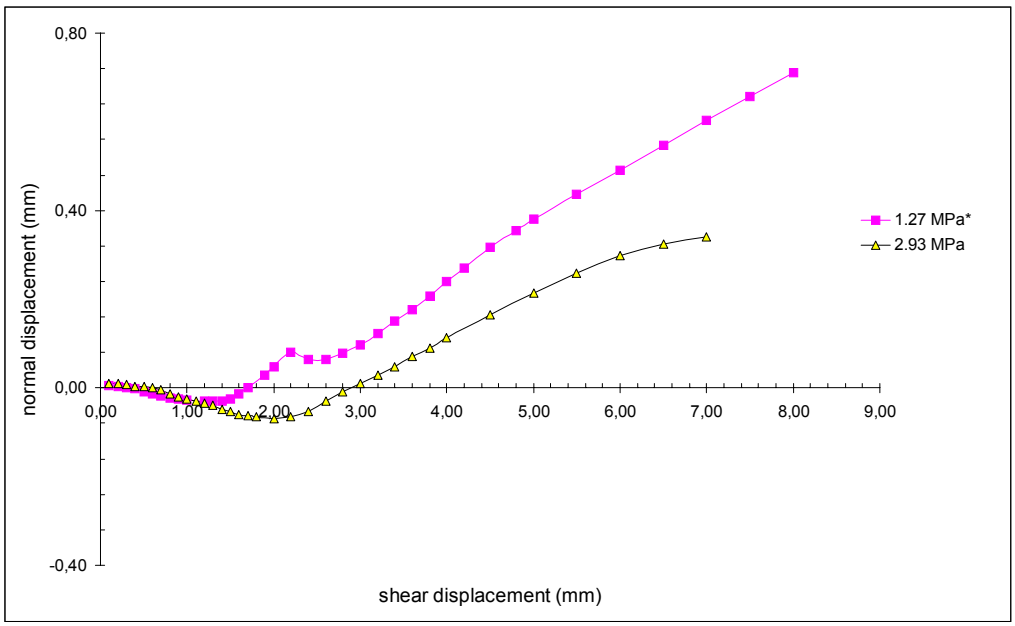

Figure A.10 Normal displacement vs. shear displacement curves for Type1, α=90° (σ_n* = 1.27 MPa)

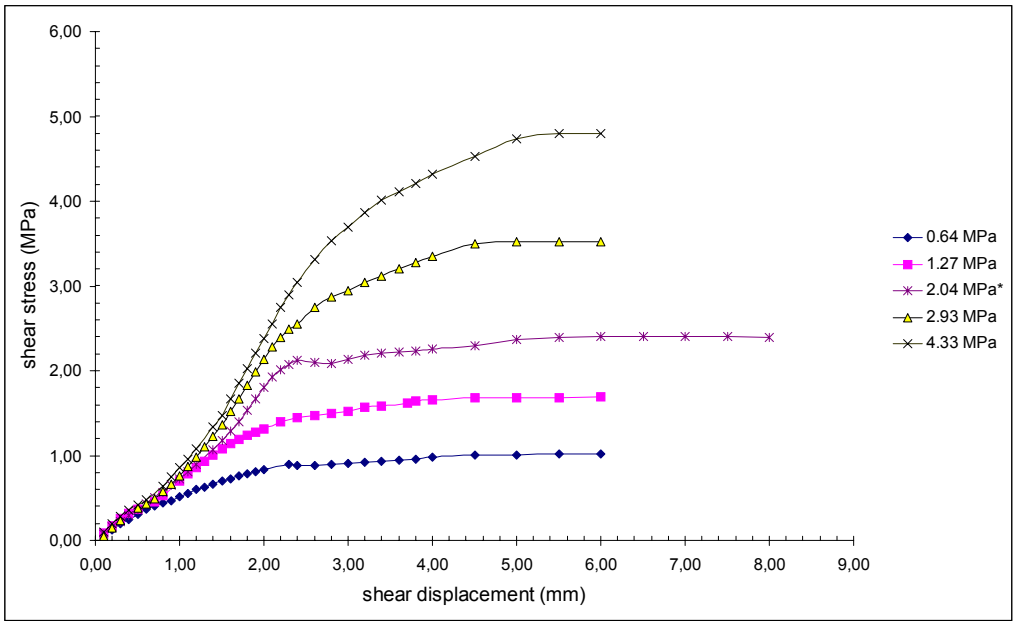

Figure A.11 Shear stress vs. shear displacement curves for Type1, α=90° (σ_n* = 2.04 MPa)

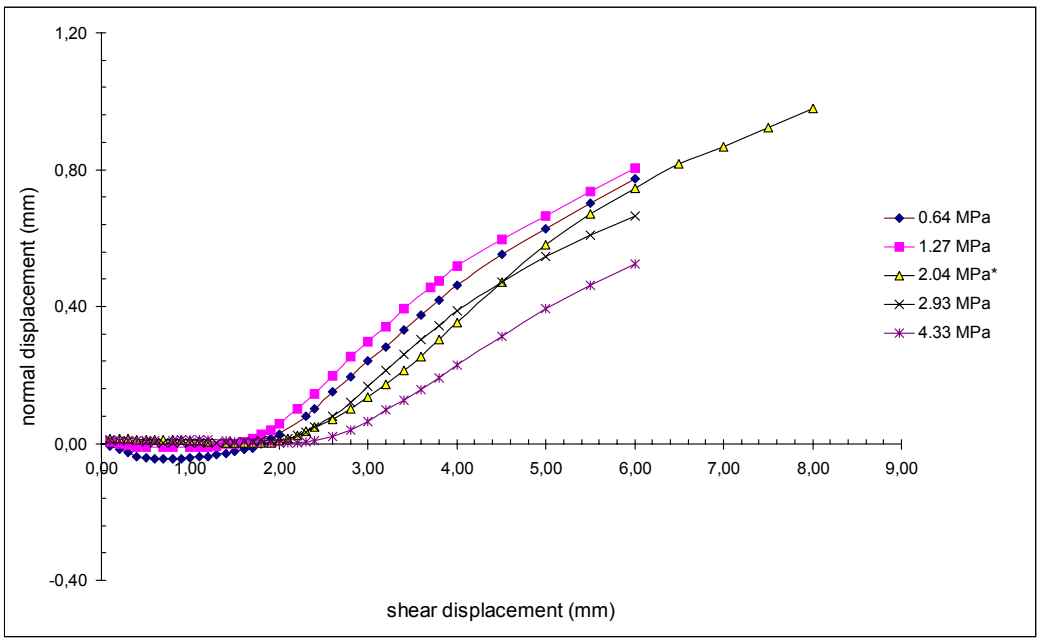

Figure A.12 Normal displacement vs. shear displacement curves for Type1, α=90° (σ_n* = 2.04 MPa)

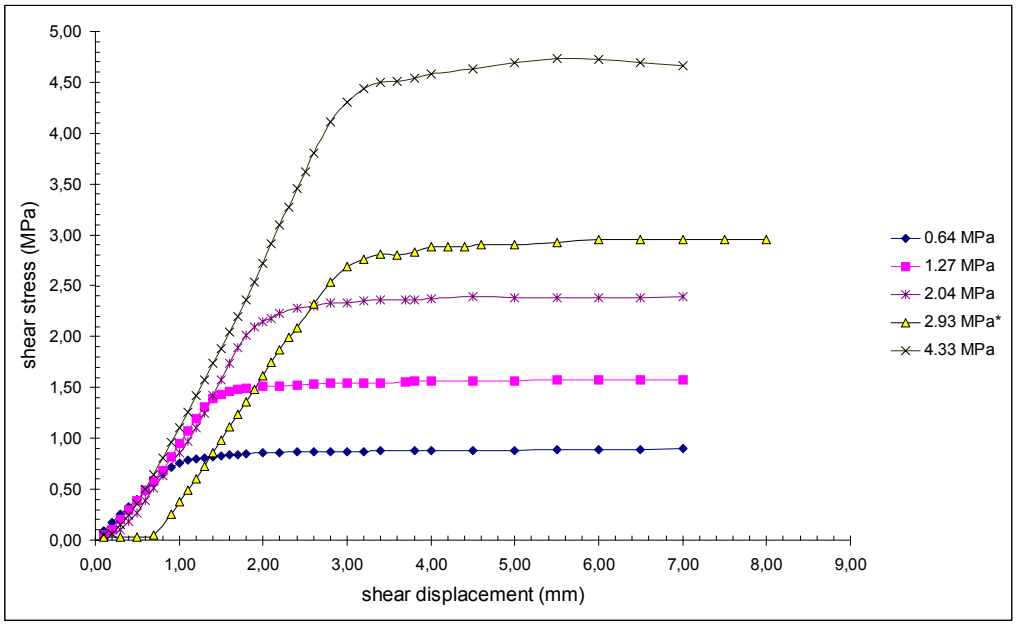

Figure A.13 Shear stress vs. shear displacement curves for Type1, α=90° (σ_n* = 2.93 MPa)

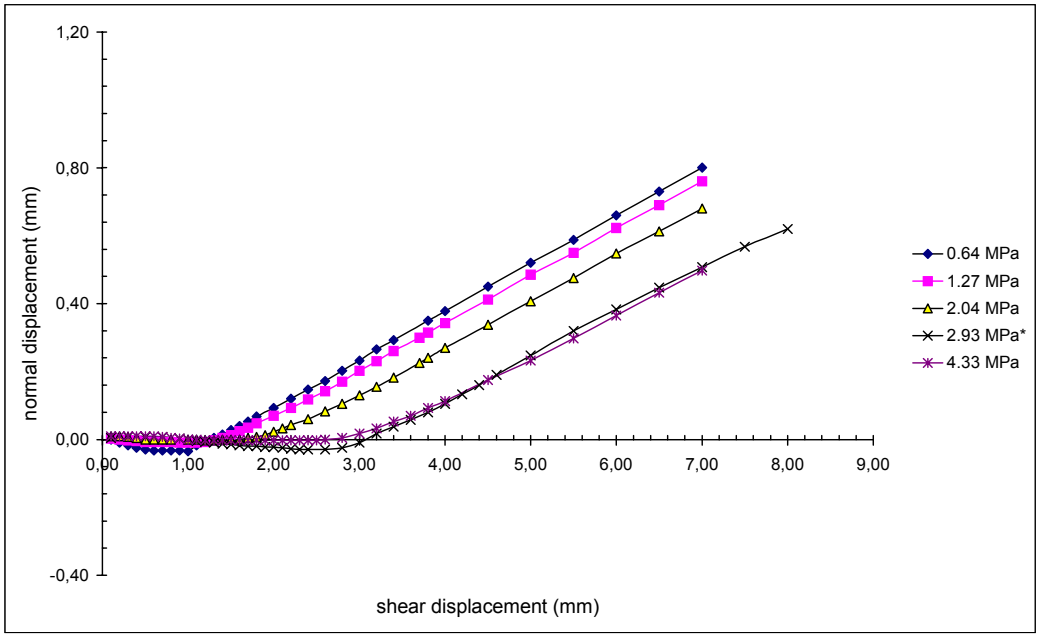

Figure A.14 Normal displacement vs. shear displacement curves for Type1, α=90° (σ_n* = 2.93 MPa)

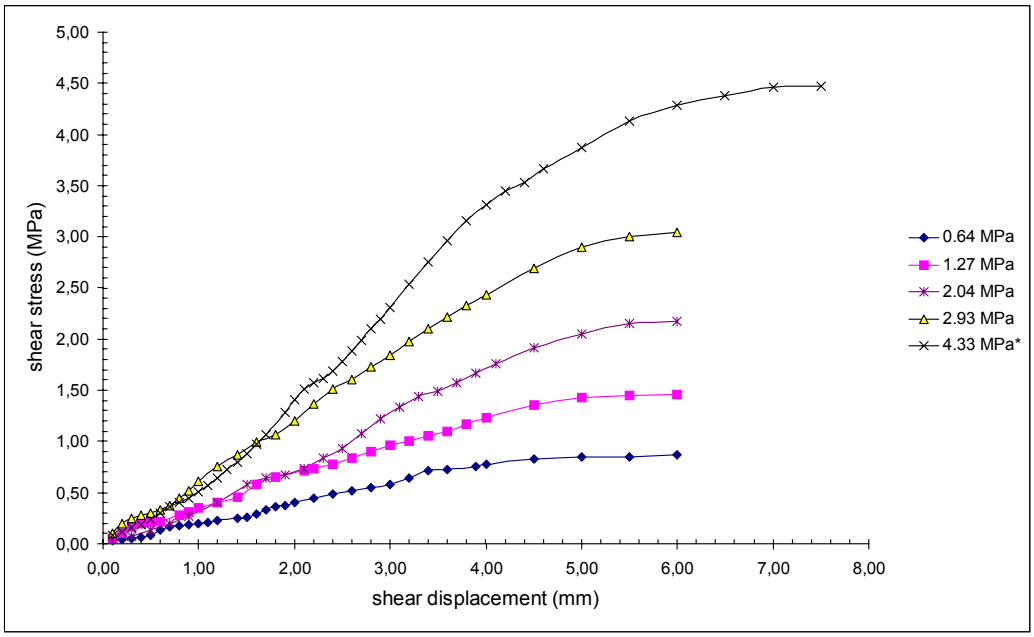

Figure A.15 Shear stress vs. shear displacement curves for Type1, α=90° (σ_n* = 4.33 MPa)

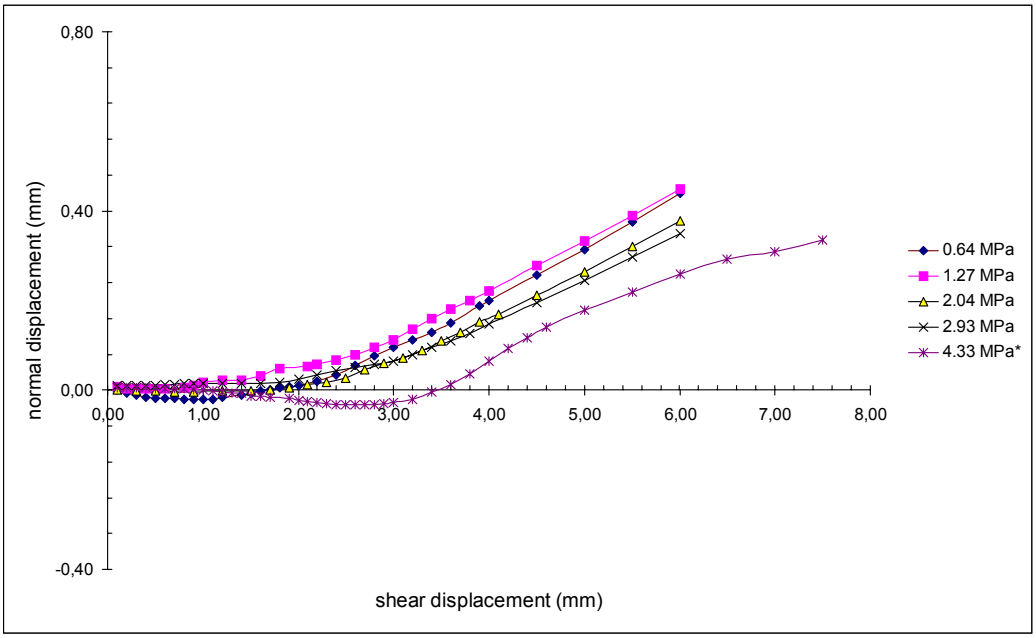

Figure A.16 Normal displacement vs. shear displacement curves for Type1, α=90° (σ_n* = 4.33 MPa)

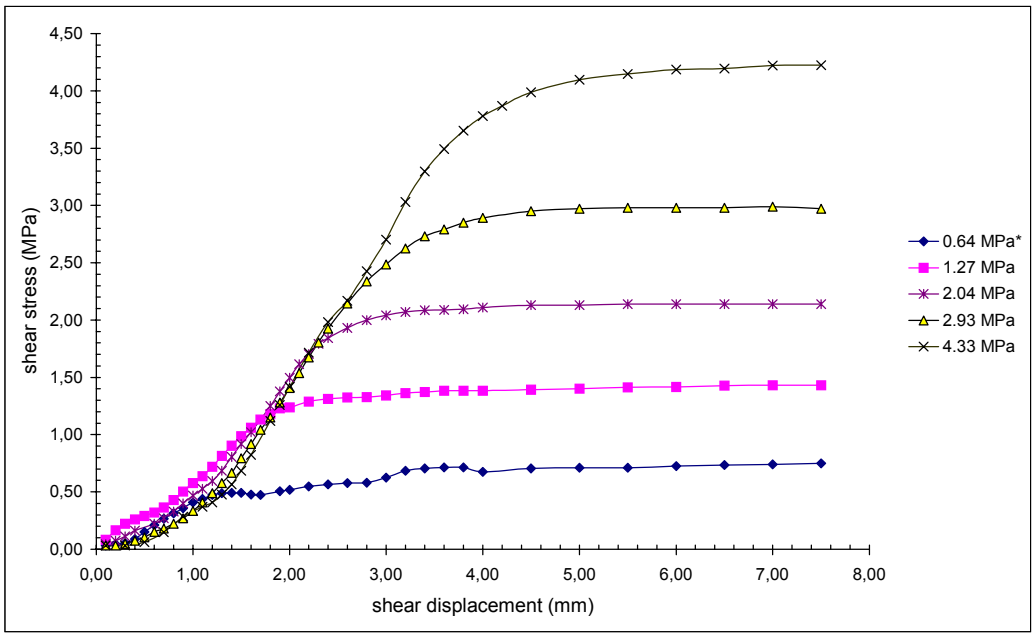

Figure A.17 Shear stress vs. shear displacement curves for Type1, α=60° (σ_n* = 0.64 MPa)

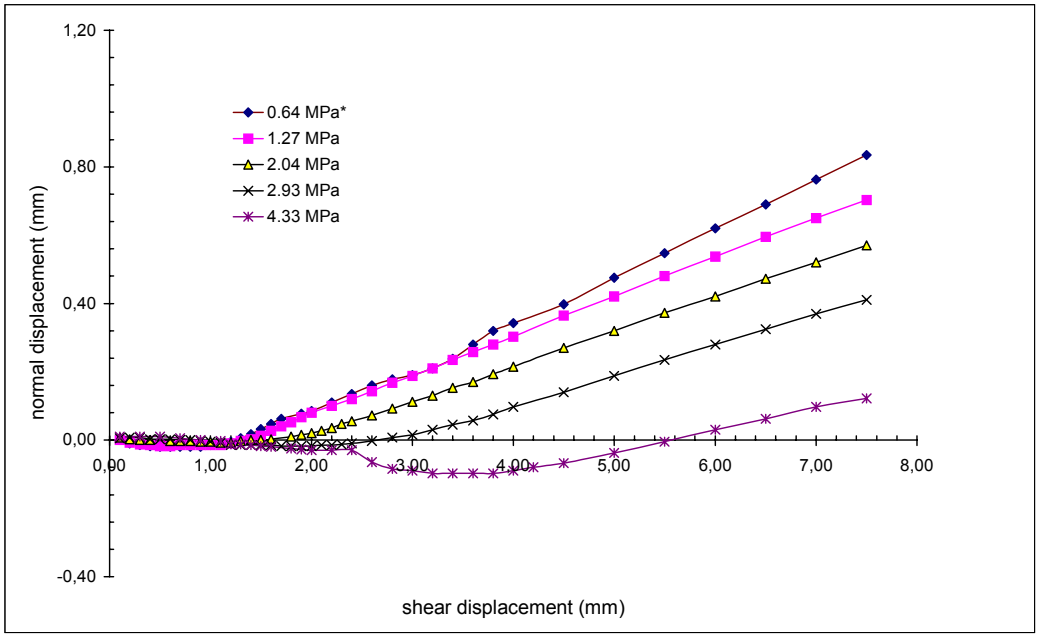

Figure A.18 Normal displacement vs. shear displacement curves for Type1, α=60° (σ_n* = 0.64 MPa)

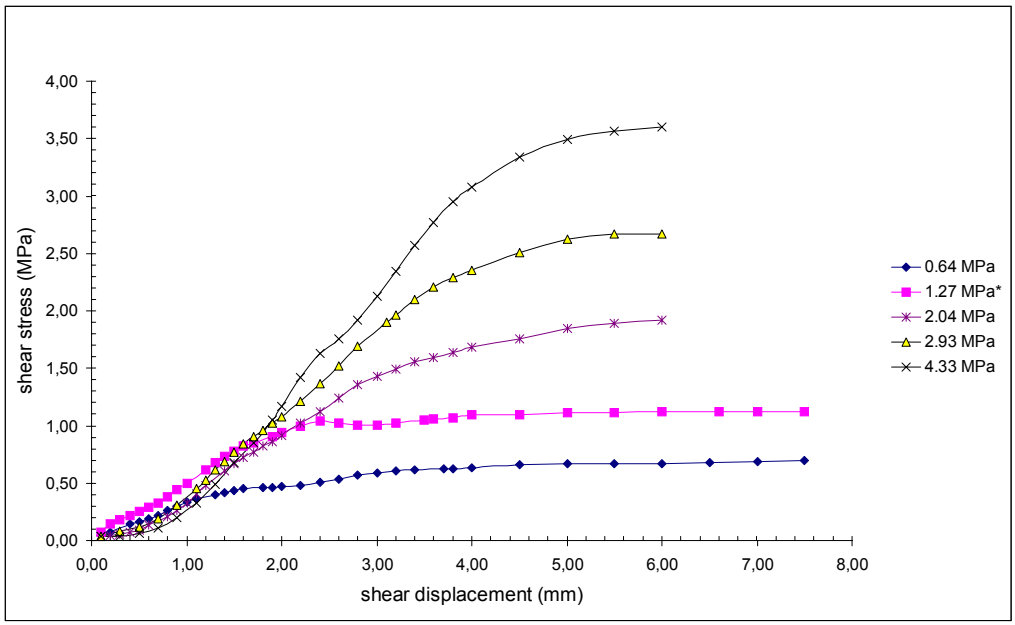

Figure A.19 Shear stress vs. shear displacement curves for Type1, α=60° (σ_n* = 1.27 MPa)

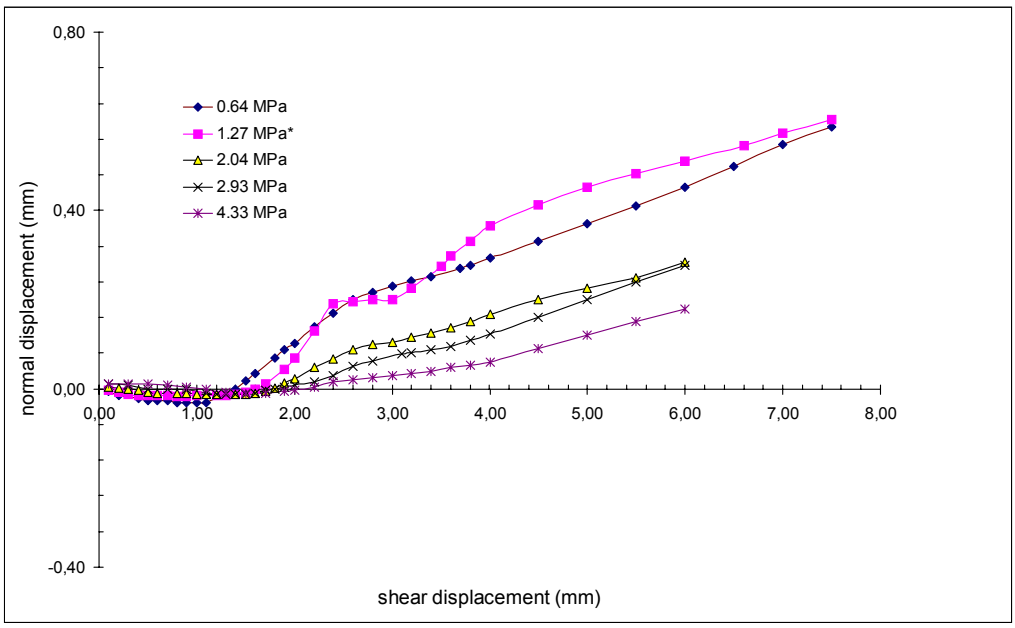

Figure A.20 Normal displacement vs. shear displacement curves for Type1, α=60° (σ_n* = 1.27 MPa)

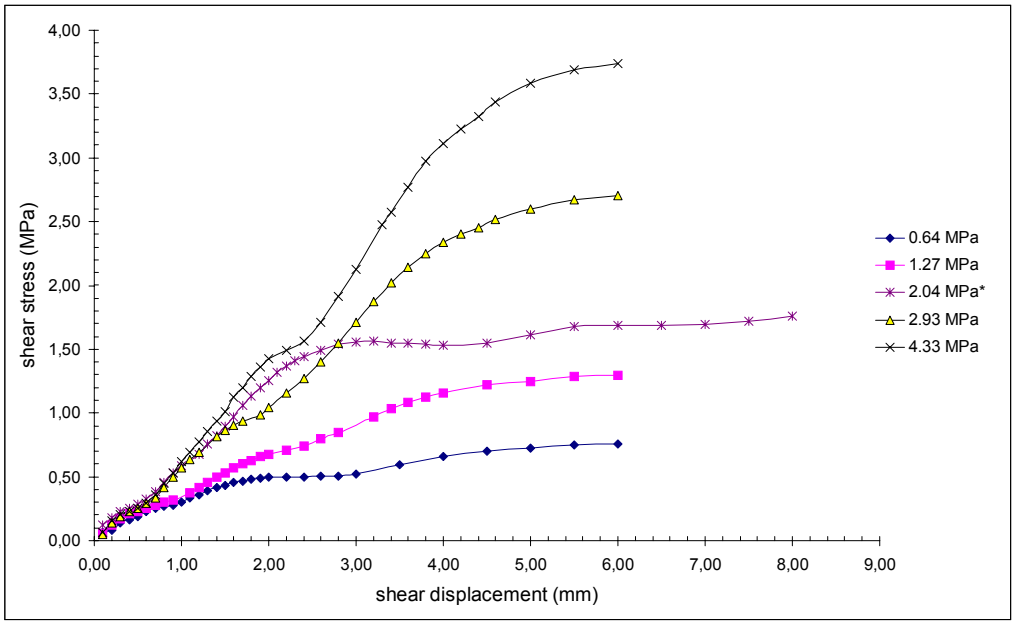

Figure A.21 Shear stress vs. shear displacement curves for Type1, α=60° (σ_n* = 2.04 MPa)

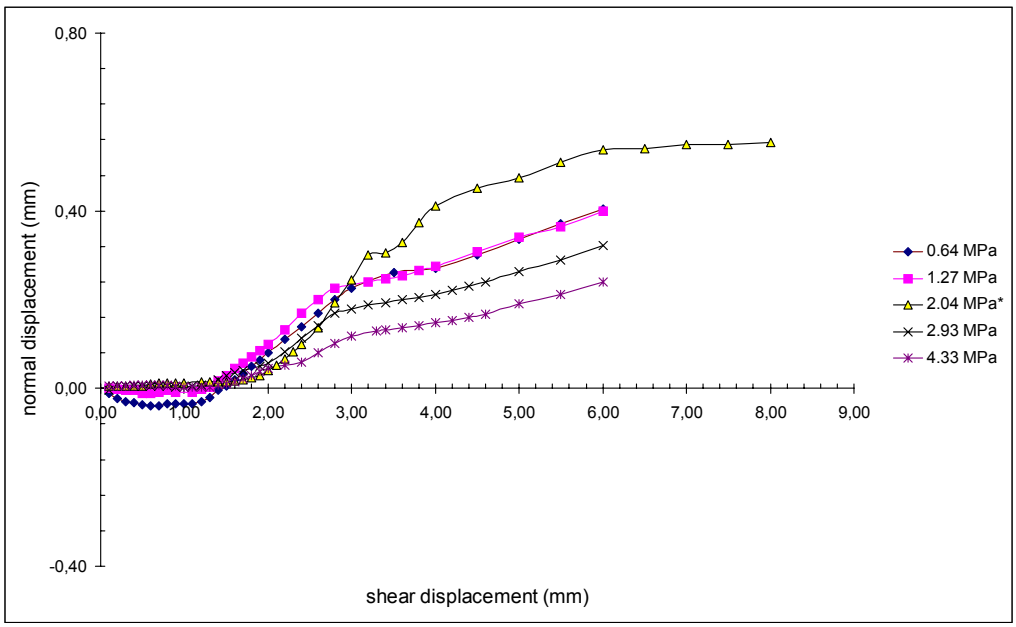

Figure A.22 Normal displacement vs. shear displacement curves for Type1, α=60° (σ_n* = 2.04 MPa)

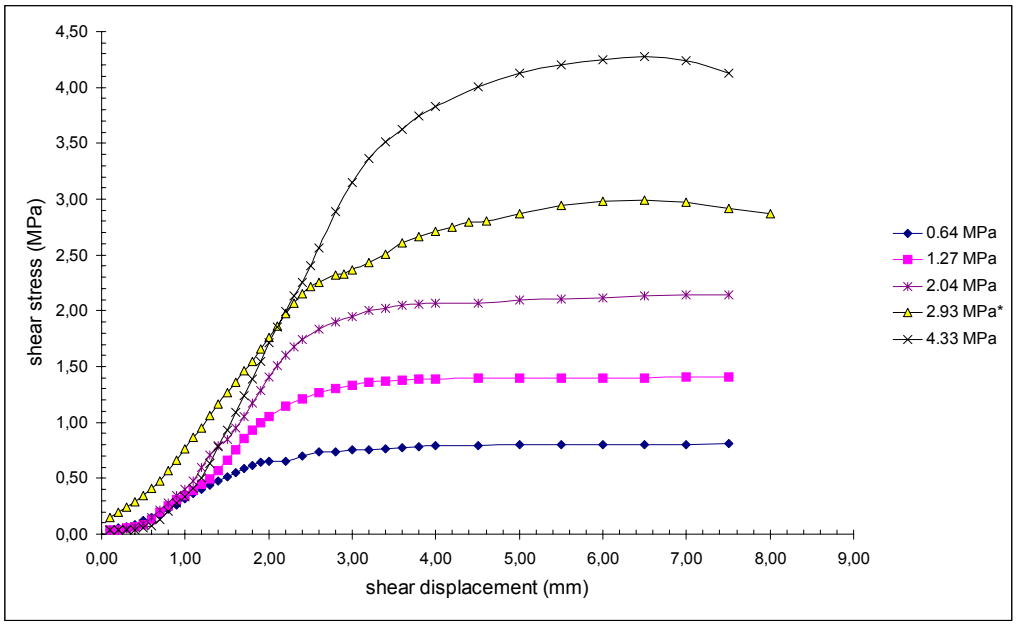

Figure A.23 Shear stress vs. shear displacement curves for Type1, α=60° (σ_n* = 2.93 MPa)

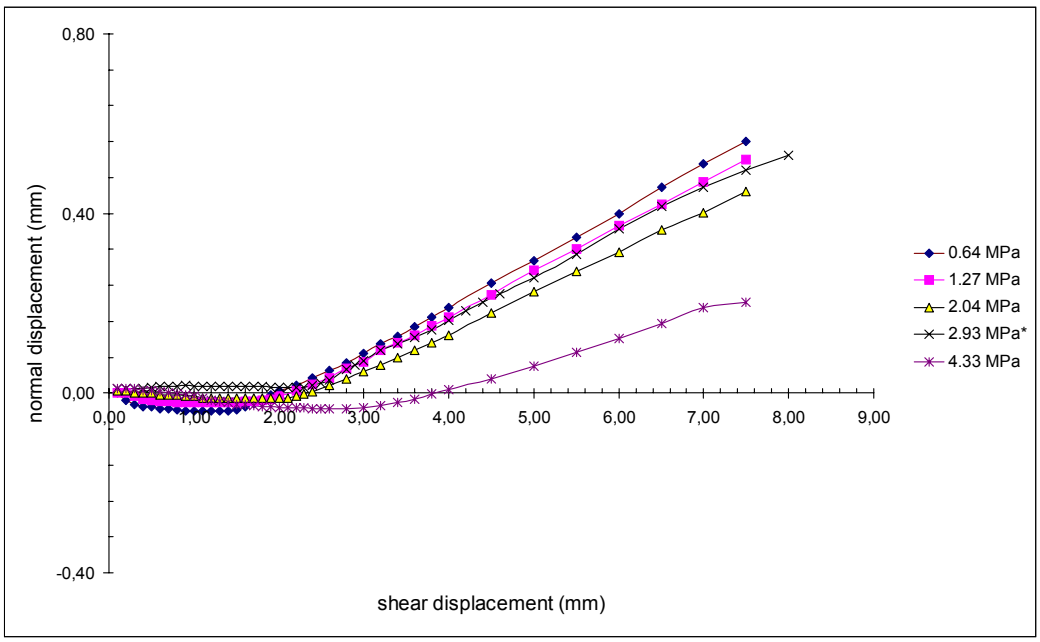

Figure A.24 Normal displacement vs. shear displacement curves for Type1, α=60° (σ_n* = 2.93 MPa)

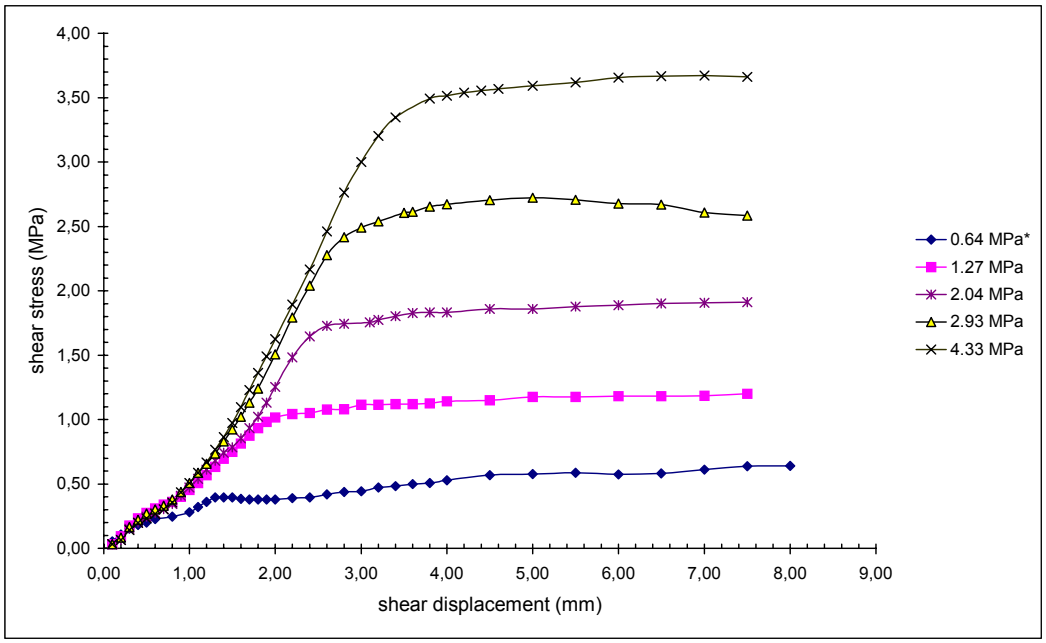

Figure A.25 Shear stress vs. shear displacement curves for Type1, α=30° (σ_n* = 0.64 MPa)

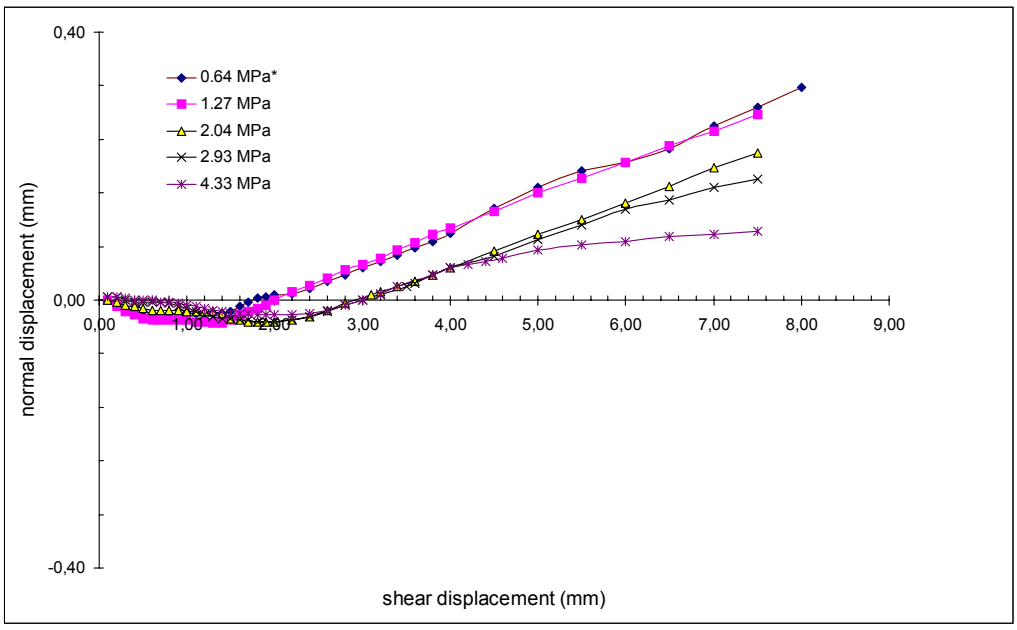

Figure A.26 Normal displacement vs. shear displacement curves for Type1, α=30° (σ_n* = 0.64 MPa)

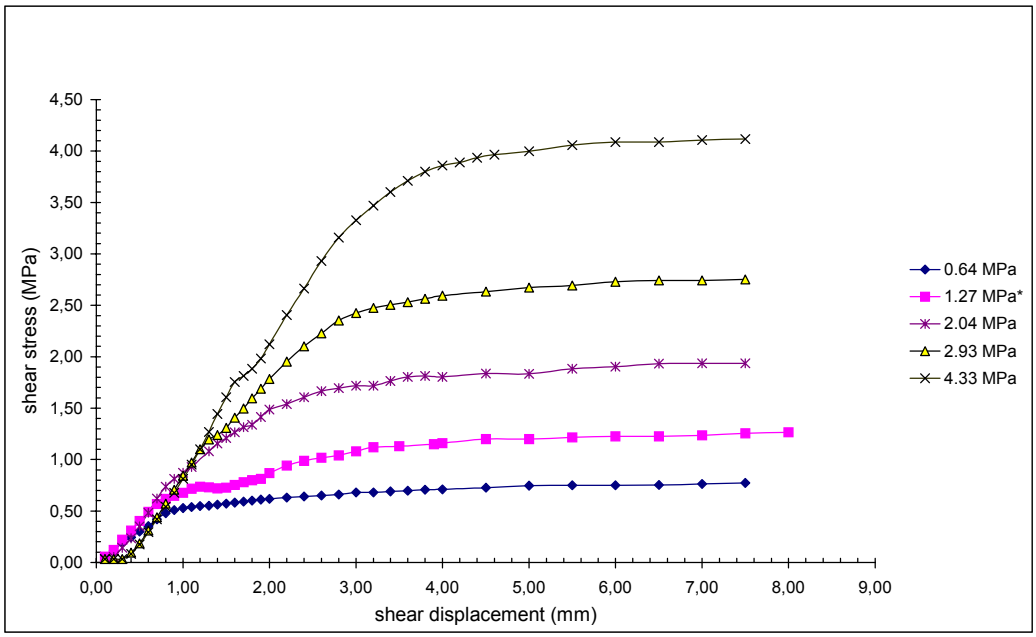

Figure A.27 Shear stress vs. shear displacement curves for Type1, α=30° (σ_n* = 1.27 MPa)

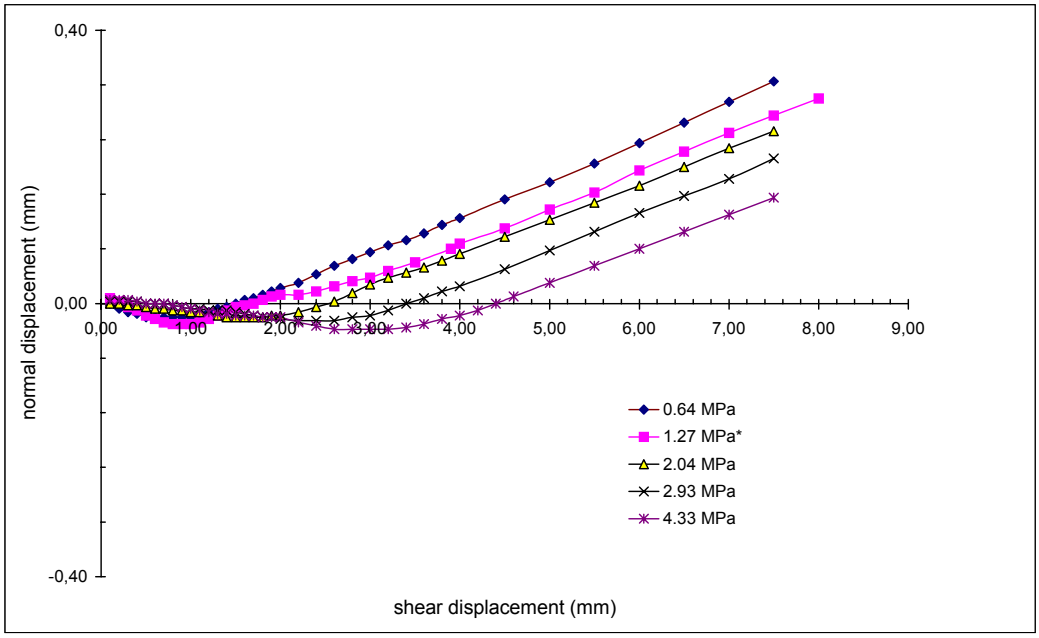

Figure A.28 Normal displacement vs. shear displacement curves for Type1, α=30° (σ_n* = 1.27 MPa)

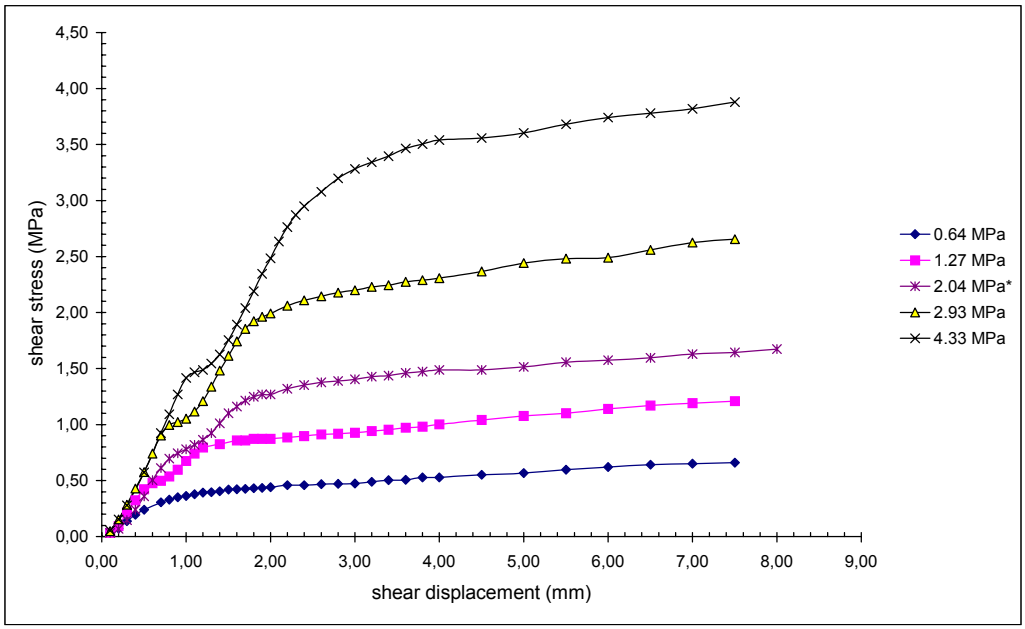

Figure A.29 Shear stress vs. shear displacement curves for Type1, α=30° (σ_n* = 2.04 MPa)

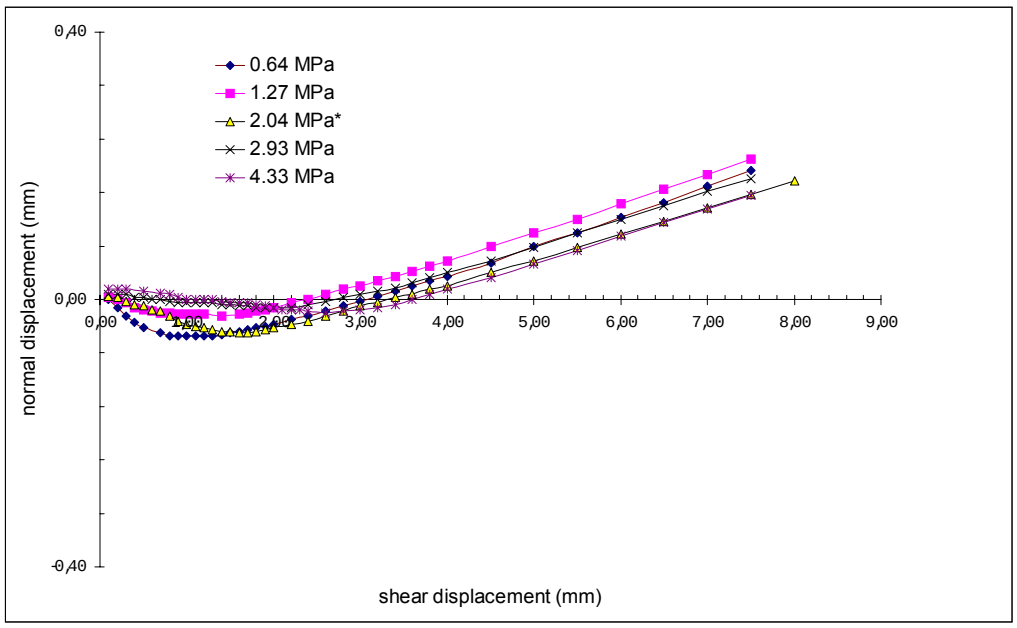

Figure A.30 Normal displacement vs. shear displacement curves for Type1, α=30° (σ_n* = 2.04 MPa)

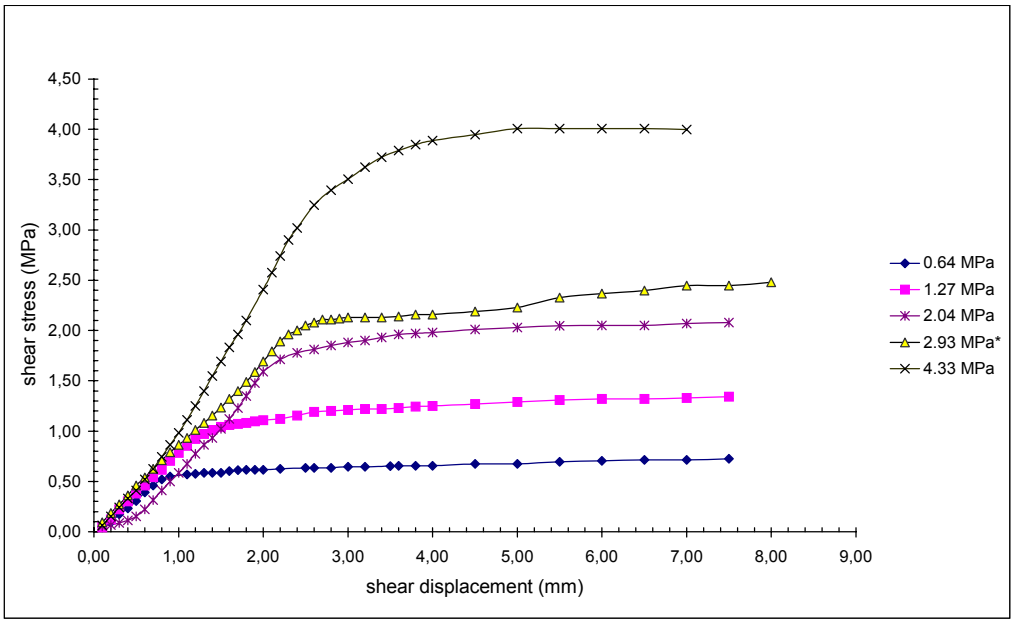

Figure A.31 Shear stress vs. shear displacement curves for Type1, α=30° (σ_n* = 2.93 MPa)

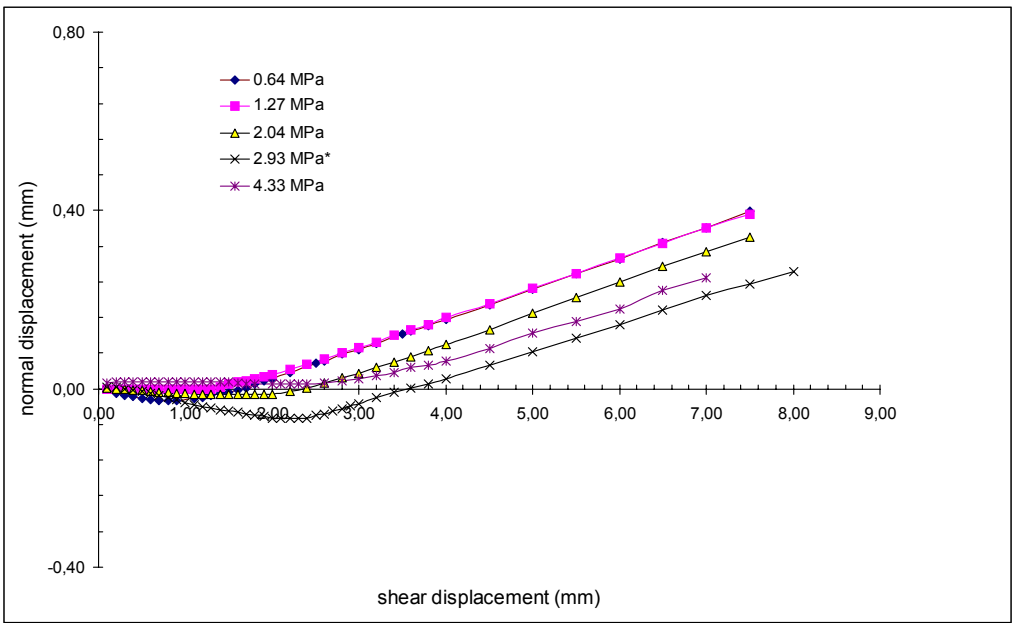

Figure A.32 Normal displacement vs. shear displacement curves for Type1, α=30° (σ_n* = 2.93 MPa)

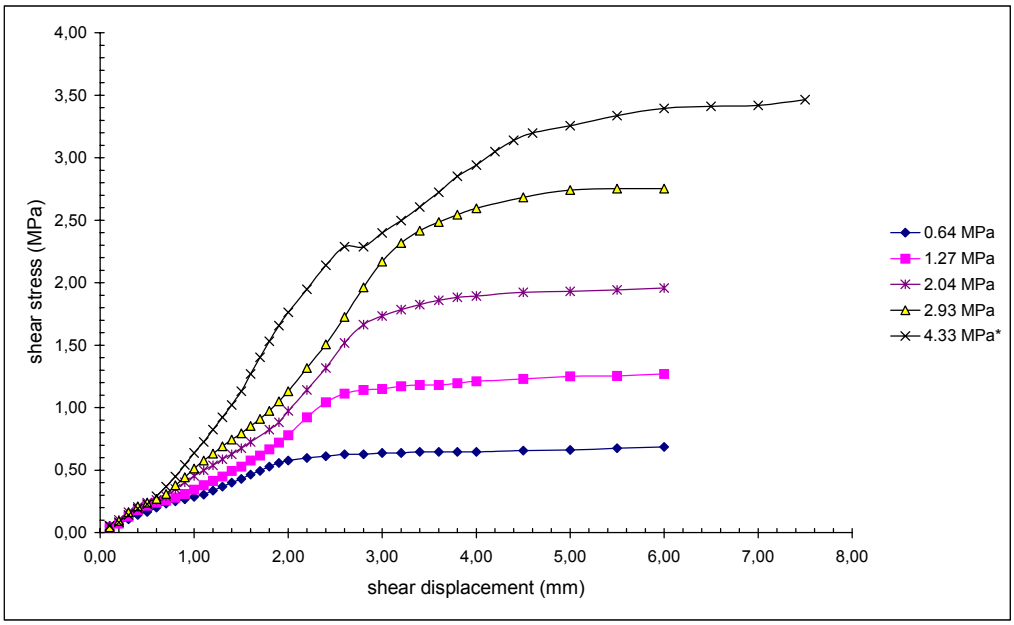

Figure A.33 Shear stress vs. shear displacement curves for Type1, α=30° (σ_n* = 4.33 MPa)

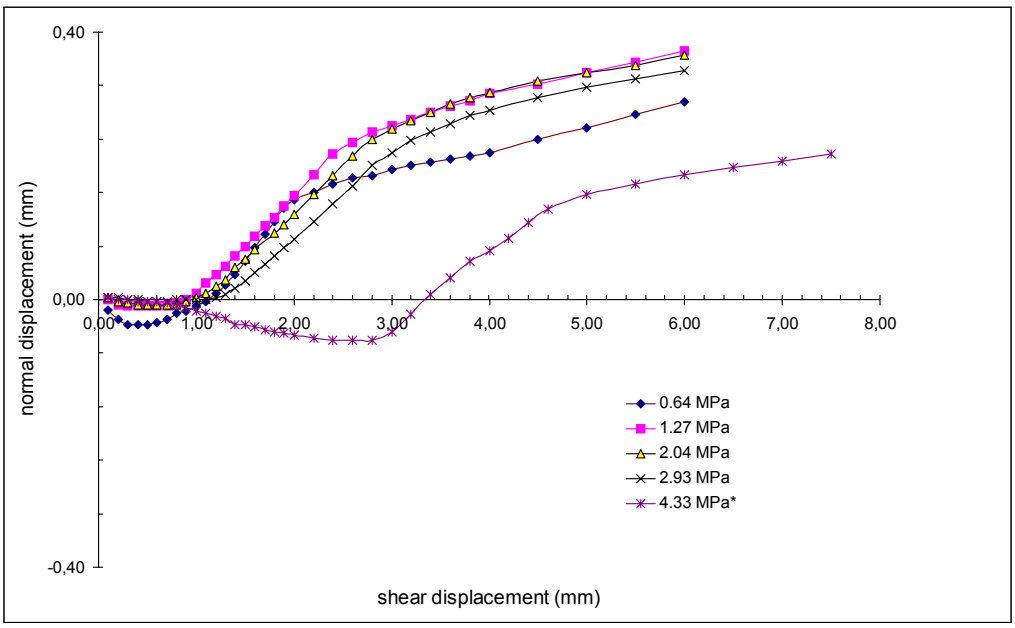

Figure A.34 Normal displacement vs. shear displacement curves for Type1, α=30° (σ_n* = 4.33 MPa)

A.3 Shear test curves of Type2 joints

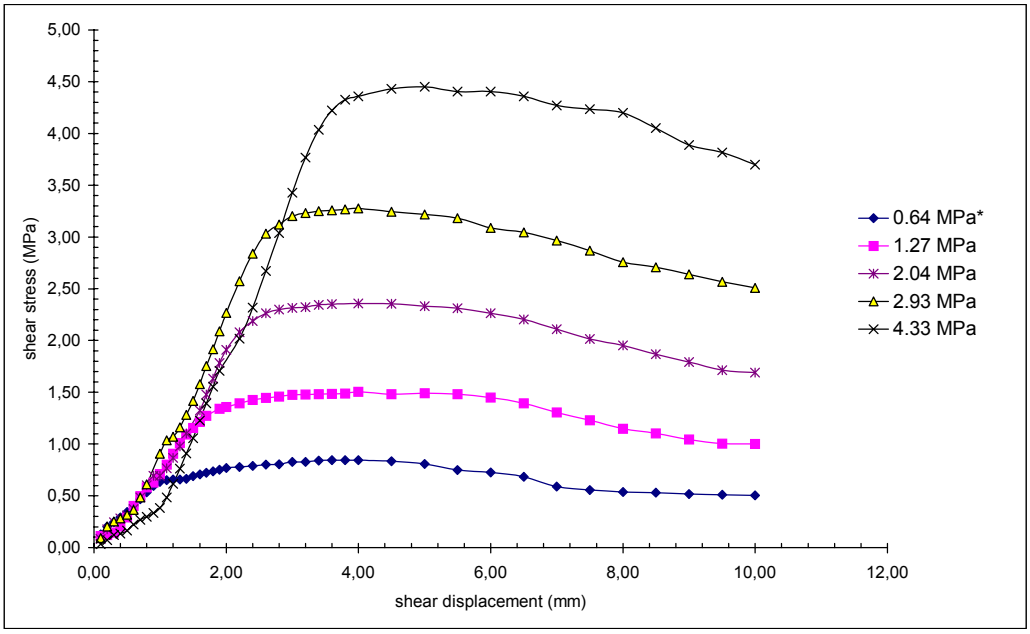

Figure A.35 Shear stress vs. shear displacement curves for Type2, α=90° (σ_n* = 0.64 MPa)

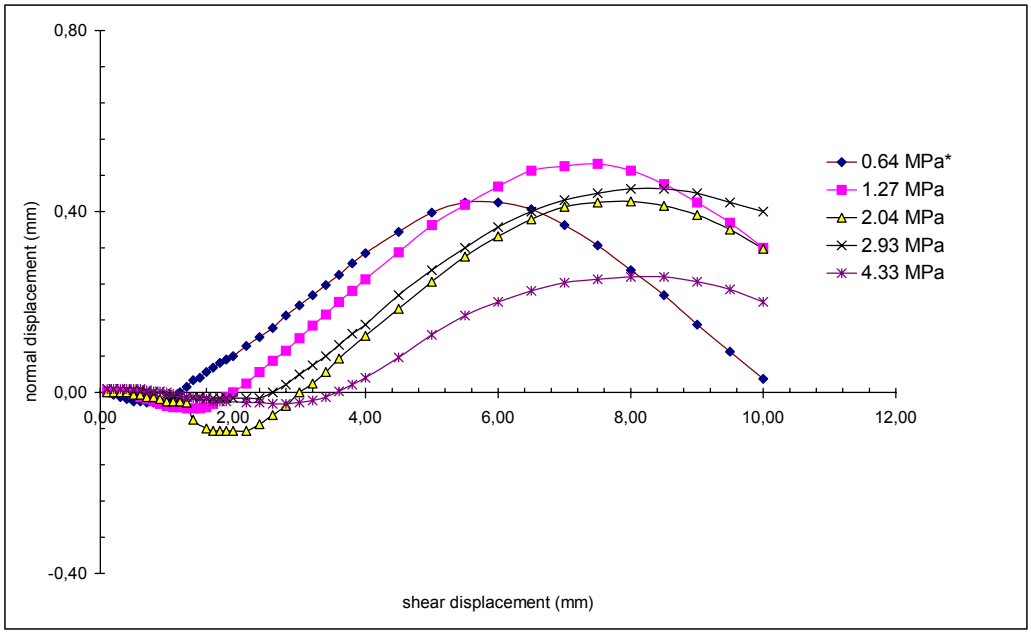

Figure A.36 Normal displacement vs. shear displacement curves for Type2, α=90° (σ_n* = 0.64 MPa)

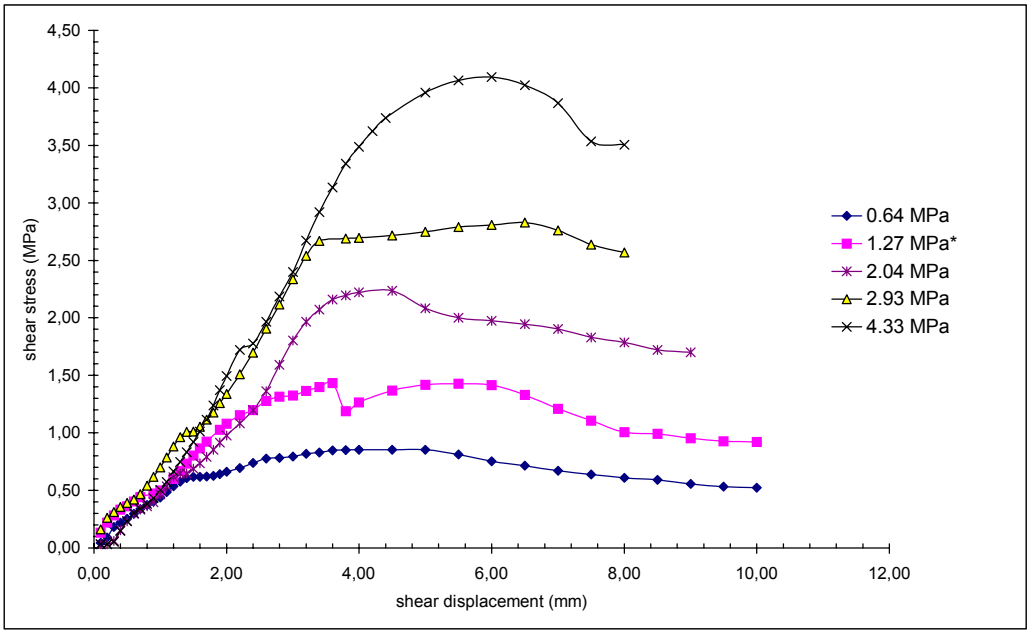

Figure A.37 Shear stress vs. shear displacement curves for Type2, α=90° (σ_n* = 1.27 MPa)

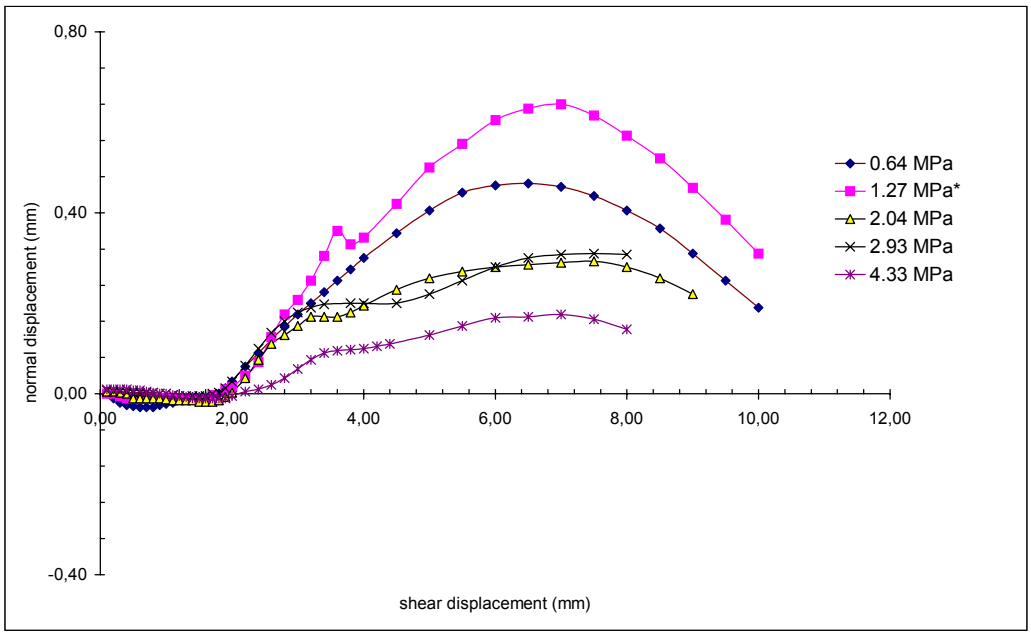

Figure A.38 Normal displacement vs. shear displacement curves for Type2, α=90° (σ_n* = 1.27 MPa)

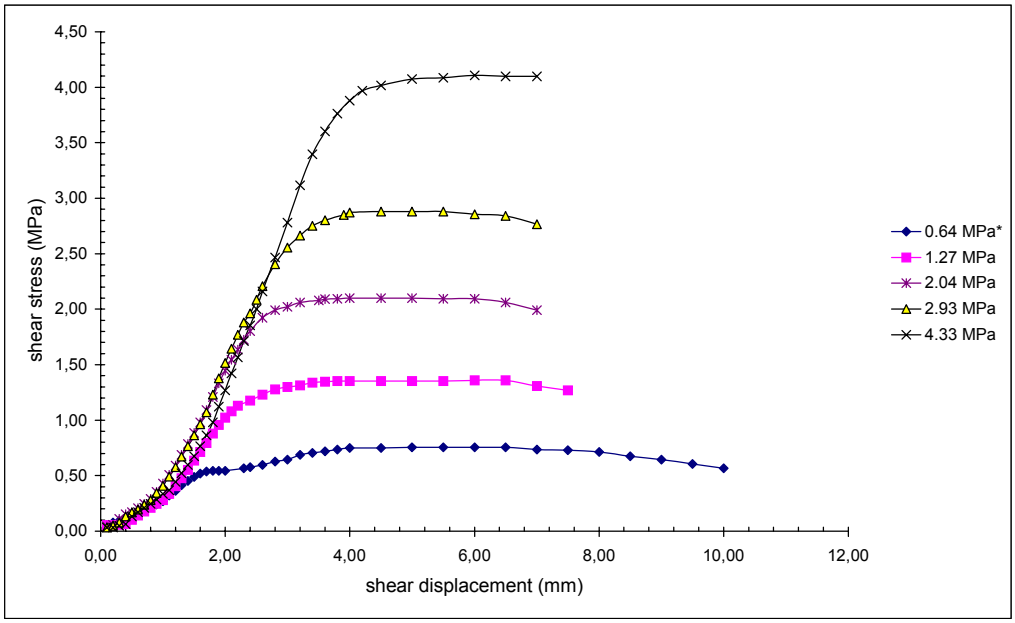

Figure A.39 Shear stress vs. shear displacement curves for Type2, α=60° (σ_n* = 0.64 MPa)

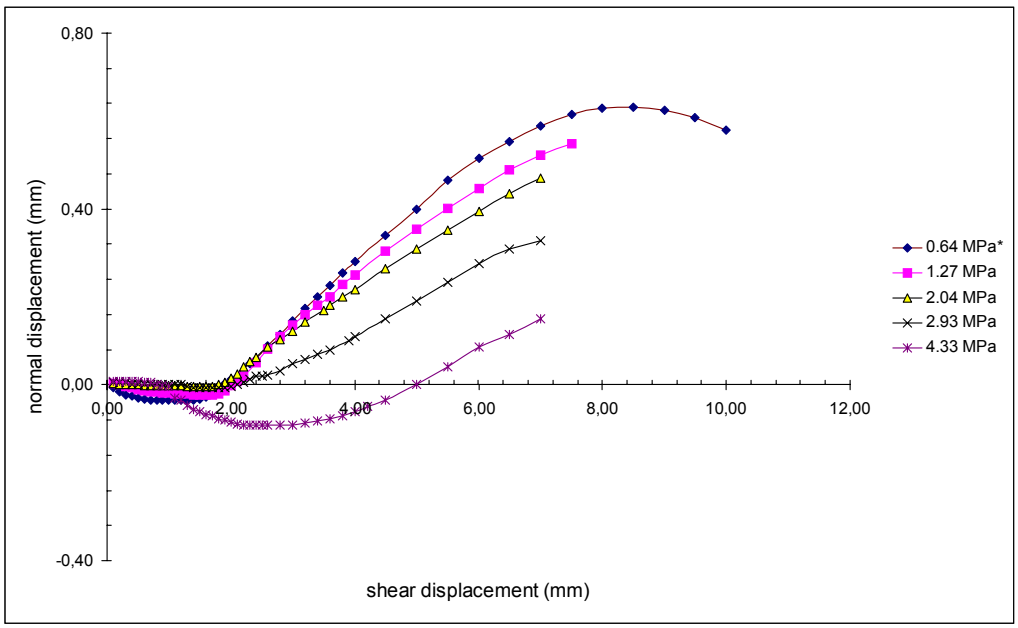

Figure A.40 Normal displacement vs. shear displacement curves for Type2, α=60° (σ_n* = 0.64 MPa)

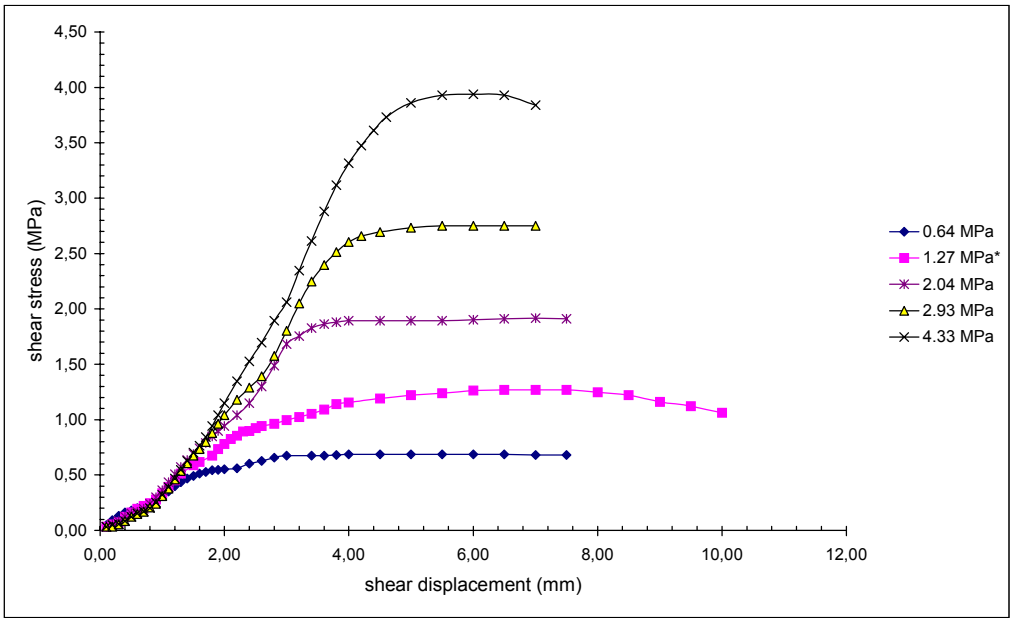

Figure A.41 Shear stress vs. shear displacement curves for Type2, α=60° (σ_n* = 1.27 MPa)

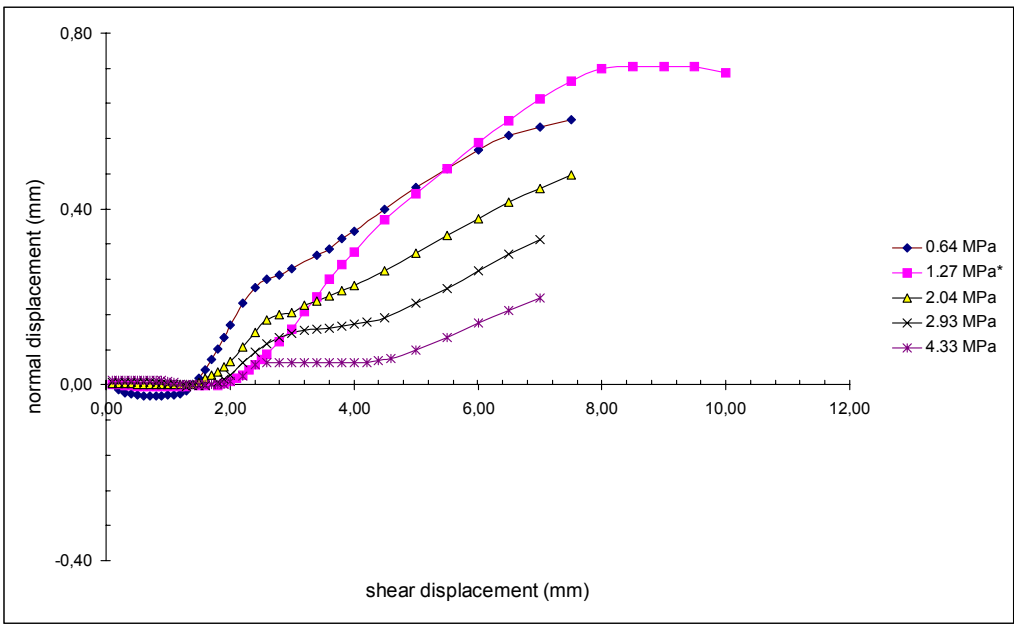

Figure A.42 Normal displacement vs. shear displacement curves for Type2, α=60° (σ_n* = 1.27 MPa)

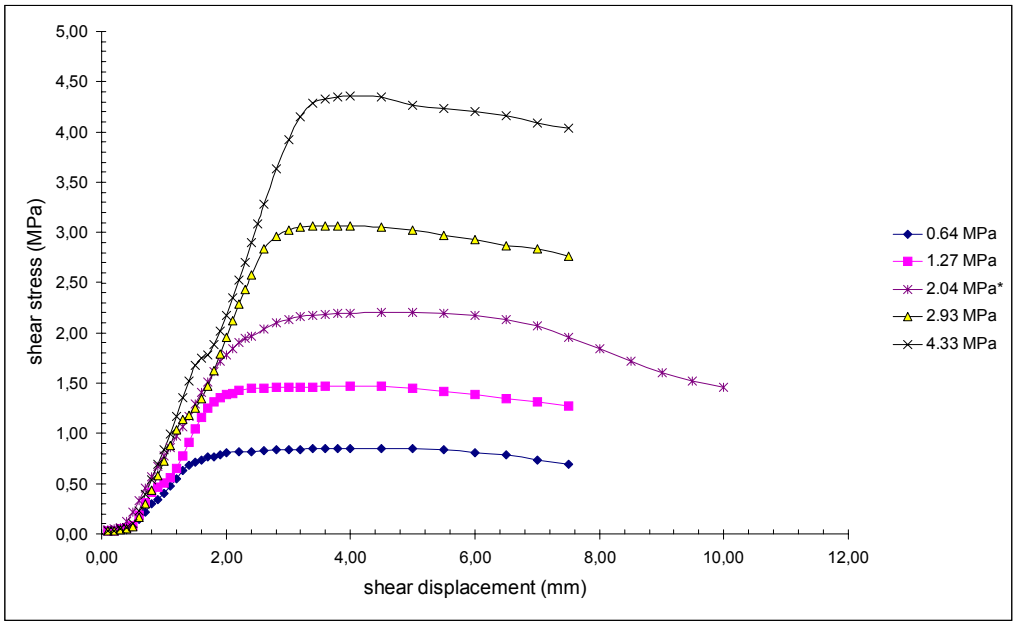

Figure A.43 Shear stress vs. shear displacement curves for Type2, α=60° (σ_n* = 2.04 MPa)

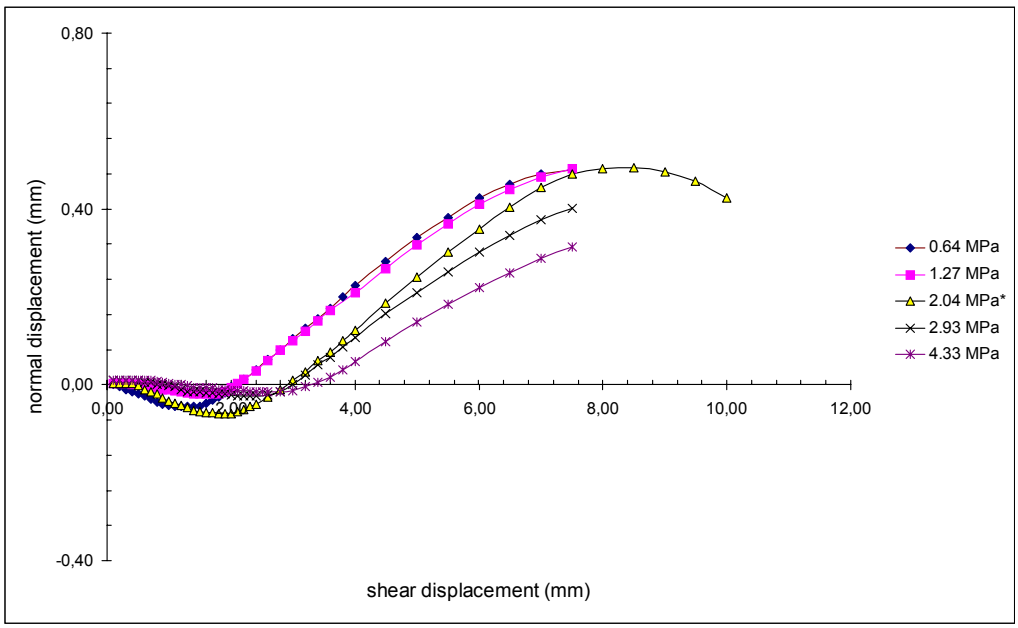

Figure A.44 Normal displacement vs. shear displacement curves for Type2, α=60° (σ_n* = 2.04 MPa)

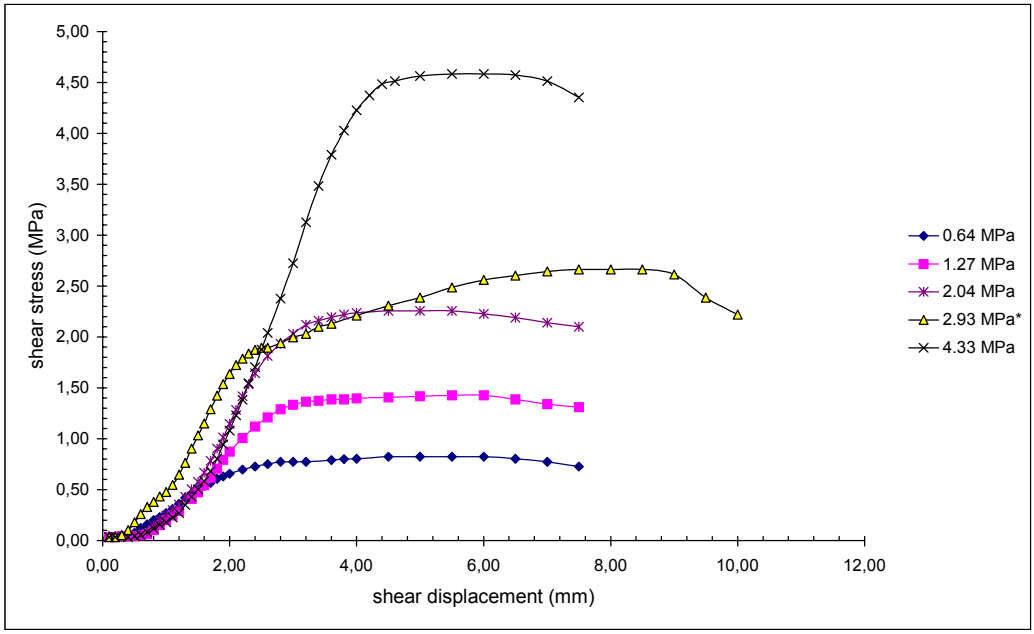

Figure A.45 Shear stress vs. shear displacement curves for Type2, α=60° (σ_n* = 2.93 MPa)

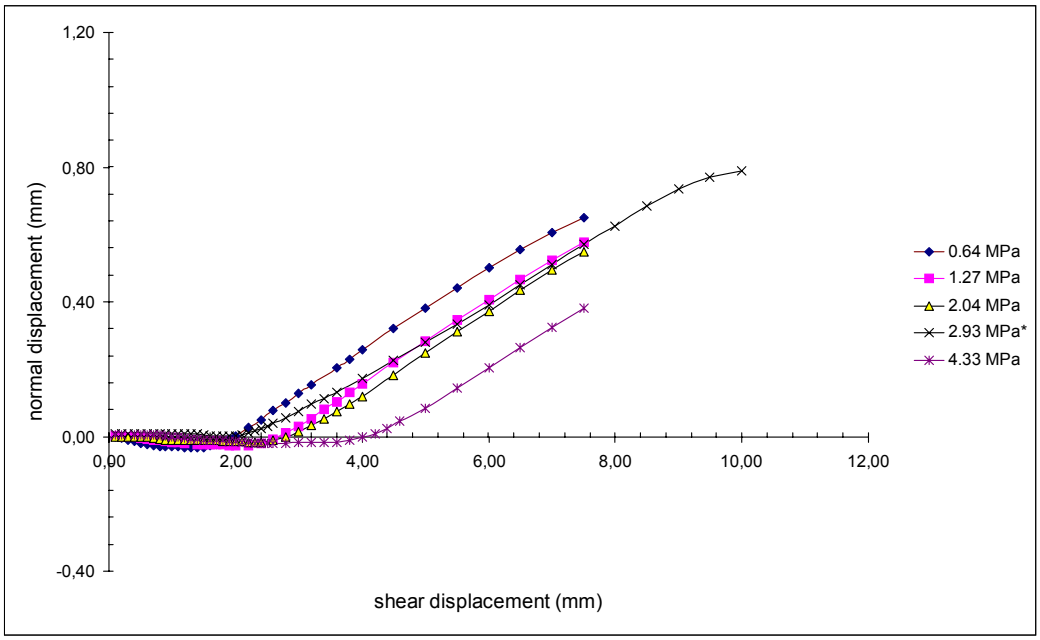

Figure A.46 Normal displacement vs. shear displacement curves for Type2, α=60° (σ_n* = 2.93 MPa)

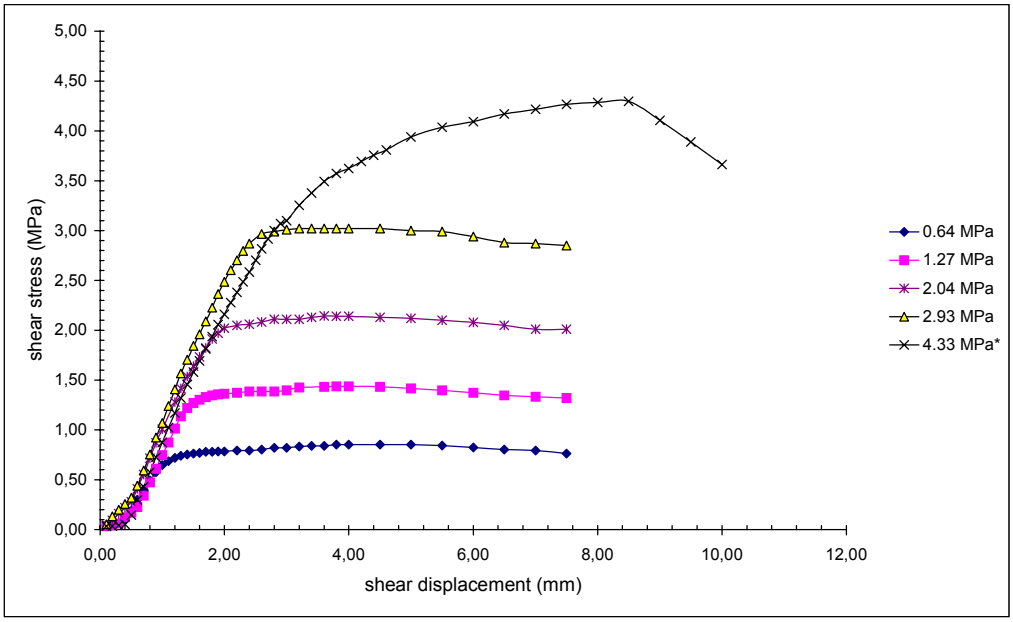

Figure A.47 Shear stress vs. shear displacement curves for Type2, α=60° (σ_n* = 4.33 MPa)

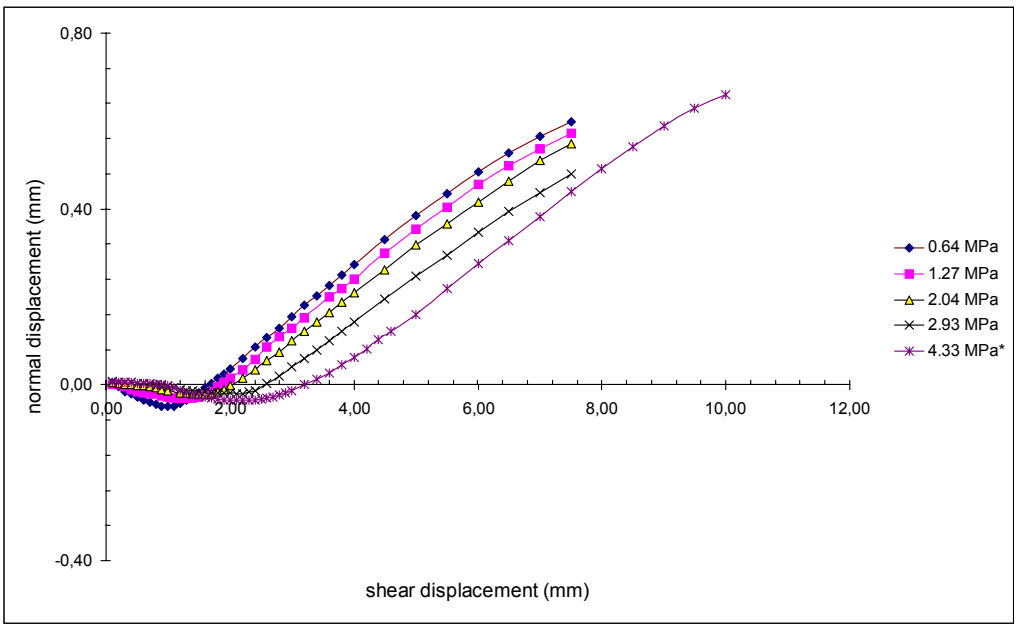

Figure A.48 Normal displacement vs. shear displacement curves for Type2, α=60° (σ_n* = 4.33 MPa)

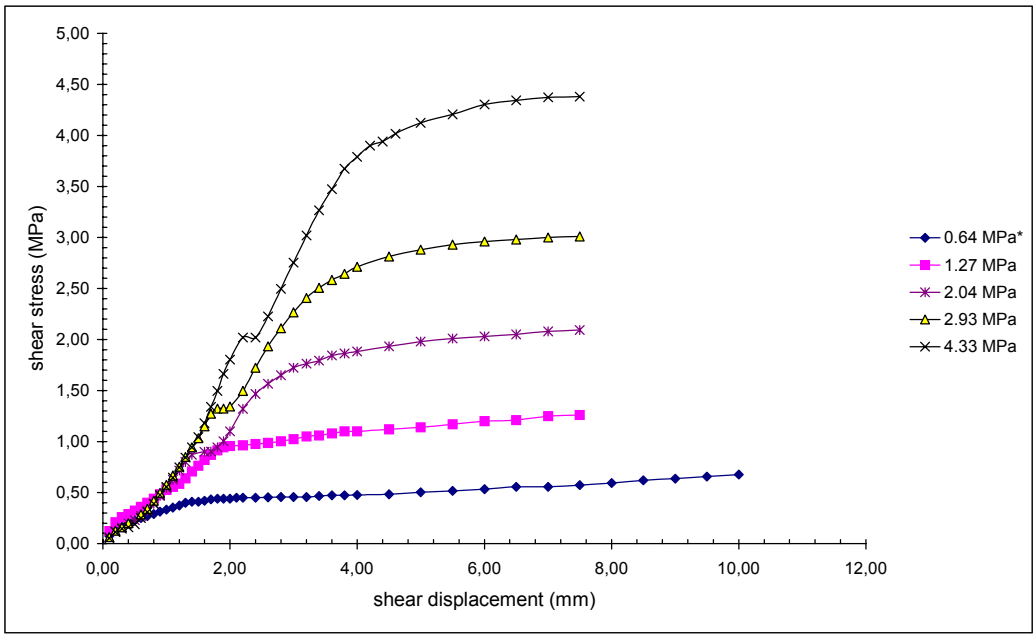

Figure A.49 Shear stress vs. shear displacement curves for Type2, α=30° (σ_n* = 0.64 MPa)

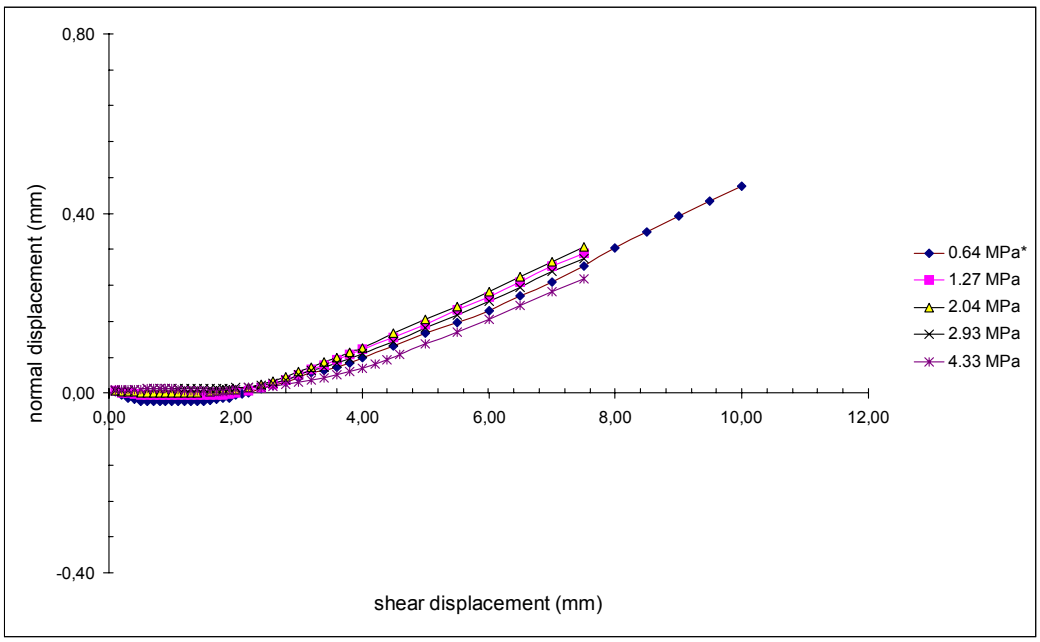

Figure A.50 Normal displacement vs. shear displacement curves for Type2, α=30° (σ_n* = 0.64 MPa)

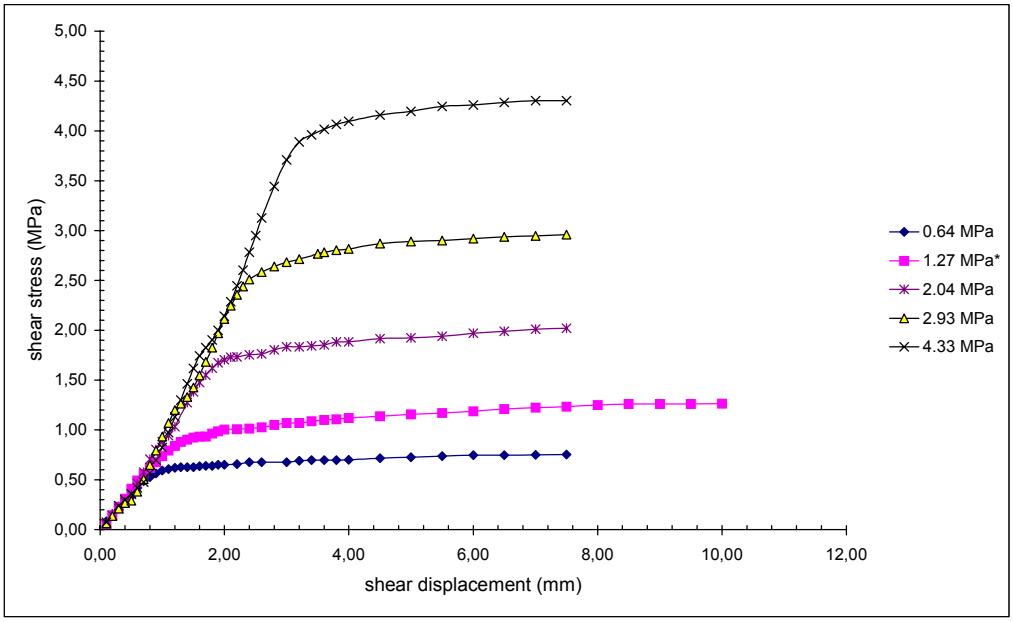

Figure A.51 Shear stress vs. shear displacement curves for Type2, α=30° (σ_n* = 1.27 MPa)

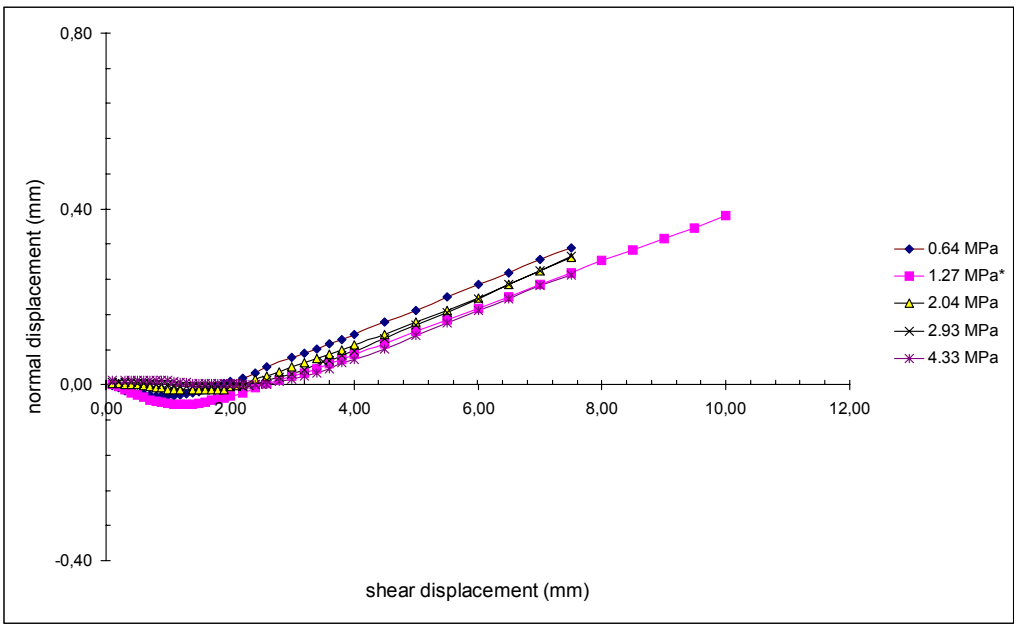

Figure A.52 Normal displacement vs. shear displacement curves for Type2, α=30° (σ_n* = 1.27 MPa)

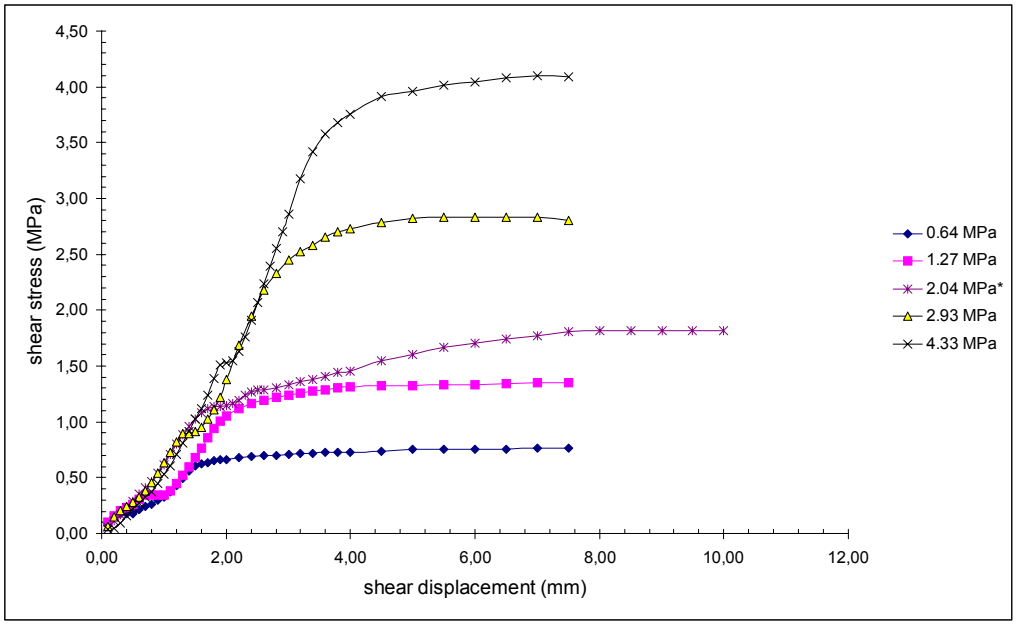

Figure A.53 Shear stress vs. shear displacement curves for Type2, α=30° (σ_n* = 2.04 MPa)

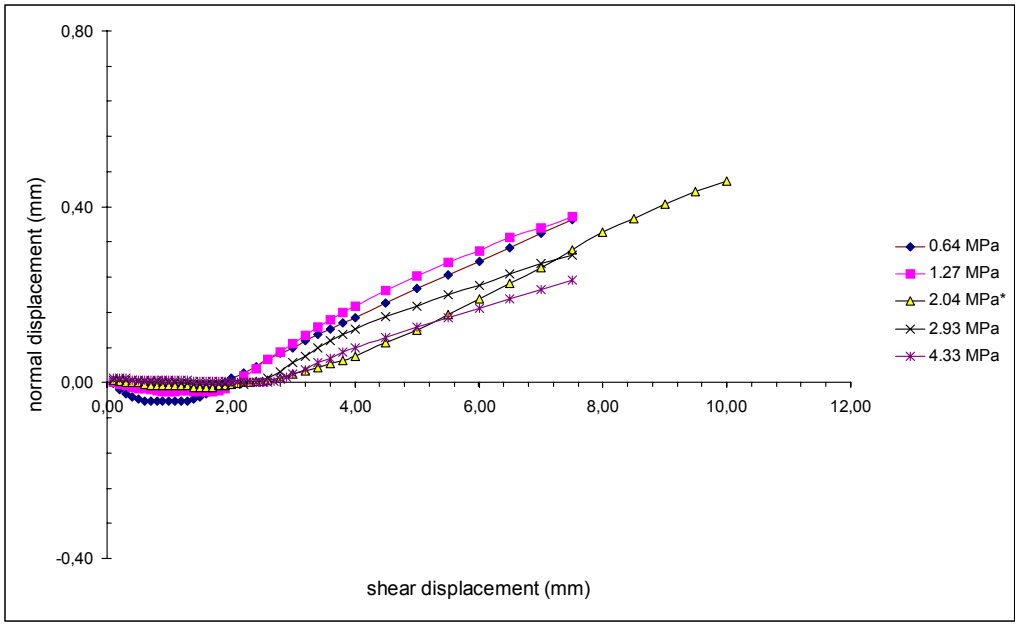

Figure A.54 Normal displacement vs. shear displacement curves for Type2, α=30° (σ_n* = 2.04 MPa)

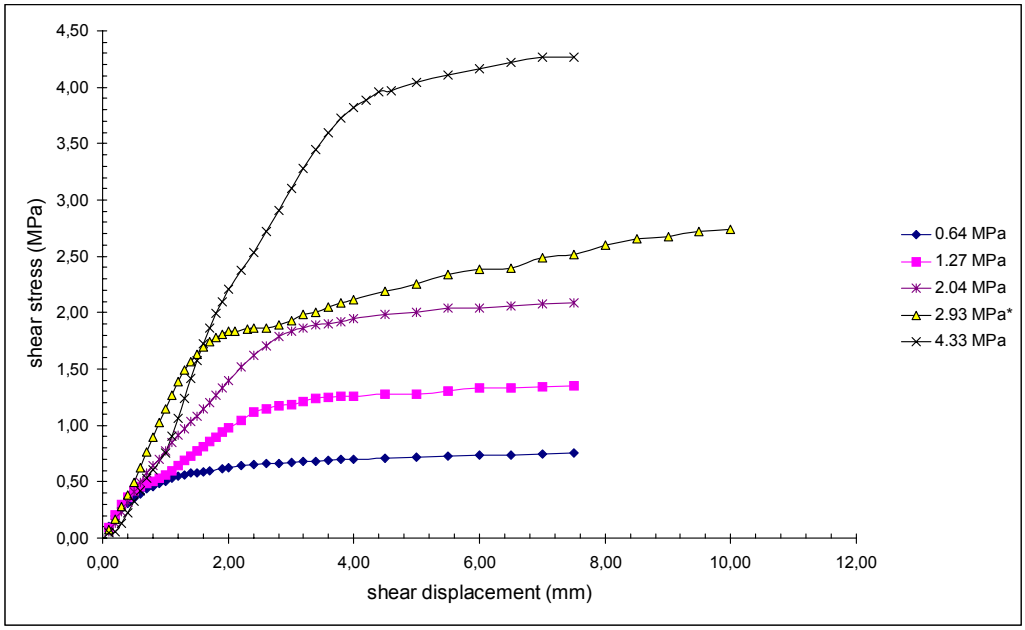

Figure A.55 Shear stress vs. shear displacement curves for Type2, α=30° (σ_n* = 2.93 MPa)

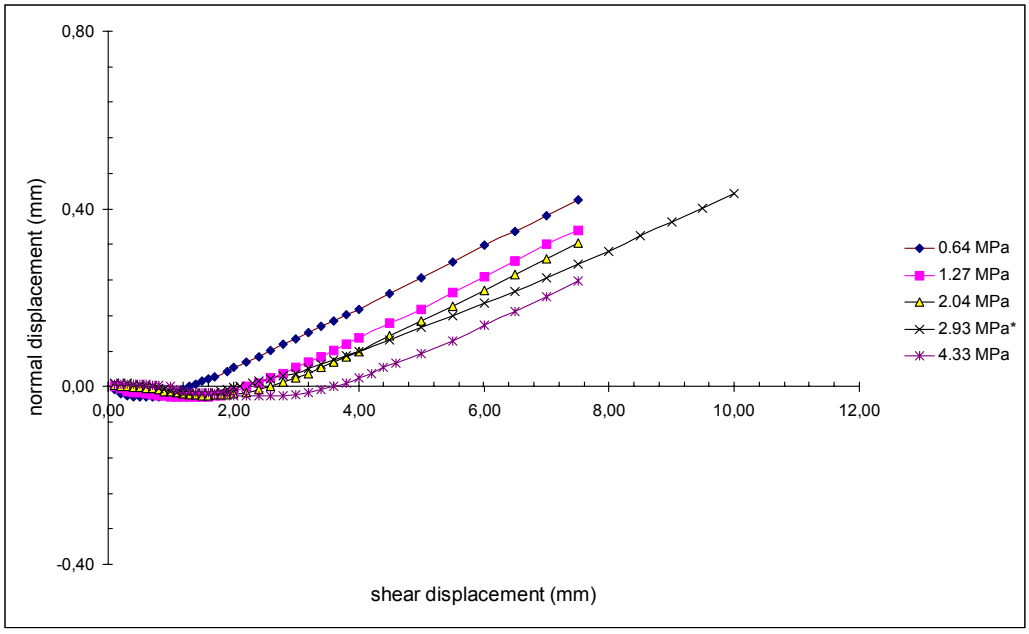

Figure A.56 Normal displacement vs. shear displacement curves for Type2, α=30° (σ_n* = 2.93 MPa)

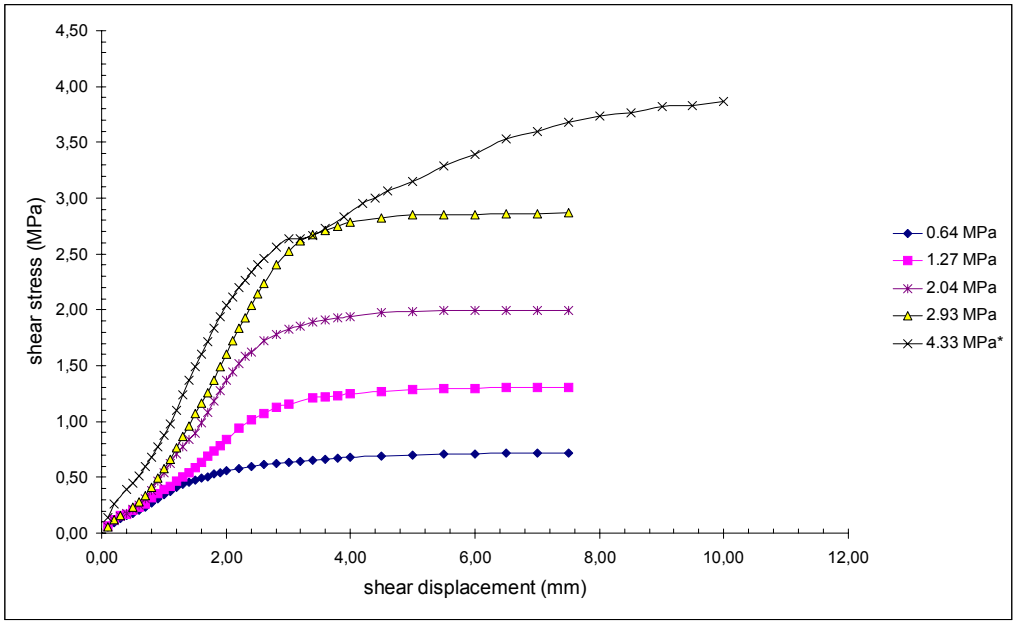

Figure A.57 Shear stress vs. shear displacement curves for Type2, α=30° (σ_n* = 4.33 MPa)

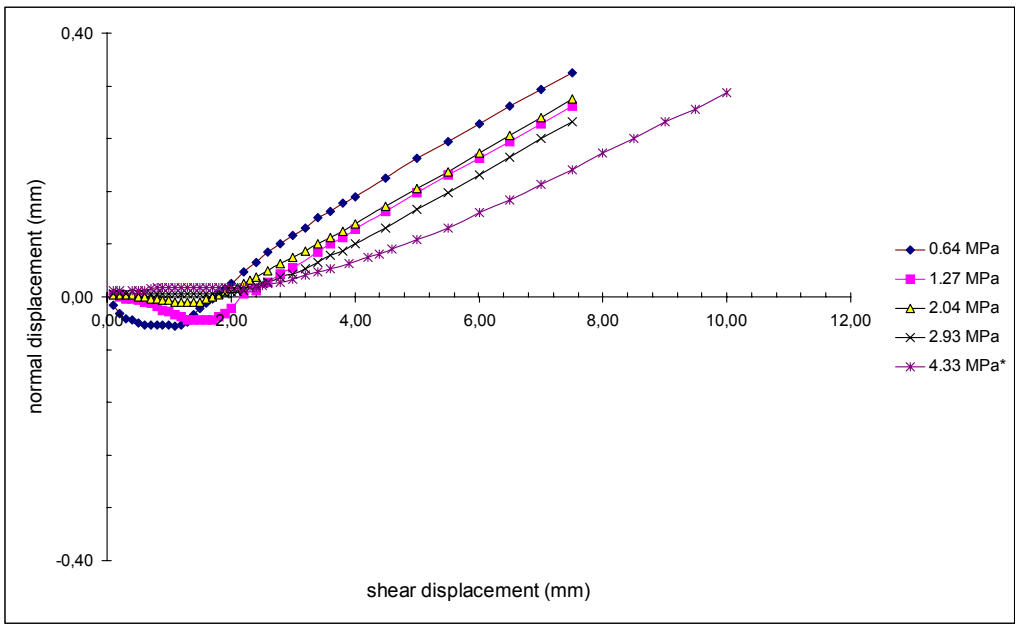

Figure A.58 Normal displacement vs. shear displacement curves for Type2, α=30° (σ_n* = 4.33 MPa)